INVESTIGATION OF FUNCTIONAL CONNECTIVITY AND NEUROVASCULAR COUPLING IN DIFFERENT VIGILANCE/BREATH-HOLD STATES OF THE BRAIN USING SIMULTANEOUS EEG-fNIRS MEASUREMENTS

by

OLAJIDE BABAWALE M

Presented to the Faculty of the Graduate School of

The University of Texas at Arlington in Partial Fulfillment

of the Requirements

for the Degree of

DOCTOR OF PHILOSOPHY

THE UNIVERSITY OF TEXAS AT ARLINGTON

MAY 2018

Acknowledgements

Firstly, I thank the Almighty God for being my strength, helper, and sufficiency throughout the period of my doctoral program. Also, my deepest appreciation goes to my doctoral supervisor, Dr. Hanli Liu, for her patience and commitment in guiding me throughout the duration of my research work. Dr. Hanli Liu constantly ensured that my work met excellent standards, and painstakingly helped with the difficulties that I encountered. In addition, Dr. Hanli Liu improved my understanding of the scientific research process. I would like to thank Dr. Khosrow Behbehani and Dr. George Alexandrakis, for their exemplary teaching. I learnt a lot from Dr. Behbehani's class in Digital Signal Processing during my first year, which helped me a great deal in my research work. He patiently answered every question that I had during the class, without complaining. Dr. George's class on Tissue Optics was my first ever introduction to functional imaging modalities. His simplicity in explaining the different concepts was vital for my understanding.

Furthermore, my doctoral journey was made productive with the help of my colleagues. Firstly, my thanks go to Thien Nguyen, who was my partner in collecting the multimodal data used for this study. Also, I greatly appreciate her doctor colleague, Dr. Tae Kim, who helped us with the sleep scoring of the simultaneous EEG-FNIRS measurements. In addition, my thanks go to Dr. Yan Wang and Ms. Ciwen, who helped in providing the code and algorithms for wavelet coherence analysis. I also thank Dr. Xinlong Wang for giving his ideas and helping me with interpretation of data. I also appreciate other members of Dr. Liu's lab who volunteered themselves as subjects for my study.

My sincere thanks also go to my loving parents, Dr. and Mrs. Babawale, who stood by me and supported me financially and materially to the best of their ability. My siblings, Modupe, Gbenga, and Odun, were all supportive and prayed for me continually. Lastly, I appreciate the Pastor and my family at Christ Embassy, Dallas, Texas. You guys were my cheerleaders, helping me up when I struggled, encouraging and believing in me all the time. One page is not enough to mention all your names. Thank you for loving me with the love of Christ. I love you all.

May 01, 2018

Abstract

INVESTIGATION OF FUNCTIONAL CONNECTIVITY AND NEUROVASCULAR COUPLING IN DIFFERENT VIGILANCE/BREATH-HOLD STATES OF THE BRAIN USING SIMULTANEOUS EEG-fNIRS MEASUREMENTS

Olajide Babawale, PhD

The University of Texas at Arlington, 2018

Supervising Professor: Hanli Liu

Functional connectivity and neurovascular coupling have been studied extensively in the neuroimaging literature. Insights gained from the knowledge of brain connectivity have provided a better understanding of how the brain organizes its subsystems in controlling different cognitive processes. In addition, knowledge gained from neurovascular coupling has been useful in understanding the relationship between cerebral blood flow and brain health. Further insights into brain connectivity and neurovascular coupling in different vigilance/breath-hold states are required to understand better on how the brain functions in these different states. Thus, my PhD research work attempted to understand the working of the brain in different vigilance states/breath-hold by analyzing both functional connectivity and neurovascular coupling. This

research work was subdivided into 3 specific aims. Aim 1 was to investigate functional connectivity of EEG in both resting-state and four different vigilance states from wakefulness to sleep. Graph theory analysis was used to quantify brain network characteristics in different vigilance states from wakefulness to sleep, while EEG source reconstruction coupled with machine learning algorithm was used to identify brain networks in resting-state. 4 brain networks (namely visual, sensorimotor, vision, and self-referential) were identified from EEG resting-state data, along with their oscillatory characteristics. Also, the functional characteristics of the default-mode network was found to be significantly altered across vigilance states from wakefulness to sleep. Aim 2 was to study neurovascular coupling in three different vigilance states from wakefulness to sleep. A recently developed method known as wavelet coherence was used to quantify neurovascular coupling in each of the vigilance states for different EEG frequency bands. Neurovascular coupling was analyzed in 3 separate frequency components which were endogenic component (0.01 – 0.02 Hz), neurogenic component (0.02 – 0.04 Hz), and myogenic component (0.04 – 0.15 Hz). Also, the analysis of neurovascular coupling was performed for four separate brain sites. The endogenic and myogenic component in coupling was shown to be significantly altered across vigilance states, with increased coupling reported in eyes-closed vigilance state (for 2 brain sites) and sleep state (one brain site). Aim 3 was to investigate neurovascular coupling in three different states of breath-hold namely normal breathing, short breath-holds, and long breath-holds. Wavelet coherence analysis was also applied here to quantify neurovascular coupling as in Aim 2. In addition, the three frequency components in neurovascular coupling (endogenic, neurogenic, and myogenic) were also studied in each of these separate states. Also, the same four brain sites used in Aim 2 were also used in Aim 3 for neurovascular coupling analysis. A significant increase in endogenic and neurogenic

components was reported for long breath-holds compared to normal breathing and short breath-holds at 3 of the brain sites. In conclusion, both functional connectivity and neurovascular coupling were significantly altered across different vigilance states/breath-hold.

Table of Contents

List of Figures

List of Tables

CHAPTER 1

1. INTRODUCTION

1.1 Functional connectivity

The brain is organized as a set of different networks, which include the default-mode network, sensorimotor network, salience network [1]. Each network is made up of specific brain regions which interact together at both the structural and functional level. The interaction of different brain regions/network elements at the functional level is known as functional connectivity. The aim of functional connectivity study is to identify functional brain networks from brain imaging recordings obtained from functional magnetic resonance imaging or FMRI, positron emission tomography or PET, and functional near infrared spectroscopy or FNIRS. Several brain networks have been identified in the resting-state condition of the brain, when no tasks are performed by the subject. These networks are commonly referred to as resting-state networks [1]. The study of resting-state networks of the brain has helped in the quicker diagnosis of different brain dementia such as Alzheimer's disease[2] and schizophrenia[3]. In addition, with functional connectivity studies, researchers can investigate the working of the whole brain at once[4]. This way, multiple brain networks are viewed simultaneously, so that the functional architecture of the brain can be readily explored and analyzed [4]

As the resting-state brain transitions from an awake restful state to a sleep state, the functional connectivity of different brain networks is altered, as shown in previous studies[5, 6]. In the neuroimaging literature, the changes in functional connectivity of brain networks during the transition from an awake, restful state to sleep state have not been studied using EEG imaging modality. EEG, or electroencephalography, is an imaging modality which records the electrical activity of neurons in the brain. Data obtained using EEG modality have a very high temporal

resolution compared to other imaging modalities such as functional magnetic resonance imaging (fMRI) and functional near infrared spectroscopy[7]. Also, EEG data contain frequencies between 2 – 60 Hz[8]. Thus, the relationship between functional architecture and different frequency bands of the brain can be readily studied using EEG modality. In addition, functional connectivity analyses of EEG data can be performed as either sensor-level analysis or source-level analysis. At the sensor-level, brain networks are identified from time series recordings of EEG electrodes. At the source level, the electrode time series recordings are first inputted into a reconstruction algorithm to convert them to EEG source images. This method improves the poor spatial resolution of EEG time series data. Then, functional connectivity analysis is performed on these source images to identify brain networks. Two common methods used in the literature for functional connectivity analysis are Independent Component Analysis, or ICA, and graph theory analysis, or GTA [9]. In addition, ELORETA is a well-developed algorithm used for EEG reconstruction analysis[10].

In Aim 1 of my doctoral dissertation, EEG modality was utilized to investigate functional connectivity of the brain using both EEG source-level and EEG sensor-level analysis. Specifically, in Chapter 2, I used ELORETA combined with ICA algorithm to investigate resting-state EEG functional connectivity in a source-level analysis across 15 healthy subjects. In addition, the functional connectivity at source-level was examined across five EEG frequency bands namely delta (1-4 Hz), theta (4 -8 Hz), alpha (8 – 12 Hz), beta (12 -30 Hz), and gamma (30 – 60 Hz). My work in Chapter 2 was a replication study of Aoki et al's work [22] to establish the validity of ELORETA-ICA method as a tool for functional connectivity analysis of EEG data at the source level. Also, in Chapter 3, I used graph theory analysis (GTA) to study EEG functional connectivity at the sensor-level in four different vigilance states which were, eyes-

open (EO), eyes-closed (EC), sleep-stage 1 (SS1), and sleep-stage 2 (SS2). This analysis was performed for 18 healthy subjects for four EEG frequency bands which were delta, theta, alpha, and beta bands.

1.2 Neurovascular coupling in different vigilance states

In the brain, neurons transmit information through electrical oscillations. Also, it is well known that these electrical oscillations produced by neurons have some form of link with cerebral hemodynamic processes. This link is referred to as neurovascular coupling in the neuroimaging literature[11]. Put more succinctly, neurovascular coupling refers to the relationship between neural electrical activity and the corresponding changes in cerebral blood flow in the brain[12]. Neurovascular coupling is a phenomenon that underlies critical processes of the brain such as cerebral autoregulation[13]. The study of neurovascular coupling is very important for the understanding and determination of brain health. In addition, the study of neurovascular coupling of the brain sheds greater light on the pathology of certain brain-related cardiovascular diseases such as ischemic stroke, small vessel disease, and heart disease [11, 12]

In the neuroimaging literature, the neurovascular coupling in the brain during the transition from awake, restful state to sleep state has not been well studied. Also, from previous studies, neurovascular coupling studies have been performed mainly using simultaneous EEG-fMRI instrumentation [14, 15]. However, EEG-fMRI is very expensive. Also, it lacks portability and ease of use. Simultaneous EEG-fNIRS is a less expensive set up for neurovascular coupling studies. EEG-fNIRS instrumentation can easily be used in a non-laboratory setting. Also, EEG-fNIRS combines the high temporal resolution of EEG with the better spatial resolution of fNIRS to investigate brain dynamics[16]. In Aim 2 of my doctoral research, a simultaneous EEG-fNIRS instrumentation set up was used to investigate neurovascular coupling in the brain during the

transition from awake, restful state to sleep state. Specifically, in Chapter 4, a method known as wavelet coherence analysis was used to quantify neurovascular coupling in three different vigilance states which were eyes-open (EO), eyes-closed (EC), and sleep-stage 1 (SS1). In addition, 3 frequency components of neurovascular coupling were quantified for each vigilance state, which are the endogenic component (in a fNIRS frequency range of 0.01 – 0.02 Hz), the neurogenic component (in a fNIRS frequency range of 0.02 – 0.04 Hz), and the myogenic component (in a fNIRS frequency range of 0.04 – 0.15 Hz). These components were examined separately for three frequency bands of EEG which were theta (4-8 Hz), alpha (8 – 12 Hz), and beta (12 – 30 Hz). Also, the neurovascular coupling analysis across vigilance states was performed in four different sites located on the head, which were the left, right frontal, left occipital, and right occipital brain sites.

1.3 Neurovascular coupling during voluntary breath-holding

Neurovascular coupling is significantly altered in the brain for respiratory disease of hypoxia, like stroke[11]. An understanding of the neurovascular coupling in normal respiratory function can provide some insight into the link between respiratory pathologies and brain function. The neurovascular coupling in different states of voluntary apnea has not been studied using simultaneous EEG-fNIRS measurements. In Aim 3 of my doctoral research, the neurovascular coupling in different periods of voluntary breath-holding was investigated using EEG-fNIRS. Specifically, in Chapter 5, wavelet coherence method was used to quantify neurovascular coupling in three different states of voluntary breath-hold which were rest/normal breathing of 5 minutes; 5 short breath-hold periods of 10 seconds each; and 5 long breath-hold periods of 20 seconds each. Also, the endogenic, neurogenic, and myogenic frequency components of

neurovascular coupling were quantified in each breath-hold state for three different frequency bands of theta, alpha, and beta, in each of four different brain locations mentioned above.

An outline of the research aims of my doctoral work is provided below in Section 1.3.

1.4 Research aims

Aim 1a: To investigate functional connectivity of the brain at EEG source level in resting state using ELORETA-ICA method;

Aim 1b: To investigate functional connectivity of the brain at EEG sensor-level in four different vigilance states (eyes-open, eyes-closed, sleep-stage 1, and sleep-stage 2) using graph theory analysis and EEG;

Aim 2: To investigate neurovascular coupling of the brain in three different vigilance states (eyes-open, eyes-closed, and sleep-stage 1) using wavelet coherence analysis and simultaneous EEG-FNIRS;

Aim 3: Investigating neurovascular coupling of the brain in two different breath-holding states (shorter breath-holding, and longer breath-holding) using wavelet coherence analysis and simultaneous EEG-FNIRS.

CHAPTER 2

2 Resting state independent networks identified by EEG measurements and analyses using ELORETA-ICA: *A replication study*

2.1 Background

Functional brain networks are defined as "sets of distant cerebral areas that are linked anatomically through white matter tracts, and functionally, through dynamics of coupled activities[17]" Resting state functional connectivity (RS-FC) implies functional brain networks that are active when the brain is in a 'no-task' or resting state. Accurate identification of RS-FC enables neuroscientists to observe multiple cortical networks at the same time, thereby providing information about the functional organization of the brain[4]. High-quality quantification and good understanding of RS-FC are also helpful for studying the brain activity in patients who may not be able to perform certain task-related activities, for example, patients in vegetative or minimally conscious states and young children [4]. The disruption of RS-FC is implicated in cognitive disorders such as Alzheimer's[2], schizophrenia[18], and dementia[19]. Thus, understanding and quantification of RS-FC can possibly be beneficial for early diagnosis of neurological disorders.

To better understand functional brain networks, their oscillatory characteristics need to be considered. Most of RS-FC studies undertaken in the literature have been performed using functional magnetic resonance imaging (fMRI), which measures hemodynamic responses to neuronal activities. While fMRI has a high spatial resolution, it suffers from a low temporal resolution (1-2s); thus, the frequencies associated with cognitive processes at frequencies higher than 1 Hz cannot be detected in fMRI-derived functional networks. Furthermore, fMRI is an

indirect method of observing resting state neuronal networks in the brain since it measures only hemodynamic activities. Electroencephalography (EEG), on the other hand, is an inexpensive, portable, and non-invasive brain imaging modality, which directly records neural activities at a high temporal resolution. It is well known that EEG signals are highly oscillatory in nature and comprise abundant information with multiple frequency bands (2-60Hz) that result directly from cognitive processes[8]. Understanding these frequency-dependent electrophysiological signals may shed light on important mechanisms of brain functions and operations.

There are three popular methods used in functional connectivity analyses: seeding, graph connectivity analyses, and independent component analysis (ICA) [9]. Of the three methods, ICA is the most appropriate for the exploratory analysis of multiple brain networks [9]. ICA is a data-driven technique which decomposes multichannel brain activity into independent components (ICs) or networks. ICA can separate physiological components from artefactual ones[20]. Moreover, a method called functional ICA has been recently developed for EEG functional connectivity analyses[21], with which an EEG resting state network can be represented in a dimension of space-frequency. In other words, using functional ICA, an EEG resting state network is represented as an image of brain regions at specific EEG frequencies that function together across a group of subjects[22]. Therefore, functional ICA helps identify not only networks that are active in resting state but also the electrophysiological oscillatory frequencies within these networks. Furthermore, cross coupling of different EEG frequencies can be readily observed using functional ICA.

In a recent study, an EEG source localization approach called exact low resolution electromagnetic tomography (eLORETA) has been combined with functional ICA to identify resting state networks and their interactions in five frequency bands (delta, theta, alpha, beta, and

gamma band) from EEG data obtained from 80 subjects [22]. They identified amongst others the "visual" network in alpha frequency band, "sensorimotor" network in beta and gamma bands, and "self-referential" network in alpha and beta bands [22]. There are several advantages of eLORETA-ICA over other network visualization methods, which are (i) to allow for decomposition of cortical electrical activity into independent components (ICs) in different frequency bands, (ii) to use all frequency information of EEG data in analysis, (iii) to obtain a complete set of EEG-based resting state independent networks across several frequency bands.

Solid replication of scientific findings is critically important, as emphasized recently in several publications [23-25]. Robust replication (1) allows scientists to determine whether a particular method or tool is suitable for broad or specific uses; (2) help discover effects, if any, of additional variables, different experimental conditions, various types of instruments, or different groups of subjects on the method being studied; (3) provide the supporting validity to a particular, new, scientific tool under study. A replication study is thus a necessary step for any novel development of methodology, protocol, and/or algorithm to ensure its respective correctness, reliability, and reproducibility for future uses.

In this study, a replication of recent work by Aoki et. al in ref. [22] was performed. The ELORETA-ICA procedure has been validated by a previous study by Marqui et al [21]. Specifically, the eLORETA-ICA method was utilized to identify EEG resting state functional networks and their activity in five EEG frequency bands based on 64-channel EEG data obtained from 15 healthy young subjects (mean age = 23.5 years; s.d = 2.7). Note that the EEG measurements acquired by Aoki et. al used only 19 electrodes. For more quantitative comparison, temporal profiles of the 19 EEG channels, which corresponded to the international 10-20 system, from the recorded 64-channel EEG data, were selected. Then, ELORETA-ICA

was used to identify EEG resting state networks at five specific frequency bands for 19-channel EEG. Then, the networks of the 64-channel and 19-channel EEG analyses were compared. Also, the networks determined using 19-channel EEG analysis were compared with those reported by Aoki et. al. The aims of this study were (1) to investigate the effect of increasing the number of EEG electrodes on results of EEG resting state functional networks, and (2) to assess the reproducibility of the eLORETA-ICA method as a general tool for EEG independent networks analyses.

2.2 Methods

Figure 2.1 shows an overall flow of the study, consisting of four major parts, which will be described in several sub-sections below. This analysis flow was followed for both 64-channel and 19-channel EEG data processing. The first sections discuss the analysis of the 64-channel EEG, while the analysis of the 19-channel EEG is discussed under the section titled "eLORETA-ICA analysis of data recorded from 10-20 EEG electrodes."

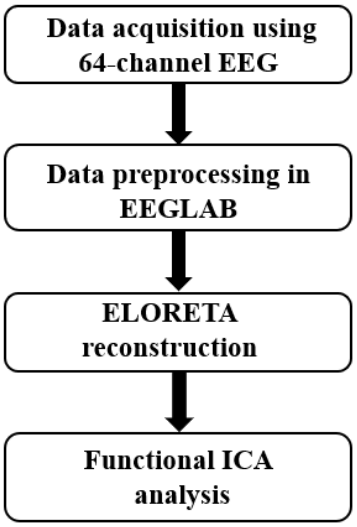

Figure 2.1: Flowchart of ELORETA-ICA study

2.2.1 Subjects

A total of 15 healthy human participants (13 males, 2 females, mean age = 23.5 years, SD = 2.7 years) were recruited from the local community of the University of Texas at Arlington. The inclusion criteria included: either sex, any ethnic background, and in an age range of 18–35 years old. The exclusion criteria included: diagnosed with a psychiatric disorder, history of a neurological condition, history of severe brain injury, history of violent behavior, have ever been institutionalized/ imprisoned, current intake of any medicine or drug, or currently pregnant. The study protocol was approved by the institutional review board (IRB) of the University of Texas at Arlington and complied with all applicable federal and NIH guidelines. Informed consent was obtained from each participant prior to the experiments. Subjects were instructed to minimize body movements during EEG data acquisition. The EEG recordings were monitored by the research assistant on duty. Phones, radios or other electromagnetic devices were not allowed in the laboratory or on the subject for the duration of the experiment.

2.2.2 EEG Data Acquisition

EEG recordings were taken in resting state (awake, eyes-closed, and sitting) for 5 minutes. Brain electrical activity was recorded using a 64-electrode EEG device (Biosemi Instruments, Netherlands). The electrodes were positioned according to the international 10-10 system montage, which requires 64 EEG electrodes. Electrooculogram (EOG) electrodes were placed on the outer canthi of both eyes. Electromyogram (EMG) electrodes were placed on the facial muscles and earlobes. The sampling rate was set at 2048 Hz. A Biosemi active electrode system uses online referencing through a Common Mode Sense (CMS) electrode.

2.2.3 EEG Data Preprocessing

After data acquisition, the 64-channel (N_e=64) EEG temporal profiles were exported to EEGLAB toolbox [26] for preprocessing. First, the data were down sampled to 500 Hz, in line

with the previous study by Aoki et al [22]. Second, a band-pass filter of 0.53 – 120 Hz (with windowed sinc high and low pass filters) was applied to the EEG data [27]. Specifically, a Blackman window between the high-pass transition band at 0.5 Hz and the low-pass transition band at 5 Hz was used for band-pass filtering [27] Channels that were considered noisy had extremely large amplitudes, and they were corrected using spherical interpolation. Then , the data were subsequently average-referenced, followed by 60-Hz line noise removal using an EEGLAB plugin with default values [28]. Next, ICA [20] was applied to each subject's multi-channel EEG data to remove artifacts of eye blinks, eye movements and muscle noise. Finally, the first set of artifact-free 120-s epochs (sixty 2-secs epochs) were selected for each subject and converted to ASCII text files for EEG source localization using eLORETA. Figure 2.2 outlines the entire data processing steps/procedures from 64-channel EEG data acquisition to five frequency-dependent source localization images.

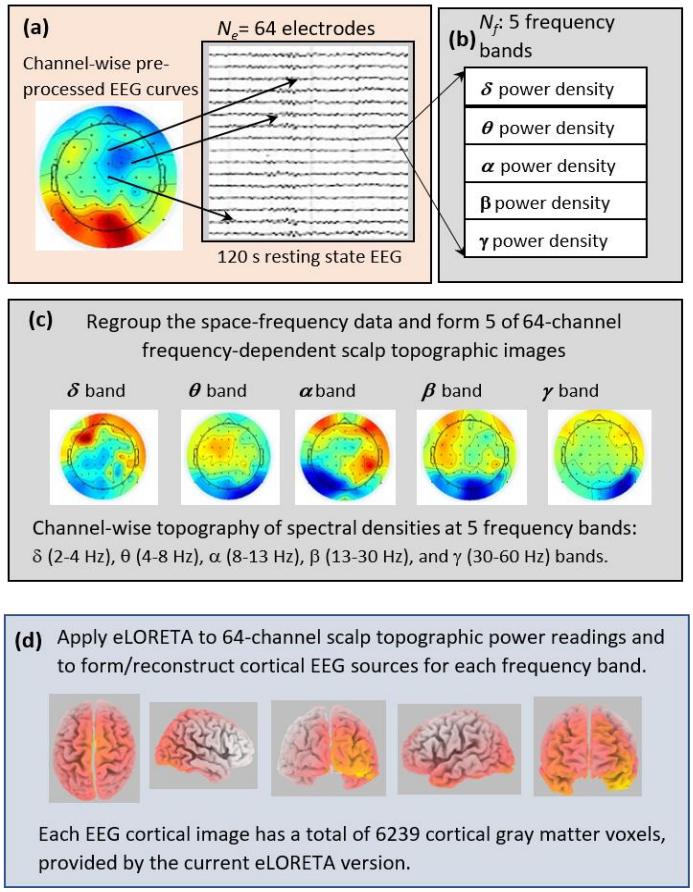

Figure 2.2: Steps of data processing of 64-channel EEG data to form frequency-dependent ELORETA images

2.2.4 ELORETA

ELORETA is publicly available free academic software (http://www.uzh.ch/keyinst/loreta.htm) and computes the cortical three-dimensional (3D) distribution of current density based on the scalp-recorded electric potential distribution. It offers a weighted minimum inverse solution with zero localization error under ideal conditions [10]. ELORETA uses a total of 6239 voxels at 5-mm spatial resolution to localize electric activity in the cortex. In this study, Eloreta was used to calculate 3D cortical current distribution at each of the five frequency bands (i.e., delta, theta,

alpha, beta, and gamma band; N_f =5) from subjects' EEG data. Figure 2.2 provides schematic illustration for the entire process.

Specifically, each of 64 EEG curves across 120 secs were decomposed into delta (δ; 2-4 Hz), theta (θ; 4-8 Hz), alpha (α; 8-12 Hz), beta (β; 13-30 Hz), and gamma (γ; 30-60 Hz) bands; their respective power spectral densities were calculated for all 64 channels. By then, the processed EEG data became a space-frequency domain (i.e., 64 electrode locations with five power spectral densities per site). To obtain frequency-dependent 3D cortical current distributions, the data were regrouped and formed into five of 64-channel scalp topographic images for respective frequency bands. Next, by applying eLORETA to each of the 64-channel scalp topographic power density images, 3D cortical EEG sources for each frequency band were reconstructed, as demonstrated in Fig. 2.2(d). Each of the EEG cortical images had a total of 6239 cortical gray matter voxels.

2.2.5 Functional ICA

The process shown in Fig. 2.2 was performed for each subject; the 5 reconstructed images represented current sources active in respective frequency bands. Then, an ICA-based method known as functional ICA was used to perform group analysis of each subject's source image solution to identify independent components (i.e., independent networks) and their respective EEG frequency bands across all subjects. The overall principle is shown in Fig. 2.3.

Specifically, the eLORETA-derived 5-frequency source images from each subject were expressed in a matrix format as voxel-by-frequency or $N_v \times N_f$, where N_v= total number of voxels given by eLORETA=6239 and N_f = 5. To identify networks across all subjects, each subject's voxel-by-frequency matrix was transformed into a voxel-frequency vector (see the left panel) of Fig. 2.3. All subjects' vectors were then concatenated, and functional ICA was applied to this

concatenated matrix to derive *K* independent components represented in space-frequency, as shown by the right panel of Fig. 2.3. In this way, common space-frequency features were emphasized and extracted across all (n=15) subjects.

The number of independent components (*K*) in this study was estimated using the sphericity test, in accordance with the previous study [22]. Also, Non-Gaussianity was used to estimate independence between networks, and fourth-order cumulant was used to calculate non-Gaussianity. For this study, the network maps were color-coded for visual representation using a z-score threshold of 2 (which corresponds to a significance level of 0.05). Voxels with positive values of cortical current density were coded yellow and those with negative values of cortical current density were coded blue.

Weighted minimum-norm inverse solutions, such as ELORETA, have a regularization parameter (α) that needs to be optimally determined for final and accurate algorithm execution. This parameter is important for calculating the eLORETA transformation matrix (T-matrix). It is important to choose an optimal value for α to prevent both over-smoothing and spurious localization of EEG sources [29]. In this study, source localization was performed using eLORETA with four different values of α in decreasing orders of magnitude. These values were 10000, 100, 1, and 0.01. Then, the respective source images obtained using four different α values were compared by observing their corresponding source distributions. Based on the comparison and observation of the reconstructed images, the most appropriate value was selected as the regularization parameter in each respective case in this study. The criteria for selecting this value were based on (i) the observed posterior voxel activation of alpha frequency band for all subjects except one, which was excluded from further analysis, and (ii) the quality of reconstructed source images. ELORETA Images obtained using α = 0.01 had a very sparse

cortical current distribution with very few voxel activations. This showed that the value of 0.01 was too stringent for reconstruction. ELORETA images obtained using $\alpha = 100$ and $\alpha = 10000$ had voxel activations distributed across the brain surface, showing that these values may be too relaxed and may produce spurious cortical current source distributions. Because of this, ELORETA images obtained using $\alpha = 1$ was used for functional ICA analysis.

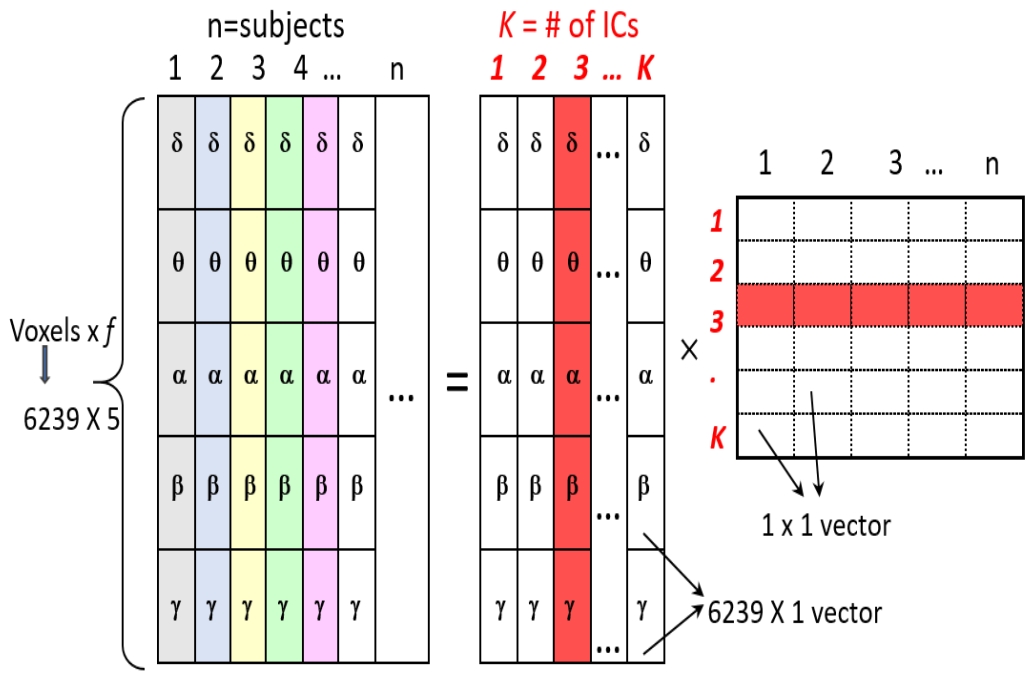

Figure 2.3: Functional ICA analysis of frequency-dependent images

2.2.6 ELORETA-ICA Analysis Using 19 electrodes to simulate 10-20 EEG System

A similar eLORETA-ICA analysis was performed on a subset of the original Biosemi 64-channel EEG dataset obtained from all subjects. This subset contained the 5-minute recordings of 19 channels which correspond to the international 10-20 system of EEG electrode placement. The processing steps were like the framework described in Sections 2.2.3-2.2.5, and illustrated in

Figs. 2.2 and 2.3. The numbers of channels were different between the two analyses. The channels chosen in the19-channel subset were Fp1, F7, F3, T3/T7, C3, P3, T5/P7, O1, Fz, Cz, Pz, Fp2, F4, F8, C4, T4/T8, P4, P8/T6, and O2 from the original 64 channels for each subject. Also, the regularization value was set to $\alpha = 1$ for the 19-channel EEG analysis, like in the 64-channel EEG analysis. Choosing the same regularization value for both analyses helped to effectively compare the results obtained in both analyses. Note that the regularization value is very important for reducing the effect of noise on the results of EEG source reconstruction.[29].

Furthermore, the alpha source localizations in the posterior location were used as a landmark or reference to quality-check the reconstructed eLORETA images. It is well accepted in the neuroimaging field that in resting state, alpha sources are in posterior areas of the human brain. If the reconstructed subject's alpha sources were in posterior locations of the brain, functional ICA was performed by grouping all confirmed subjects' images at 5 frequency bands together for a simultaneous, subject-based ICA analysis (see Fig. 2.3). Two subjects' data were excluded from further analysis because their alpha sources were not localized in posterior locations, and this was probably due to noisy artifacts. Then, functional ICA was performed on the remaining 13 subjects' frequency-dependent eLORETA images.

2.3 Results

2.3.1 ELORETA-ICA Analysis of 64-channel EEG Data

Using the sphericity test [22], the number of independent networks (*K*) was calculated as 7.8. Consequently, eLORETA-ICA analysis was performed with K = 7. Of the 7 components, four resting state networks were identified with their respective frequency bands, based on comparison of their spatial current distributions to well-known RSNs in the neuroimaging literature. Specifically, independent component 2 (IC2) was identified as the "visual" network,

and it had activation in all five frequency bands (see Figs. 2.4A-4E). Independent component 5 (IC5) was identified as the "dual-process of vision perception" network, and it was active in four frequency bands (all bands except delta), as shown in Figs. 2.5A-5G. Independent component 6 (IC6) was identified as the "sensorimotor" network, and it had activation in four (delta, theta, alpha, and gamma) bands, as marked in Figs. 2.6A-6D. Independent Component 7 (IC7) was identified as "self-referential" network (see Figs. 2.7A-7D); it was active also in four frequency bands (all bands except delta).

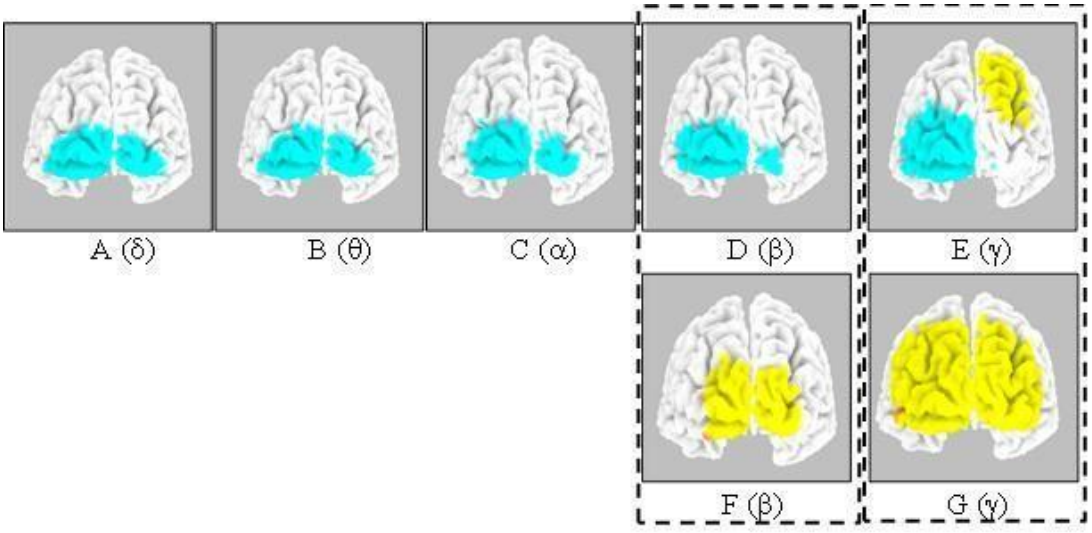

Figure 2.4: Visual Network for 64-channel and 19-channel analysis. In 64-channel, this network was identified in (A) delta, (B) theta, (C) alpha, (D), beta, and (E) gamma bands. In 19-channel, this network was identified only in (F) beta, and (G) gamma bands.

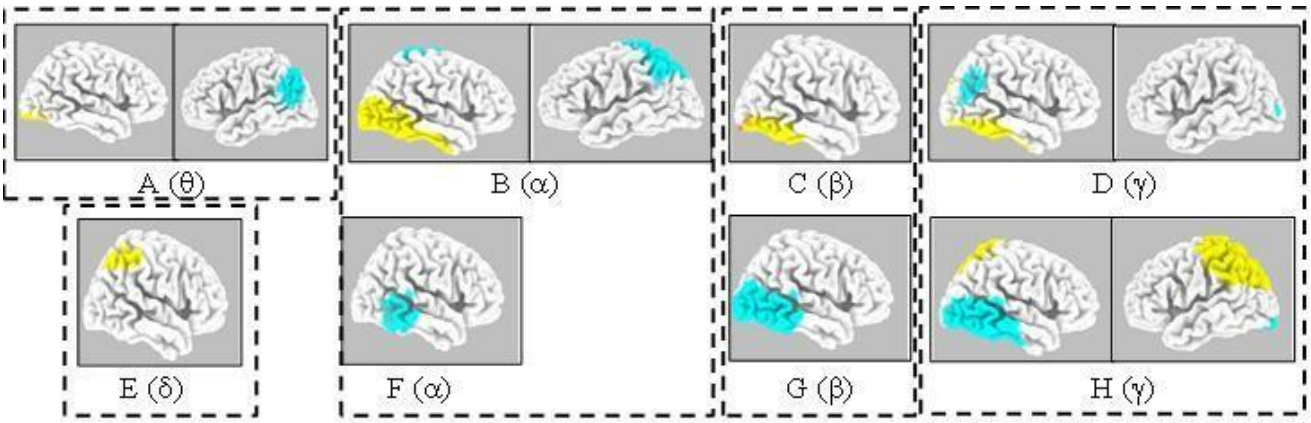

Figure 2.5: Dual-process of vision perception network, identified in both 64-channel and 19-channel EEG. In 64-channel, this network was identified in (A) theta, (B) alpha, (C) beta, and (D) gamma bands. While in 19-channel, it was identified in (E) delta, (F) alpha, (G) beta, and (H) gamma bands

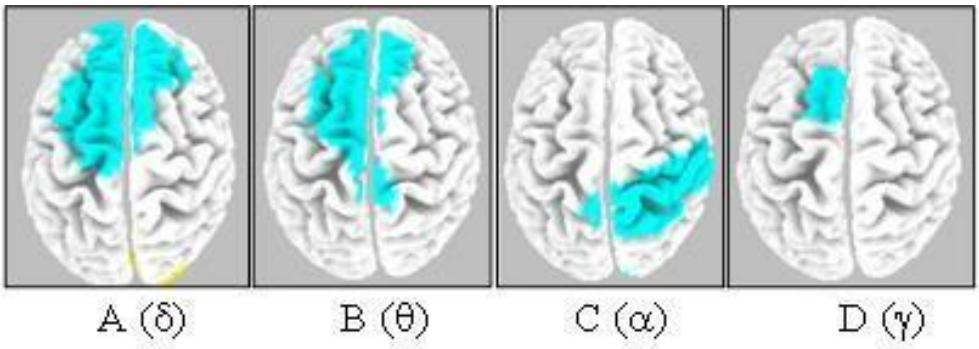

Figure 2.6: Sensorimotor network, identified in only 64-channel EEG. This network was identified in (A) delta, (B) theta, (C) alpha, and (D) gamma bands

.

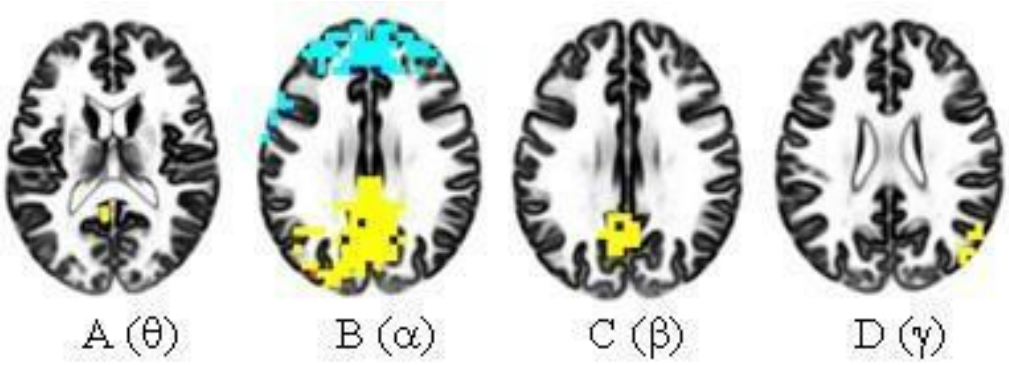

Figure 2.7: Self-referential network, identified in only 64-channel EEG. This network was identified in (A) theta, (B) alpha, (C) beta, and (D) gamma bands.

.

2.3.2 ELORETA-ICA Analysis of 19-channel EEG Selected from 64-channel Data

The sphericity test calculated the number of components as 6.568. Consequently, the value of 6 was chosen as the number of components, K. From the 6 components, only 2 EEG networks and their activity in different EEG frequency bands were identified. The identified EEG networks were: IC2 as the "visual" network in beta and gamma bands (Fig. 2.4F & 2.4G); and IC3 as the "dual-process of vision perception" network in delta, alpha, beta, and gamma bands (Figs.2.5H-L).

2.4 Discussion

In this study, a replication of a previous EEG-resting state independent networks study by Aoki et al was performed. The study was conducted in a two-part analysis. First, the eLORETA-ICA method was utilized to analyze 64-channel EEG resting state data obtained from 15 subjects and to identify EEG resting state networks at respective frequency bands. The international 10-10 system for data acquisition with 64 EEG electrodes was used, while the previous work by Aoki et al. utilized the international 10-20 system with 19 electrodes. For better comparison with the results by Aoki et al, the second part of the analysis was to carry out eLORETA-ICA on time

series of 19 channels (those used in the 10-20 system) selected from the original 64-channel EEG data. Electrophysiological data was collected from a much smaller sample size (n=15) with a much smaller age span (23.5±2.7 years of age) compared to the previous study (n=80; an estimated mean age=45 with an age range from 18-87 years). The aim of this study was two-fold: (i) To compare EEG independent networks identified with a denser electrode system (64 channels) versus a sparse electrode system (19 channels), and (ii) to examine the reproducibility and possible generalization of the eLORETA-ICA method as a tool for analyzing frequency-dependent EEG resting state independent networks.

In the analysis of the 64-channel EEG data, four EEG resting state independent networks and their respective neural oscillations were identified. Analysis of 19-channel EEG identified only two EEG resting-state networks with their respective oscillations. All of these networks found in both analyses were in good agreement with the previous study by Aoki et al [22]; however, fewer networks were identified in the 19-channel EEG analysis compared to the previous study by Aoki et al [22]. For clear and detailed comparison, Table 2.1 summarizes the EEG independent networks and their respective frequency bands that were identified in this study and the previous work [22]. Crosses 'X' indicate the frequency bands that were found to be active within the networks, and spaces left blank indicate that the frequency band was absent or inactive. In the following sub-sections, each of the networks are discussed in more detail, and the similarities and differences between the results obtained in the two studies.

Table 2.1: Resting-state networks and their respective neural oscillations, identified in 64-channel and 19-channel for this study (columns 1 and 2) and the previous study by Aoki et al (column 3). Places marked 'X' show that the corresponding neural oscillation was identified in this network. Places shown as blank indicate that the corresponding neural oscillation was not identified in this network.

EEG networks in 5 frequency bands	64-channel analysis in this study	19-channel analysis in this study	19-channel analysis by Aoki et al.
Visual network			
Delta	X		
Theta	X		
Alpha	X		X
Beta	X	X	
Gamma	X	X	
Dual-process of vision perception			
Delta		X	
Theta	X		
Alpha	X	X	X
Beta	X	X	X
Gamma	X	X	
Sensorimotor			
Delta	X		
Theta	X		
Alpha	X		
Beta			X
Gamma	X		X
Self-referential			
Delta			
Theta	X		
Alpha	X		X
Beta	X		X
Gamma	X		

2.4.1 Visual Network

IC2 was identified as the "visual" network in the 64-channel EEG data (Figure 2.4A-4E), and as IC2 in the 19-channel EEG data (Figure 2.4F-4G). This network was characterized by activation of voxels in the occipital region, specifically BA 17 and 18 (Figs. 2.4A-2.4G). In the 64-channel EEG, this component had activation in all five frequency bands that were identified in this study (Figs. 2.4A-E). However, in the 19-channel EEG, this network had activation in only two frequency bands (Figs. 2. 4F-G). The visual network consists of brain regions that are involved in the processing and interpretation of visual stimuli. These brain regions include the primary visual cortex (V1, located in BA 17) and the secondary visual cortex (V2, located in BA 18). Numerous neuroimaging studies have shown that V1 and V2 are in the occipital lobe of the brain.

In the previous study by Aoki et al, the visual network was also identified at only the alpha frequency band [IC4 in [22]]. While some neuroimaging studies have shown that the alpha band plays a major role in visual processing, other studies have also reported that the visual network may employ more than one neural oscillation to perform its tasks. For example, an EEG-fMRI study by Mantini et al [30] identified the five major cerebral oscillations (delta, theta, alpha, beta, gamma) to be active in this network, with all of them except one (gamma) having statistically significant correlations with the network's BOLD time course. Some other studies have shown that the gamma frequency band may be involved in a neural phenomenon known as "visual feature binding" [31]. The studies are consistent with this study's findings of multiple EEG frequency bands within the visual network. In addition, the identification of visual network at multiple frequency bands by both 19-channel and 64-channel EEG analyses show good

reliability and reproducibility of the eLORETA-ICA method as an excellent tool for identifying resting-state independent networks in EEG data.

2.4.2 "Dual-process of vision perception" Network

IC5 was identified in the 64-channel EEG data as the "dual-process of vision perception" network in four frequency bands (Figs 2.5A-5G), which was also recognized as IC3 in the 19-channel EEG with four frequency bands. Based on the 64-channel EEG analysis, this network was characterized by activations in right occipitotemporal cortex (Fig. 2.5A) and left occipito-parietal cortex (Fig. 2.5B) in theta band; activations in right occipitotemporal cortex (Fig.2.5C) and left posterior parietal cortex (Fig. 2.5D) in alpha band; activation in right temporal cortex in beta band (Fig. 2.5E); and activations in right temporal cortex and middle temporal area (Fig. 2.5F) and activation in left occipital cortex (Fig. 2.5G), both in gamma band. In the 19-channel EEG, this network was characterized by activation in right posterior parietal cortex (Fig. 2.5H) in delta band; activation in right temporal cortex (Fig. 2.5I) in alpha band; activation in right occipitotemporal cortex (Fig. 2.5J) in beta band; activations in right occipitotemporal cortex (Fig. 2.5K) and in left posterior parietal cortex (Fig. 2.5L), both in gamma band.

The dual-process of vision perception network consists of brain regions that are actively involved in the flow of visual information from the visual cortex to other parts of the brain for further cognitive processing. Specifically, this network consists of two pathways; one, a dorsal visual pathway (DVP), is involved in automatic visual guidance of spatial movements [22], and another, a ventral visual pathway (VVP), compares visual information from occipital lobe to spatial memory in right temporal cortex. Together, these two separate visual pathways are necessary for both visual perception and action [32].

In the previous study by Aoki et al, this network was also identified with two frequency bands [IC5 in [22]]. The DVP in the previous study comprised the left posterior occipitoparietal cortex, the caudal intraparietal sulcus (cIPS) and middle temporal (MT+) in alpha band, while the VVP comprised the right occipitotemporal cortex, temporo-parietal junction (TPJ), parahippocampal gyrus, fusiform gyrus, and ventral pre-frontal cortex (vPFC). Furthermore, the VVP linked the occipitotemporal cortex in alpha band to vPFC in beta band, and it was negatively correlated with the DVP [22]. In this study, similar areas were identified for the DVP, specifically the MT+ (Fig. 2.5F) and left occipitoparietal cortex (Fig. 2.5B). Similarly, for VVP, the right occipitotemporal cortex (Figs. 2.5A, J & K) and the right temporal cortex (Figs. 2.5E, F& I) were identified. Also, the DVP was negatively correlated with VVP (Figs. 2.5A-B, C-D, & K-L), like that seen in the previous study [22]. However, the posterior parietal cortex (BAs 3, 5&7) was also identified for this network (Figs. 2.5D, H, & L), which was not identified in the previous study. The posterior parietal cortex is a brain region that is also a part of the dorsal visual pathway [32]. This study's identification of this network in both 19-channel and 64-channel EEG analyses show the reproducibility of the eLORETA-ICA method in EEG connectivity analyses.

2.4.3 Sensorimotor Network

IC6 was identified as the "sensorimotor" network in the 64-channel data (see Fig. 2.6). However, this network was not identified in the 19-channel EEG data. Based on the 64-channel analysis, this network was active in four frequency bands. It was characterized by activation in areas of the frontal cortex (BAs 4, 6, 8, 9, &10) in delta band (Fig. 2.6A); activation in frontal cortex (BAs 6 & 8) and medial post central region in theta band (Fig. 2.6B); activation in right

postcentral gyrus (BAs 3&5) in alpha band (Fig. 2.6C); and activation in premotor cortex (BA 6) in gamma band (Fig. 2.6D).

In the previous study, the sensorimotor network was characterized by activation in medial postcentral region in beta band and pre-supplementary motor area (SMA) in gamma band [IC10 in [22]]. Similar regions for the sensorimotor network were also identified in this study. Specifically, the post central region in alpha band was identified (Fig. 2.6C) and pre-SMA in delta, theta, and gamma bands (Figs. 2.6A, 2.6B, 2.6D) in the 64-channel EEG. The primary somatosensory cortex is located on the postcentral gyrus. In addition, the premotor cortex helps in motor planning. Furthermore, the alpha oscillation was identified within this network (Fig. 2.6C). Alpha rhythm is one of the resting state oscillations observed in sensorimotor network [33].

2.4.4 Self-referential Network

IC7 was identified in the 64-channel EEG as "self-referential" network (Fig. 2.7). This network was not identified in the 19-channel EEG data. In the 64-channel EEG, IC7 had activation in posterior cingulate cortex (BA 30) in theta band (Fig. 2.7A); activation in the prefrontal cortex (PFC; BAs 8 & 10) which was negatively correlated with activation in precuneus (BA 31) and posterior cingulate (BA 30) in alpha band (Fig. 2.6B); activation in precuneus/posterior cingulate (BA 31) in beta frequency band (Fig. 2.7C); and activation in right TPJ (BA 39) in gamma band (Fig. 2.7D).

In the previous study, activation in right TPJ and in PFC was also reported [22], but in only alpha and beta frequency bands. The previous study did not report activation in precuneus and posterior cingulate cortex for this network, which this study revealed. The precuneus is a major

hub of the default-mode network and is implicated in several self-referential processes [34]. Furthermore, the posterior cingulate cortex is also involved in self-referential processing [35].

2.4.5 Comparison of Networks Identified by 64- and 19-channel Analyses in this study

Both 64- and 19-channel analyses identified the "visual" network, but this network was active in different frequency bands in both studies. Specifically, the visual network derived from the 64-channel analysis was active in all five frequency bands (IC2; Figure 2.4A-E), while the same network was active in only two bands based on the 19-channel analysis (IC2; Figure 2.4F-G). Mantini et al [30] conducted an EEG-fMRI study of functional brain networks and showed that brain networks could be active in more than one EEG frequency band. This study also found that the visual network had 4 significantly active bands [30], which supports the observations of multiple oscillations within the visual network derived from the 64-channel EEG and 19-channel EEG analysis conducted in this study. Due to the increased number of channels, the 64-channel EEG may have helped or enhanced capture of more information about the temporal characteristics of the visual network compared to the 19-channel data analysis.

In addition, the 64-channel EEG analysis allowed to identify more EEG networks than the 19-channel EEG analysis. Specifically, two more networks were identified in 64-channel EEG, which were the sensorimotor network (Figs. 2.6A-D) and the self-referential network (Figs. 2.7A-D). These networks were not identified in the 19-channel EEG analysis. Studies have shown that an increased number of EEG electrodes leads to more improved EEG source reconstruction [36]. The improved source localization of the 64-channel EEG could therefore have been a factor in identifying these two additional brain networks. Also, multiple frequency bands within these two networks were identified. Mantini's study of these two networks also

identified multiple frequency bands within these two networks [30]. Thus, in addition to identifying other brain networks active within EEG data, the 64-channel EEG measurement and analysis could help identify other neural oscillations that are active within these EEG networks. This added information provides researchers with a better understanding of the brain's organizational structure.

The dual-process of vision perception network was identified in four frequency bands (with three overlapped) in both 19-channel data (IC3; Figure 2.4H-2.4L) and in 64-channel data (IC5; Figure 2.4A-G). The previous study by Aoki et al [22] identified two of the four bands (alpha and beta) that this study identified in this network. The findings of gamma in this network in both 19-channel and 64-channel EEG analyses suggest that the gamma band may also play an active role within this network. It is suggested that an EEG-FMRI study of this network could be performed to properly identify the neural oscillations that are present within this network.

Taken together, this study shows or confirms that multiple neural oscillation frequencies can coexist within brain independent networks and can be detected or identified by multi-channel EEG measurements. Furthermore, this study clearly demonstrates that more EEG channels can help identify other brain networks that are represented in EEG data and improve detection sensitivity to other frequency bands that are active within these networks.

2.4.6 Comparison between Results of current study and Those by Aoki et al. Using 19-channel Analysis

It would be more appropriate to compare results with 19-channel EEG analysis obtained in this study with those by Aoki et al. who utilized only 19 electrodes in their EEG measurements. As

shown in Table 2.1, the previous study identified more EEG networks compared to this study. In addition, more active frequency bands were identified in the two networks that were identified in this study compared to the previous study.

There are several possible reasons for the differences between the two studies. First, the demography of the subjects in both studies was quite different. The subjects in this study were all young adults (mean age = 23.5 ± 2.7 years), while the subjects in the study by Aoki et al. were older with an extremely large range from 18-87 years of age. Studies have shown that brain networks change along aging, which have been documented by previous studies[37] ([38], [39], [40]). Thus, the large difference in subjects' age between the two studies could be an important contribution to the disparity between the oscillation bands of the identified independent networks. In other words, an aging brain may reduce its brain network connections across its oscillation frequencies, resulting in fewer frequency bands observed by the 19-channel EEG measurements. This speculation needs further investigation, possibly using a denser EEG (such as a 10-10 system) device. A second reason could attribute to the lower z- score (z = 2) that was used as a network imaging threshold in this study. A low threshold for the networks could have resulted in larger-area network images with more frequency bands, but with a lower statistical power. Since the sample size here (n=15) was much smaller than the other study (n=80), this study could not select the same threshold as theirs (z=3). Thus, it is possible that some frequency bands with low significance were shown as active in the results of this study, whereas those frequency bands would not be significant under a higher threshold. Last, the small sample size (n=15) in this study may have made it difficult to identify other networks which were identified in Aoki et al.; for example, the dual-process of memory perception network was not

seen using either 19- or 64-channel data analysis. The low sample size of this study could also be responsible for identifying only two networks in the 19-channel EEG data analysis.

2.4.7 Limitations of Study

The eLORETA-ICA study was performed under some limitations. First, the sample size of subjects (n=15) was quite small compared to the previous study (n=80). However, this study was still able to identify four networks in the 64-channel EEG data that were consistent with those reported by Aoki et al. Second, a z score of 2 was utilized as statistical threshold for network images because of limited sample size, which could overestimate independent networks with more frequency bands than the actual ground truth. Third, the age spans of the subjects were quite different between the two studies, which was a confounding factor and made it difficult to directly compare the results of this study with those of the other study. It could also be the reason why the networks observed in the 19-channel data analysis had different frequency characteristics to those obtained in the previous study.

2.5 Conclusion

In this study, a previous investigation by Aoki et. al in ref. [22] was replicated, which utilized an independent networks analysis tool known as eLORETA-ICA to identify EEG resting state networks and their interactions in different frequency bands. Additional variables were included in this replication study, such as an increase in the number of EEG electrodes (from 19 to 64) and the use of a younger group of subjects (mean age = 23.5 years). A limitation of this study was the small sample size (n=15). The analysis identified 4 resting state independent networks that were also identified in the previous study. In addition, the results revealed that each of these resting state networks had electrophysiological activities with more frequency bands than those found in the other study. This difference was discussed and attributed majorly to a large age

difference between the study groups and possibly the small sample size. Overall, this study was in good agreement with the findings by Aoki et al. that multiple neural oscillation frequencies coexist within brain independent networks and can be detected or identified by multi-channel EEG measurements. Furthermore, this study clearly demonstrates that more EEG channels can help identify other active brain networks that are represented in EEG data and improve detection sensitivity to more frequency bands that are active within these networks. Also, this replication study proves that eLORETA-ICA is a valid and reliable methodology for investigating EEG resting state networks

CHAPTER 3

3. Alterations in functional connectivity of EEG brain networks during transition from wakeful to sleep state quantified by graph theory analysis

3.1 Background

Functional connectivity studies the functional relationship between different regions of the brain. Functional connectivity analysis is obtained from time series recordings of brain imaging data and it describes patterns of statistical dependence among neural elements[41]. The study of functional connectivity of the brain helps neuroscientists to identify brain regions that have some functional relationship. These brain regions are known as a brain network. Research has shown that certain brain networks are active during rest, while some others are active when the brain is engaged in an active task [1, 42]. The study of functional connectivity and brain networks is helpful in the early detection of cognitive disorders like Alzheimer's disease [43], schizophrenia [44], and other dementia [2]. Also, the study of brain networks has been performed using different neuroimaging modalities which include functional magnetic resonance imaging or FMRI[45], positron emission tomography or PET[46], functional near-infrared spectroscopy or FNIRS[47], and electroencephalography or EEG[48]. In functional connectivity analyses, functional coupling between different brain regions does not signify a causal relationship between these regions[41]. In a nutshell, functional connectivity analyses give insight into the functional organization and architecture of the brain and enables researchers to observe activity of multiple brain networks at the same time [4]

Brain networks are known to undergo changes in functional connectivity as the brain goes from a wakeful rest state to sleep state. These changes have been studied mainly in fMRI data. For example, a FMRI study found a significant difference in default mode connectivity between

wakeful rest and sleep[5]. Specifically, there was a loss of connectivity between the frontal cortex and the posterior cingulate cortex in sleep [5]. In addition, Monti et al [49] reported a decrease in global information-processing capacity of the brain during a state of anesthesia-induced unconsciousness. Furthermore, Spoormaker et al [6] showed in an FMRI study that frontoparietal connectivity disintegrated in stage 1 of sleep, and was completely absent in deeper sleep stages. In another fMRI study, thalamocortical connectivity was reduced during the transition from wakefulness to light sleep; while corticocortical connectivity was increased, which subsequently disintegrated in deeper sleep[50]. Taken together, these studies show that functional brain networks experience changes in functional connectivity as the brain goes from wakeful consciousness to an unconscious state or sleep.

However, these changes have not been studied directly from neuronal recordings. EEG is a non-invasive brain imaging modality that directly captures neural activity at a very high temporal resolution[8] EEG measurements contain abundant information about frequencies (2-60 Hz) that mediate various cognitive processes [22]. In addition, EEG is portable and easy to use compared to other imaging modalities such as fMRI. Using EEG to study functional connectivity of the brain along different vigilance states will help researchers to better understand the neuronal characteristics of functional brain networks. Furthermore, neuroscientists can better understand how the neuronal characteristics of brain networks are altered in different vigilance states. Also, neuroscientists would be able to better relate the neuronal characteristics of these brain networks to their hemodynamic characteristics. This extends the understanding of the changes in functional connectivity of the brain that occur in different vigilance states.

Graph theory analysis, or GTA, is a mathematical tool that is used for the analysis of complex networks [51]. In neuroscience, GTA is one of the three major methods that is used to investigate

the functional connectivity of the brain.[9]. GTA has been used to study brain networks in fMRI [52], FNIRS [53], and EEG datasets [54]. In GTA, a brain network is characterized as either a graph or a connectivity matrix with nodes and edges [55]. For EEG-GTA analyses, the nodes correspond to EEG electrodes. Also, edges represent the magnitude or strength of the functional coupling between signals from pairs of EEG electrodes. The correlation coefficient has been used to quantify edges in a brain network[56]. Furthermore, graph theory parameters can quantify both functional segregation and functional integration properties of brain networks. Functional segregation refers to the separation of a brain network into different modules or clusters[57]. Two graph parameters that describe functional segregation are global clustering coefficient and nodal clustering coefficient [57]. Functional integration, on the other hand, refers to the interaction of several brain regions for information transfer[57]. Also, two graph theory metrics that quantify functional integration are global efficiency and nodal efficiency [57]. Graph theory analyses utilize different network thresholds to give a comprehensive picture of brain connectivity. In short, graph theory analyses provide a quantitative analysis of brain connectivity. Also, graph theory analyses can measure both global and local metrics of brain connectivity. Finally, graph theory parameters provide physiological interpretation of the characteristics of brain networks.

In this study, GTA was used to analyze brain networks in EEG data during the transition from wakeful rest to sleep state. Resting-state EEG data was acquired from eighteen subjects (mean age = 23.5 years; standard deviation = 2.7) in both eyes-open state (EO) and eyes-closed state (EC). Furthermore, sleep scoring of the eyes-closed EEG data was performed to separate the data into both sleep stage 1 (SS1) data and sleep stage 2 (SS2) data for each subject according to the American Association of Sleep Medicine (AASM) standard [94]. Then, the EEG data was

processed in each of the different vigilance states and transformed into power in four different EEG frequency bands (delta, theta, alpha, and beta) for each state. Then, using graph theory analysis (GTA) and statistical analyses, the changes in EEG functional brain networks across different vigilance states for different frequency bands were analyzed and observed.

3.2 Methods

3.2.1 Subjects

18 young subjects (fifteen males and three females) with a mean age of 23.5 years (standard deviation = 2.5 years) were recruited for this study. These subjects were chosen from the student population of University of Texas at Arlington. The inclusion criteria were as follows: either sex (male or female), and in an age range of 18 – 29 years old. The exclusion criteria were as follows: (1) diagnosed with a psychiatric or sleeping disorder, (2) history of a neurological condition, or severe brain injury, or violent behavior, (3) have ever been institutionalized/imprisoned, (4) current intake of any medicine or drug, or (5) currently pregnant. In addition, none of the participants were smokers or had diabetes. The study protocol was approved by the institutional review board (IRB) at The University of Texas at Arlington and complied with all applicable federal and NIH guidelines. Informed consent was obtained from each participant prior to the experiments.

3.2.2 Simultaneous EEG-fNIRS Instrumentation

Resting-state brain activity was acquired using a dual-modality instrumentation set up. Specifically, the data were collected using both a 64-channel EEG instrument (Biosemi, Netherlands) and a 133-channel fNIRS instrument (Shimadzu corporation, Japan). Furthermore, a dual-modality cap (Shimadzu corporation, Japan) was used to acquire both EEG and fNIRS measurements from each subject. The dual-modality cap positioned the 133 fNIRS channels

according to a standard whole-head layout which was already designed in the Shimadzu fNIRS machine. In addition, the 64 EEG electrodes were inserted into cap holes that covered specific FNIRS channels. The FNIRS machine uses three wavelengths of 780nm, 805nm, and 830nm to calculate oxy-, deoxy-, and total hemoglobin concentrations at each channel location. Furthermore, the sampling rate for the EEG data acquisition was 1 kHz, while the sampling rate for the fNIRS data acquisition was 8Hz. In addition, the simultaneous EEG-FNIRS acquisition was controlled by a desktop computer which was connected to both the EEG instrument and fNIRS instrument via a USB port. Figure 3.1 shows the instrumentation setup which was used for this study.

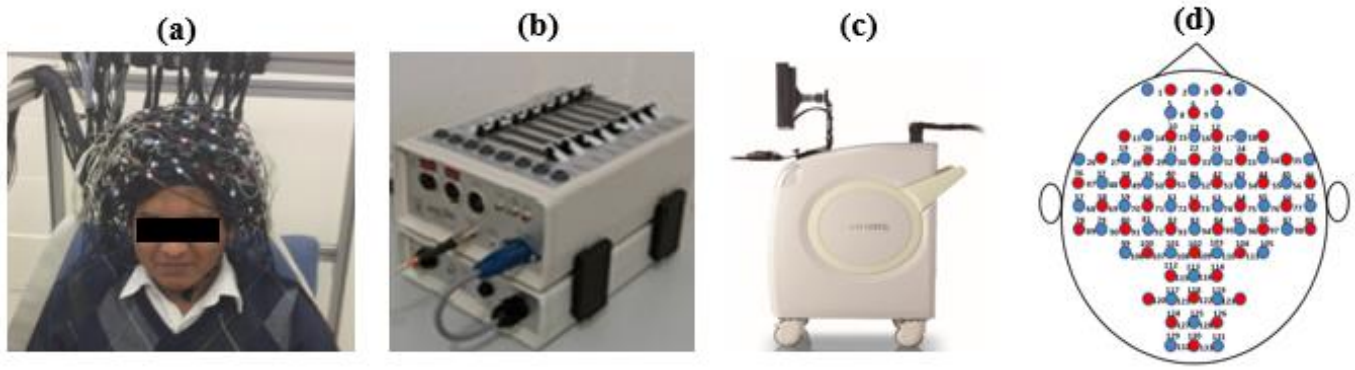

Figure 3.1: Instrumentation setup used for functional connectivity study. The simultaneous EEG-FNIRS acquisition was carried out on a subject using a dual-modality (10-10) head cap worn on the subject's head as shown in (a). The simultaneous EEG-FNIRS acquisition was performed using (b) 64-channel EEG instrument and (c) 133-channel FNIRS measurement. The 133 channels of FNIRS were positioned according to the channel layout shown in (d). Red circles in the channel layout correspond to FNIRS sources (40 sources), while blue circles correspond to FNIRS detectors (40 detectors).

3.2.3 Experiment and Protocol

Each subject was seated in a comfortable chair for the whole duration of the experiment. Simultaneous EEG-fNIRS acquisition of resting-state brain activity was performed in two

separate stages. In the first stage of data acquisition, each subject was asked to keep his or her eyes open for five minutes. Then, resting-state brain activity of each subject under this condition was acquired. In the second stage, each subject was asked to close his or her eyes and fall asleep for ten minutes. Then, resting-state brain activity of each subject under this condition was also acquired. In addition, the measurements were conducted in a well-ventilated room with minimal noise. Also, phones and other electromagnetic devices were not allowed in the lab or on the person of the subject during the whole duration of the experiment. In addition, each subject was positioned away from electrical sources to prevent contamination of the data by 60 Hz power line noise.

3.2.4 EEG Data preprocessing

Data preprocessing of EEG data in both eyes-open and eyes-closed resting states was performed using the EEGLAB toolbox. EEGLAB is a well-known electrophysiological toolbox that has been developed for EEG data analysis [26]. Firstly, all the EEG datasets were imported into the EEGLAB toolbox which was installed in MATLAB 2016 software. Next, the EEG data for each subject was down-sampled to 256Hz. Next, a FIR bandpass filter with a frequency range of 1 – 80 Hz was applied to each EEG dataset to remove unwanted signals. Furthermore, each subject's EEG data channel locations was set to match standard MNI coordinates in EEGLAB. Then, the EEG time series signal at each EEG electrode was inspected for extremely large amplitudes and electromyographic (EMG) artifacts. Such electrodes were corrected using spherical interpolation method which was implemented using the EEGLAB toolbox. After channel interpolation, the EEG data for each subject was re-referenced to an average reference. Furthermore, power line noise in the data was removed using the Clean line algorithm in EEGLAB, with the parameters set to default values. Finally, an Independent Component Analysis (ICA) algorithm was applied

to the EEG data for each subject to remove eye movement artifacts, muscle noise, and eye blink artifacts. This algorithm was also implemented in the EEGLAB toolbox using the command "runica".

3.2.5 Sleep scoring of eyes-closed EEG data

For each of the EEG datasets in the eyes-closed (EC) state, they were further examined for sleep stages with the help of a qualified medical doctor. Specifically, the whole ten-minute resting-state eyes-closed EEG data for each subject was first segmented into separate thirty-second (30 s) epochs. Then, with the help of the doctor, each thirty-second (30 s) epoch was assigned to either stage 0 (eyes-closed and awake, or EC), stage 1 (sleep stage 1 or SS1), or stage 2 (sleep stage 2 or SS2). into either eyes-closed (EC), sleep-stage 1 (SS1), or sleep-stage 2 (SS2) data. This step was performed in accordance with the American Association of Sleep Medicine (AASM) guidelines for sleep scoring. After sleep scoring, each subject's resting-state eyes-closed EEG dataset was separated into both sleeping-stage 1 EEG dataset and sleeping-stage 2 EEG dataset, in preparation for functional connectivity analysis. Table 3.1 shows the total duration (in minutes) of each subject's EEG dataset in the eyes-opened state (EO), eyes-closed state (EC), sleeping-stage 1 (SS1), and sleeping-stage 2 (SS2). In addition, Figure 3.2 shows the flowchart for EEG data preprocessing of all EEG datasets in Table 3.1.

Table 3.1: The table shows the total duration (in minutes) of eyes-opened (EO), eyes-closed (EC), sleep-stage 1 (SS1), and sleep-stage 2 (SS2) EEG datasets for each of the eighteen subjects that were recruited for functional connectivity study.

Subject	1	2	3	4	5	6	7	8	9	10	11	12	13	14	15	16	17	18
EO	5	5	5	5	5	5	5	5	5	5	5	5	5	5	5	5	5	5
EC	10	9.5	8.5	10	5	10	5.5	1.5	1	9.5	2	5.5	0	3	0.5	10	10	0.5
SS1	0	0.5	1.5	0	5	0	4.5	4.5	4	0.5	3	4.5	3	1.5	2.5	0	0	1.5
SS2	0	0	0	0	0	0	0	4	5	0	5	0	7	5.5	7	0	0	8

.

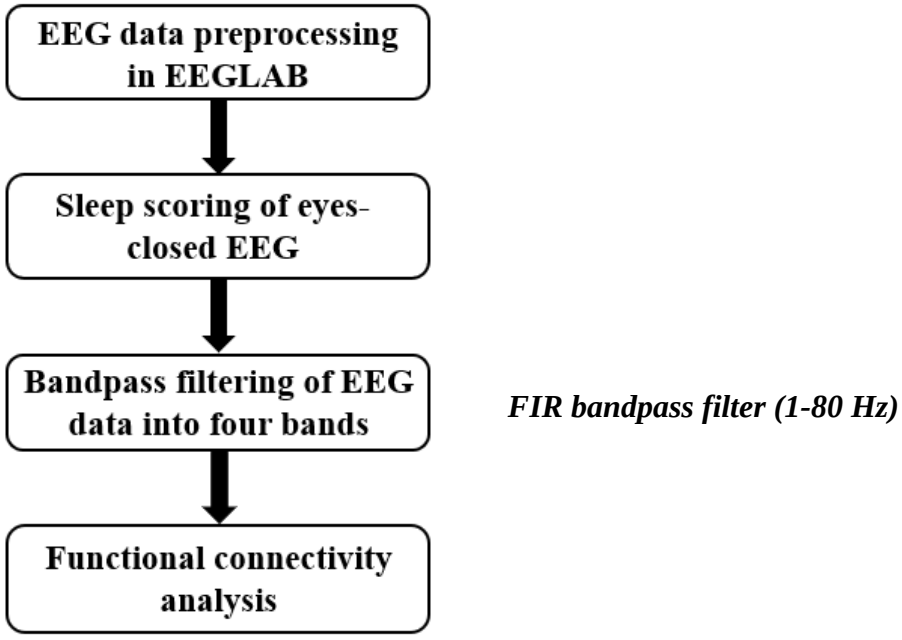

Figure 3.2: Flowchart of EEG data processing for functional connectivity study. A bandpass filter of range 1 – 80 Hz was used to filter the EEG signal into four separate EEG bands of delta, theta, alpha, and beta.

3.2.6 Functional connectivity analysis of EEG data in different vigilance states

Firstly, bandpass filtering into separate EEG frequency bands was performed for each subject. Specifically, each subject's EEG dataset in each vigilance state was sectioned into four separate EEG frequency bands which were delta band (1-4Hz); theta band (4-8Hz); alpha band (8-12Hz); and beta band (13-30Hz). Furthermore, the bandpass filtering was performed using the FIR filter in EEGLAB. Next, each subject's EEG dataset in a specific frequency band was transformed into a 64-channel power dataset using the Hilbert transform. This procedure was done for each vigilance state. The Hilbert transform is a well-known method used for calculating the power of EEG signals[58, 59]. Then, for each frequency band, each subject's 64-channel time series of power data was then converted into a 64-by-64 power connectivity matrix. To get this connectivity matrix, the Spearman correlation coefficient for each possible pair of electrodes was calculated. This step was done for all the 64 EEG electrodes. This step yielded a 64-by-64 matrix of correlation coefficients. Again, this procedure was performed separately for each vigilance state. The Spearman correlation coefficient is more suitable for calculating the correlation of power time series data [58]. Figure 3.3 shows the steps in performing functional connectivity analysis of all the EEG datasets in Table 1

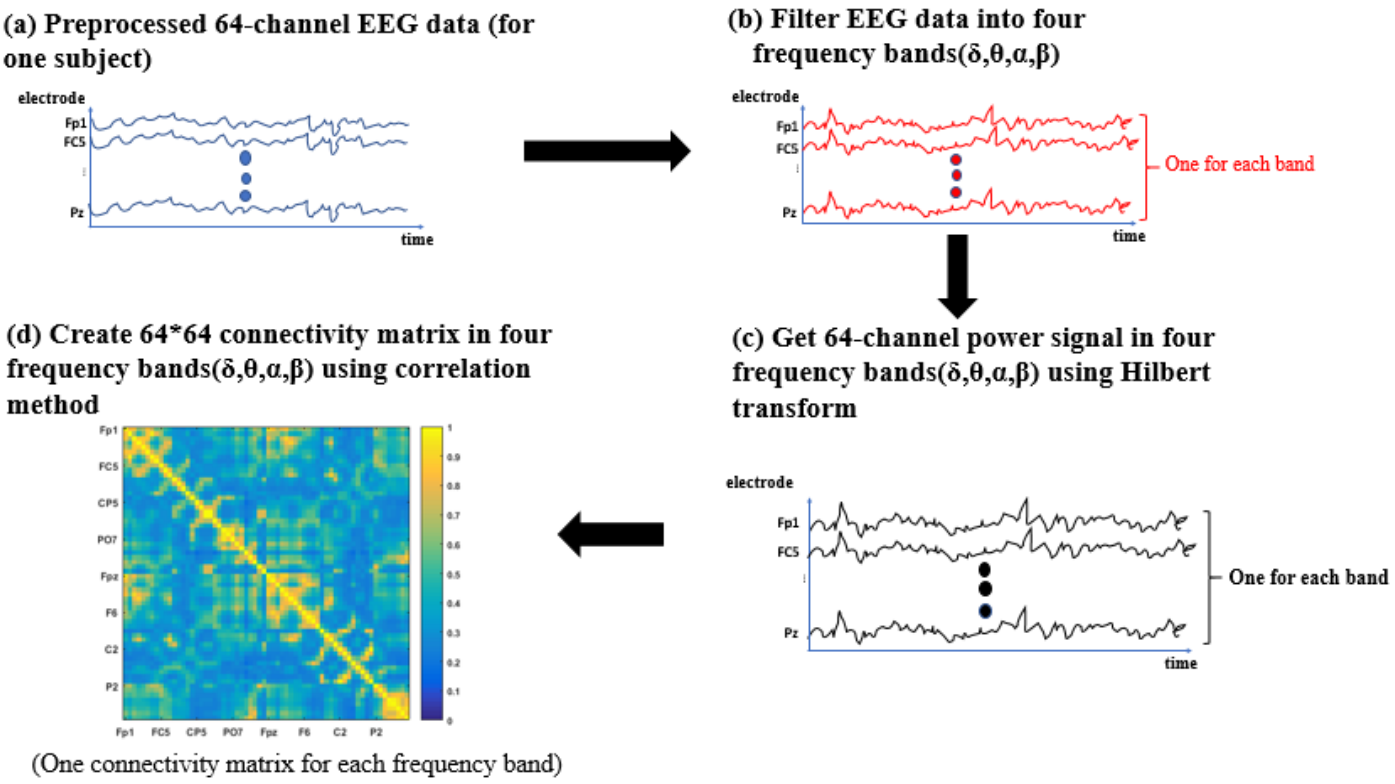

Figure 3.3: Functional connectivity analysis of all EEG data for each subject in Table 1. The preprocessed 64-channel EEG data in (a) was filtered into four separate bands which were delta (δ), theta (θ), alpha(α), and beta(β). Then, each of the frequency-band time series data in (b) was converted to 64-channel power signal in each frequency band, using Hilbert transform. Then, the power series for each frequency band in (c) was transformed into a 64*64 connectivity matrix in each frequency band, shown in (d). The rows and columns of the connectivity matrix represent the 64 EEG electrodes, while the colored pixels in the matrix represent the calculated Spearman correlation coefficient between the power signal from one EEG electrode and power signal from another EEG electrode. The correlation approach was performed between all possible pairs of EEG electrodes, and for each vigilance state.

3.2.7 Graph theory analysis (GTA)

To perform graph theory analyses, a graph theory analysis software known as GRETNA was used [60]. GRETNA is a freely downloadable tool that is used for imaging network connectomics in fMRI, fNIRS, and EEG data [60]. For each frequency band, all the 64*64 power connectivity matrices for each subject were fed into GRETNA to calculate graph theory

parameters. This procedure was performed separately for power connectivity matrices in each vigilance state. In the Network Analysis module of GRETNA, network metrics were set as follows: **Network Type:** binary**; Network Member:** absolute**; Threshold Type:** sparsity**; Threshold Range:** 0.1:0.01:0.9**; Random Networks:** 100**; Selected Mode:** Network-Small World**,** Network-Efficiency**.** Then, the GRETNA graph theory algorithms were run on these matrices to calculate both global and local network metrics of brain connectivity in each vigilance state, for all frequency bands.

3.2.8 Statistical analysis of both global and local network metrics

Statistical analysis was performed for both global and local network metrics as follows: four graph theory metrics were calculated, which were the global clustering coefficient, global efficiency, nodal clustering coefficient and nodal efficiency. The global clustering coefficient and global efficiency represent global network metrics, while the nodal clustering coefficient and the nodal efficiency represent local network metrics. For global network metrics, the clustering coefficient and global efficiency values at each threshold were first averaged across all subjects. This was done in each vigilance state and for each frequency band. Then, a repeated ANOVA test using Greenhouse-Geiser correction ($p < 0.05$) was calculated on both mean clustering coefficient and mean global efficiency values across all vigilance states. Specifically, the ANOVA test was performed for values of clustering coefficient and global efficiency at each of nine separate network thresholds from 0.1 to 0.9 in increments of 0.1. This step was performed for each frequency band.

For the local network metrics, the values of both nodal clustering coefficient and nodal efficiency at each EEG electrode in each of four separate network thresholds of 0.1, 0.3, 0.5, and 0.7 were extracted for each subject, in each vigilance state. Then, a repeated ANOVA test using

Greenhouse-Geiser correction ($p < 0.05$) was performed on values of nodal clustering coefficient and nodal efficiency at each of 64 electrodes across all vigilance states. This step was performed for each threshold of 0.1, 0.3, 0.5, and 0.7 respectively, and for each frequency band. After ANOVA test, a post-hoc test using the Tukey-Kramer method was performed for electrodes that showed a significant p-value from ANOVA. For the posthoc tests, only three pairwise comparisons were considered for statistical evaluation: eyes-open and eyes-closed (EO-EC); eyes-closed and sleep-stage 1 (EC-SS1); and, sleep-stage 1 and sleep-stage 2 (SS1-SS2). If there were any significant pairwise comparisons at a specific electrode as revealed by Tukey posthoc test, we reported the t-value for the electrode. Then, the t-values were then plotted on a two-dimensional topographic map for each of the pairwise comparisons considered. This step was performed at each threshold of 0.1, 0.3, 0.5, and 0.7 respectively. Furthermore, this step was performed for each frequency band. All statistical tests were performed using MATLAB 2016 software.

3.3 Results

3.3.1 Clustering coefficient in four frequency bands

The mean clustering coefficient in each vigilance state increased as the network threshold increased from 0.1 to 0.9, for all frequency bands (Figure 3.4). Also, the mean clustering coefficient were higher for wakeful states (both eyes-opened and eyes-closed) than sleep states (both sleep-stage 1 and sleep-stage 2), for all frequency bands (Figure 3.4). In delta band, the mean clustering coefficient in the eyes-opened vigilance state (EO) was the highest among all vigilance states for thresholds from 0.3 to 0.6 (Figure 3.4a). Also, the mean clustering coefficient in delta band was lowest in sleep-stage 2 vigilance state (SS2) for thresholds from 0.3 to 0.6 (Figure 3.4a). In addition, ANOVA test reported a significant difference ($p < 0.05$) in mean

clustering coefficient in delta band across all vigilance states only at a threshold of 0.4 (Figure 3.4a). In theta band, the mean clustering coefficient in the eyes-opened vigilance state (EO) was the highest among all vigilance states for thresholds from 0.3 to 0.5 (Figure 3.4b). Also, the mean clustering coefficient in the eyes-closed vigilance state (EC) was the highest among vigilance states for thresholds of 0.1 and 0.6 for theta band (Figure 3.4b). The mean clustering coefficient in SS2 vigilance state for theta band was the lowest among vigilance states for thresholds from 0.1 to 0.6 in increments of 0.1 (Figure 3.4b). ANOVA test reported a significant difference ($p < 0.05$) in mean clustering coefficient in theta band across all vigilance states at thresholds of 0.3 and 0.5 only (Figure 3.4b). In the alpha band, the mean clustering coefficient in eyes-closed vigilance state (EC) was the highest among vigilance states from thresholds of 0.3 to 0.8 (Figure 3.4c). Also, the mean clustering coefficient in sleep-stage 2 (SS2) for the alpha band was the lowest among vigilance states from thresholds of 0.3 to 0.9 (Figure 3.4c). In addition, ANOVA test reported a significant difference ($p < 0.05$) in mean clustering coefficient in alpha band across all vigilance states for threshold of 0.1, and thresholds from 0.3 to 0.9, in increments of 0.1 (Figure 3.4c). Finally, in beta band, the mean clustering coefficient in eyes-closed vigilance state (EC) was highest among vigilance states from thresholds of 0.3 to 0.7 (Figure 3.4d). Also, the mean clustering coefficient in sleep-stage 2 (SS2) was lowest for thresholds from 0.3 to 0.7 (Figure 3.4d). In addition, ANOVA test reported a significant difference ($p < 0.05$) in mean clustering coefficient in beta band across all vigilance states for threshold of 0.1, and thresholds from 0.3 to 0.6, in increments of 0.1 (Figure 3.4d).

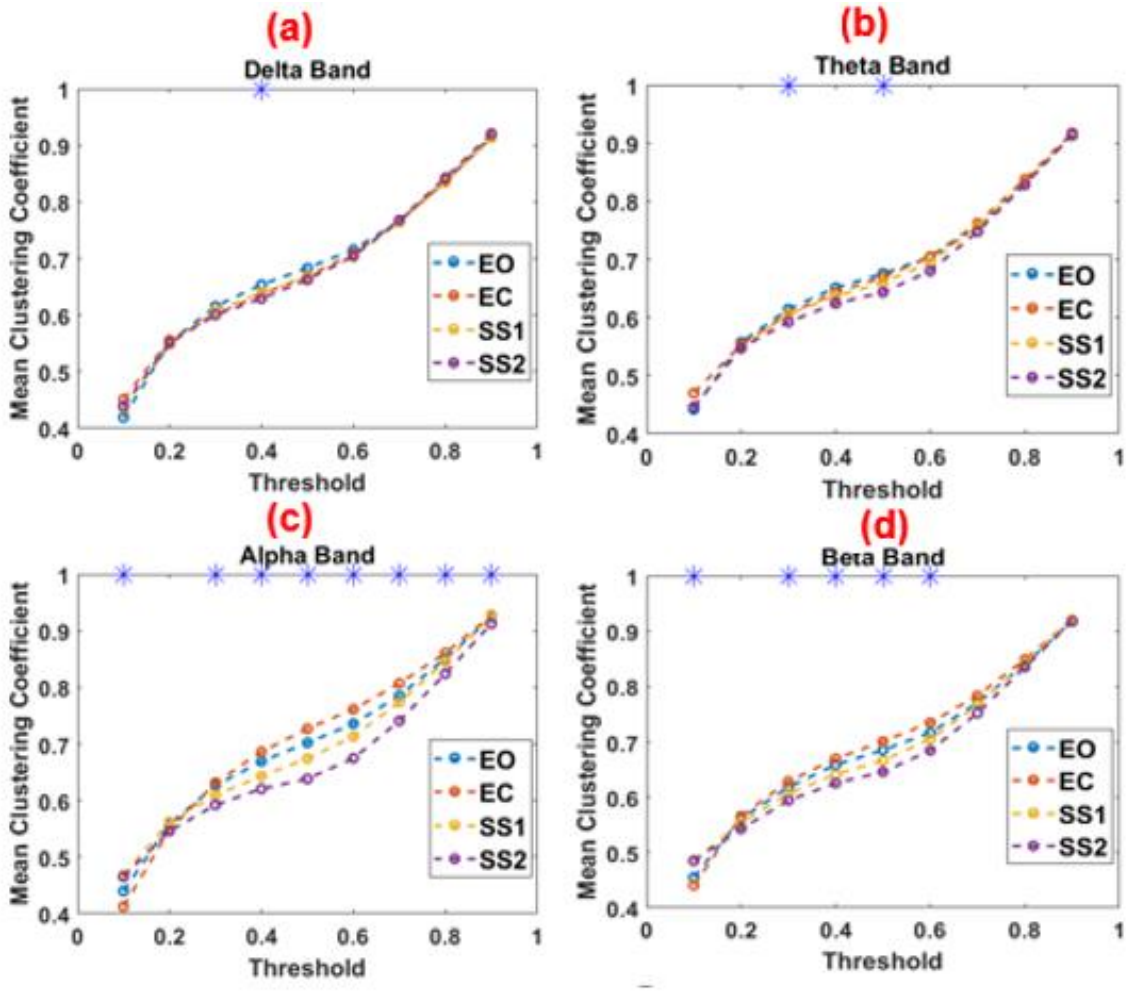

Figure 3.4: The mean clustering coefficient for each of eyes-open (EO), eyes-closed (EC), sleep-stage 1 (SS1), and sleep-stage 2 (SS2) in (a) delta, (b) theta, (c) alpha, and (d) beta bands. Blue crosses marked '*' on the plots indicate significant difference ($p < 0.05$) in mean clustering coefficient across the four vigilance states as revealed by repeated ANOVA test with Greenhouse-Geiser correction.

3.3.2 Global efficiency in four frequency bands

The mean global efficiency in each vigilance state increased as the network threshold increased from 0.1 to 0.9 in increments of 0.1, for all frequency bands (Figure 3.5). Also, the mean global efficiency values showed an increase from a wakeful state to sleep state in all bands (Figure 3.5). In delta band, ANOVA test reported a significant difference ($p < 0.05$) in mean global efficiency

across all vigilance states at thresholds of 0.1 and 0.2 (Figure 3.5a). In theta band, ANOVA test reported a significant difference ($p < 0.05$) in mean global efficiency across all vigilance states at the threshold of 0.3 only (Figure 3.5b). In alpha band, the mean global efficiency in sleep-stage 2 (SS2) vigilance state was the highest among vigilance states from thresholds of 0.1 to 0.4 (Figure 3.5c). Also, the mean global efficiency in eyes-closed vigilance state (EC) was the lowest among vigilance states from thresholds of 0.1 to 0.4 (Figure 3.5c) In addition, ANOVA test reported a significant difference ($p < 0.05$) in mean global efficiency in alpha band across all vigilance states for thresholds of 0.1 to 0.4 (Figure 3.5c). Finally, in beta band, the mean global efficiency in SS2 vigilance state was highest among vigilance states from thresholds of 0.1 to 0.3 (Figure 3.5d). Also, the mean global efficiency in EC vigilance state was lowest for thresholds from 0.1 to 0.3 (Figure 3.5d). In addition, ANOVA test reported a significant difference ($p < 0.05$) in mean global efficiency in beta band across all vigilance states for thresholds of 0.1 and 0.2 (Figure 3.5d).

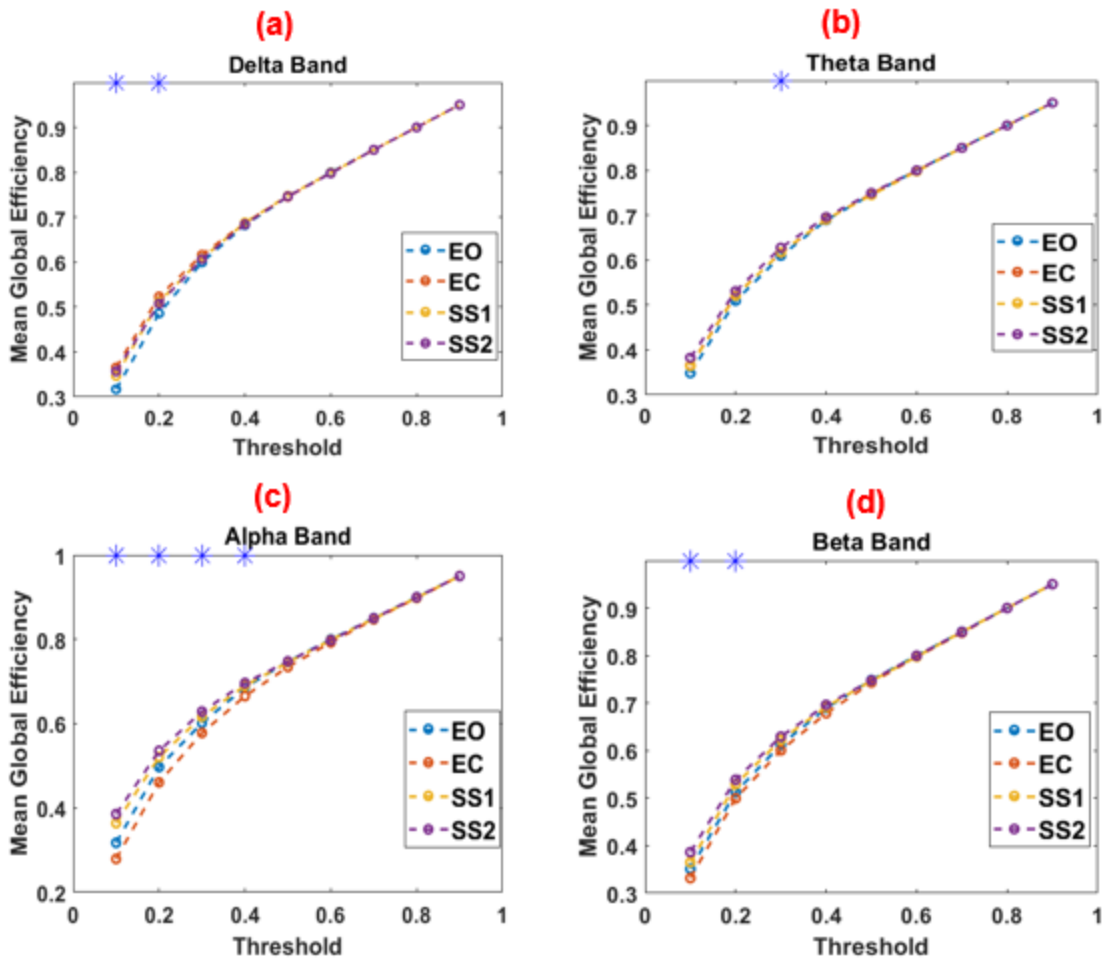

Figure 3.5: The mean global efficiency for each of eyes-open (EO), eyes-closed (EC), sleep-stage 1 (SS1), and sleep-stage 2 (SS2) in (a) delta, (b) theta, (c) alpha, and (d) beta bands. Blue crosses marked '*' on the plots indicate significant difference ($p < 0.05$) in mean global efficiency across the four vigilance states as revealed by repeated ANOVA test with Greenhouse-Geiser correction.

3.3.3 Nodal clustering coefficient in alpha and beta bands

Significant differences in nodal clustering coefficient were reported for both alpha and beta bands (Figure 3.6). In alpha band, significant differences in nodal clustering coefficient were reported in the transition from eyes-opened state to eyes-closed state (EO-EC), and in the transition from eyes-closed state to sleep-stage 1 (Figure 3.6a). Also, no significant differences in

the transition from sleep-stage 1 to sleep-stage 2 (SS1-SS2) were reported for alpha band (Figure 3.6a). The significant differences in nodal clustering coefficient were situated at frontal locations for thresholds of 0.1, 0.3, 0.5, and 0.7 in both EO-EC and EC-SS1 transitions; and parietal locations for thresholds of 0.5 and 0.7 in EC-SS1 (Figure 3.6a). In beta band, significant differences in the nodal clustering coefficient were reported only in the transition from eyes-closed state to sleep-stage 1 (Figure 3.6b). For beta band, the significant differences in nodal clustering coefficient were located at frontal sites for thresholds of 0.1, 0.3, 0.5, and 0.7; and parietal sites for only the threshold of 0.5 (Figure 3.6b).

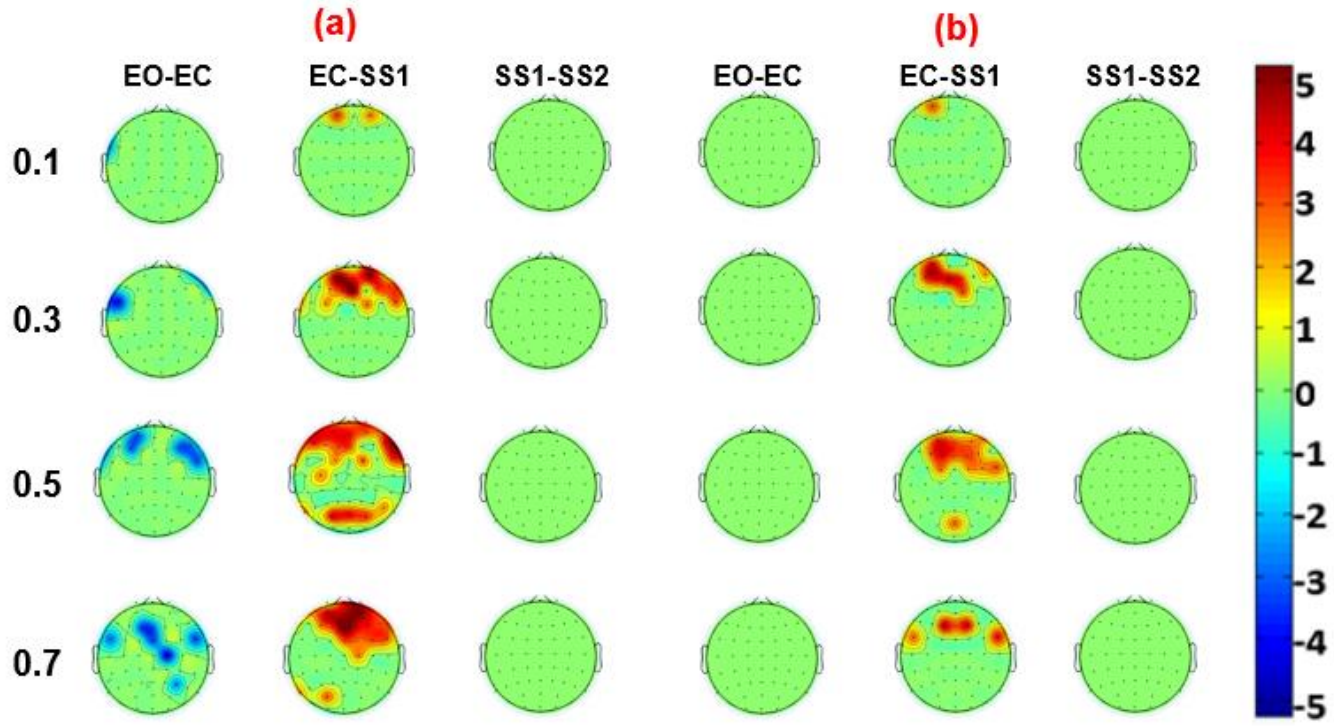

Figure 3.6: EEG topographical plots showing nodal clustering coefficient changes in eyes-opened to eyes-closed transition (EO - EC); eyes-closed to sleep-stage 1 transition (EC – SS1); and sleep-stage 1 to sleep-stage 2 transition (SS1 – SS2) in (a) alpha band and (b) beta band. The color bars represent significant t-values (uncorrected, $p < 0.05$). The EEG topographical maps were constructed using EEGLAB software.

3.3.4 Nodal efficiency in alpha and beta bands

Significant differences in nodal efficiency were reported for both alpha and beta bands (Figure 7). In alpha band, significant differences in the nodal efficiency were reported in the transition from eyes-opened state to eyes-closed state (EO-EC), and in the transition from eyes-closed state to sleep-stage 1 (Figure 3.7a). No significant differences were reported in the transition from sleep-stage 1 to sleep-stage 2 (Figure 3.7a). The significant differences in nodal efficiency were situated at temporoparietal locations for thresholds of 0.1, 0.3, 0.5, and 0.7 in both EO-EC and EC-SS1 transitions (Figure 3.7a). In beta band, significant differences in the nodal efficiency were reported in the transition from eyes-open state to eyes-closed state (EO-EC), and in the transition from eyes-closed state to sleep-stage 1 (Figure 3.7b). These significant differences were located at temporoparietal sites for thresholds of 0.1, 0.3, 0.5, and 0.7 in EO-EC transition, and in temporoparietal sites for thresholds of 0.1, 0.3, and 0.5 in EC-SS1 transition (Figure 3.7b). Also, no significant differences were reported in the transition from sleep-stage 1 to sleep-stage 2 (SS1-SS2) for beta band (Figure 3.7b).

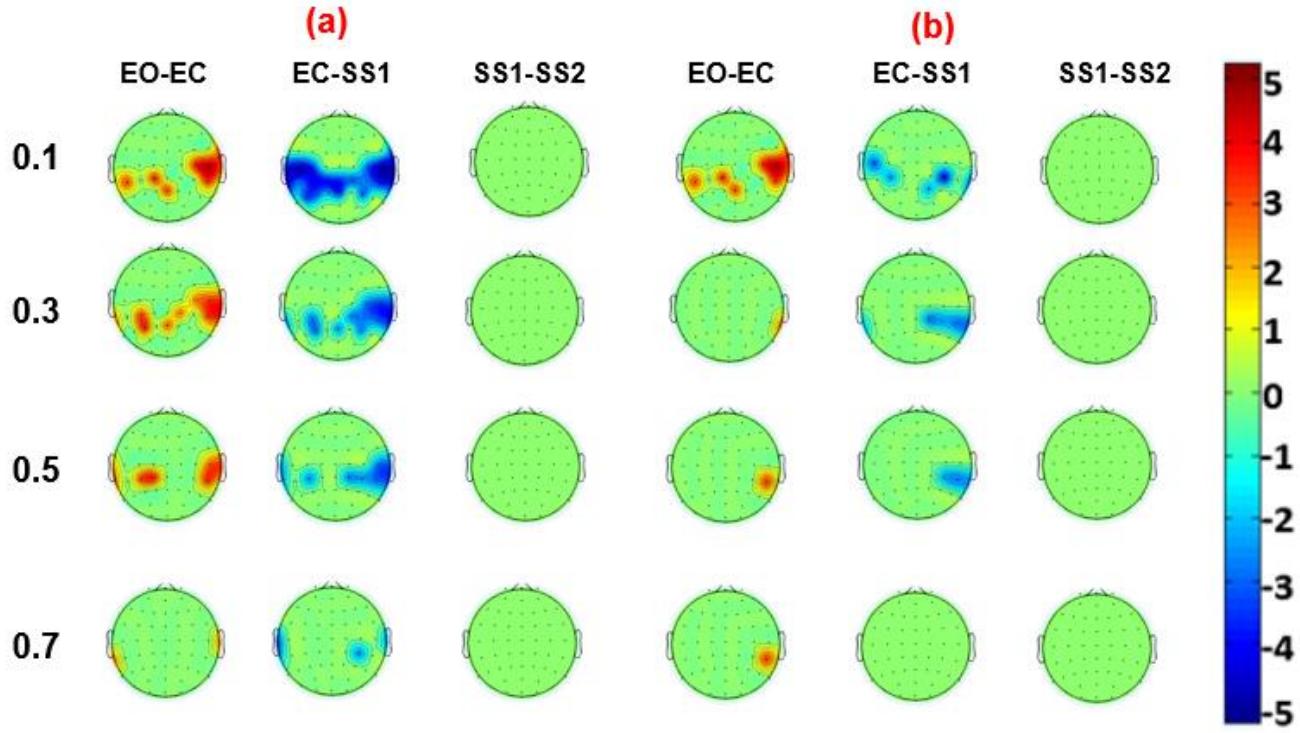

Figure 3.7: EEG topographical plots showing nodal global efficiency changes in eyes-opened to eyes-closed transition (EO - EC); eyes-closed to sleep-stage 1 transition (EC – SS1); and sleep-stage 1 to sleep-stage 2 transition (SS1 – SS2) in (a) alpha band and (b) beta band. The color bars represent significant t-values (uncorrected, $p < 0.05$). The EEG topographical maps were constructed using EEGLAB software.

3.4 Discussion

In this chapter, I investigated EEG functional connectivity in four separate vigilance states from wakefulness to sleep using graph theory analysis. Metrics of both functional segregation (which were global clustering coefficient and nodal clustering coefficient) and functional integration (which were global efficiency and nodal efficiency) were compared across vigilance states in four EEG frequency bands of delta, theta, alpha, and beta, by using appropriate statistical analyses.

3.4.1 Changes in clustering coefficient across vigilance states

Firstly, the study reported higher values of the global clustering coefficient of EEG brain network in wakeful states of both eyes-open and eyes-closed, compared to sleep states of both sleep-stage 1 and sleep-stage 2, for all frequency bands (Figure 3.4). This occurred predominantly/very significantly in both alpha and beta bands (Figures 3.4c&d). In addition, frontal nodes mostly showed significant differences ($p < 0.05$, uncorrected) in nodal clustering coefficient across vigilance states (Figure 3.6). This finding was also reported also in both alpha and beta bands (Figures 3.6a&b). Taken together, the results indicate that frontal EEG brain network becomes more clustered or segregated as the brain transitions from eyes-open state to eyes-closed state, and this clustering disintegrates during sleep state. This finding could represent the activity of the well-known default mode network (DMN) of the brain across different vigilance states. The default-mode network is preferentially activated when the brain is in eyes-closed state [34]. In addition, the DMN is composed of two major subsystems, which are the anterior subsystem and the posterior subsystem [62]. Parts of the anterior subsystem of DMN include the prefrontal cortex and superior frontal gyrus, which are located within the frontal lobe of the brain [62]. In a previous study, Ward et al [90] has linked daytime sleepiness to reduced functional connectivity of the DMN in both young and elderly subjects. In addition, Horovitz et al's study [5] has reported a reduction in frontal DMN connectivity during sleep. These studies corroborate our findings of reduced clustering/connectivity during sleep. A previous study has also linked alpha rhythm activity with default mode network in the brain [95]. This finding also agrees with the results of significant alpha activity within DMN observed here. Together, the results here suggest that the anterior subsystem of the DMN is significantly altered in clustering connectivity during the brain's transition from wakeful state to sleep state in the brain.

3.4.2 Changes in global efficiency across vigilance states

Secondly, this study reported higher values of global efficiency in sleep states of both sleep-stage 1 and sleep-stage 2, compared to wakeful states of both eyes-open and eyes-closed, in all frequency bands (Figure 3.5). This finding was quite prominent in alpha and beta bands (Figures 3.5c&d). In addition, the study also reported significant changes ($p < 0.05$, uncorrected) in nodal efficiency for temporo-parietal nodes of the brain (Figure 3.7). This finding was also reported for both alpha and beta bands (Figures 3.7a&b). In other words, the results here indicate that the efficiency of posterior EEG brain network is reduced as the brain goes into an eyes-closed state, and it is increased when the brain proceeds to the sleep state. In the DMN, there is a posterior subsystem. Parts of the posterior subsystem include the temporoparietal junction and the parietal lobule [62]. A FMRI study has shown changes in nodal efficiency during stage 1 sleep in nodes of the posterior DMN [93]. Therefore, the results here indicate/suggest that the posterior subsystem of the DMN is significantly altered in functional connectivity of integration during the brain's transition from a state of wakeful rest to sleep. However, a discrepancy between results of nodal efficiency in this study and that of the previous FMRI study is that while the FMRI study reported a significant decrease in nodal efficiency during sleep-stage 1, the current study of EEG reported an increase in nodal efficiency in stage 1 sleep (Figure 3.7a). This discrepancy could be because the t-values reported for nodal efficiency in this study were not corrected for multiple comparisons; hence they could be prone to statistical error of false positives.

Overall, the results of this study suggest that the functional connectivity of the DMN plays an important role in determining the state of consciousness within the brain. According to Guldenmund et al [61], it is expected that the network integrity of the DMN is significantly affected during an altered state of consciousness like sleep or anesthesia. This notion is observed

in the current study. Furthermore, other studies have shown that the connectivity of the default-mode network is altered along different states of consciousness [91,92]. Therefore, this study extends our understanding of the changes in functional connectivity of the DMN during different states of consciousness.

3.4.3 Limitations

The limitations of the current study were as follows: Firstly, the statistical analyses of the nodal metrics of functional connectivity (nodal clustering coefficient and nodal efficiency) did not correct for multiple comparisons. Hence, the t-values reported for the analyses of nodal metrics are prone to statistical error. Secondly, it is possible that a generalized statistical model may be more appropriate for the statistical analysis of EEG data for the different frequency bands. Also, it is unclear whether the short thirty-second epoch of sleep-stage 1 is enough to perform functional connectivity analysis in. sleep state, although thirty second epoch is sufficient to identify sleep stages according to the AASM standard [94]. Lastly, the results could be affected by volume conduction, due to use of correlation coefficient. However, the Spearman correlation coefficient gives a less biased estimate of EEG connectivity [58]

3.5 Conclusion

In this study, EEG instrument was used to quantify changes in functional connectivity of brain network across vigilance states of wakefulness and sleep. This study shows that the EEG modality can be used along with other imaging modalities to explain the changes in functional architecture and organization of the brain during different states of consciousness. This study will prove helpful to explain disorders of consciousness from a functional connectivity perspective. Furthermore, the study was able to show that the default mode network is greatly involved in consciousness processes of the brain, which agrees with previous studies.

CHAPTER 4

4. Wavelet coherence analysis of neurovascular coupling during transition from wakeful to sleep states

4.1 Background

Neurovascular coupling in the brain refers to the tight coupling between neuronal fluctuations and the corresponding hemodynamic response in the brain [66]. The brain requires a continuous supply of blood to provide energy for its many activities; this continuous supply of blood to the brain is induced by coupling between neuronal activity, cerebral blood flow, and metabolism [67]. According to previous studies, neurovascular coupling is necessary to maintain the cerebral autoregulation in the brain [68]. Also, the impairment of neurovascular coupling in the brain has been linked to some diseases such as ischemic stroke, hypertension, and Alzheimer's disease[11]. In addition, neurovascular coupling may also be impaired in small vessel disease [12].

The exact mechanism of neurovascular coupling in the brain is still an ongoing study in the neuroimaging literature. A study has shown that that neurovascular coupling in awake animals occurs differently when compared to neurovascular coupling in anaesthetized animals [69]. Also, Willie et al have shown that neurovascular coupling in humans remained unaltered during exercise, even though there was an increase in cerebral blood velocity in both the posterior and middle cerebral arteries [70]. Furthermore, an fMRI study of neurovascular coupling in rats showed that it is brain region-dependent; whereas local field potentials in the cortex showed a linear positive relationship with BOLD signals, local field potentials in the brain stem and thalamus showed a different relationship with BOLD signals [15]. In addition, Zanatta et al have proposed a subcortical pacemaker in the brain that drives synchronized neurovascular coupling

[71]. Furthermore, different studies have shown that the gamma-band activity is tightly coupled with hemodynamic signals in both non-pathological brain states [72, 73] and pathological brain states [74] .

Neurovascular coupling in the brain is controlled by several processes. Some of these processes include endogenic, neurogenic, and myogenic processes [66]. The endogenic processes refer to the processes of neurovascular coupling that take place in endothelial cells surrounding the brain. Also, the neurogenic processes take place in the nerves of the brain, while the myogenic processes occur due to contractions of the smooth muscle cells and fibers in the brain. According to an fNIRS study, the endogenic component of neurovascular coupling in fNIRS signals occurs within a frequency range of 0.003-0.02 Hz [75]. Also, the neurogenic component of neurovascular coupling in FNIRS signals occurs within a frequency range of 0.02-0.04 Hz [75], and the myogenic component of neurovascular coupling in FNIRS signals occurs within a frequency range of 0.04-0.15 Hz [75].

Wavelet coherence analysis is a recently developed method that has been used to quantitatively investigate neurovascular coupling [76]. It provides a time-frequency quantitative analysis of the tight coupling between neuronal and hemodynamic signals in real-time [76]. Moreover, wavelet coherence method serves as a potential clinical tool for quick and easy diagnosis of neurovascular pathologies [13]. In wavelet coherence method, coupling between neuronal and hemodynamic signals is calculated/computed using values from zero to one. Zero represents a complete independence of both neuronal and hemodynamic signals, while one represents a complete coherence of neuronal and hemodynamic signals [58].

However, the changes in neurovascular coupling of the human brain during the transition from resting (wakeful) state to sleep states are not well discovered. Studies of neurovascular coupling

in neonates are mostly done during sleep state [13, 77]. In addition, the endogenic, neurogenic, and myogenic processes that underlie neurovascular coupling have not been studied in different vigilance states of the human brain. In the neuroimaging literature, no study has used wavelet coherence method to study neurovascular coupling during the transition from wakeful rest to sleep states by simultaneous EEG-fNIRS data. Study on the changes in neurovascular coupling across the different vigilance states of the brain would provide researchers with better understanding of how human brain organizes its processes in the different vigilance states. Also, understanding of neurovascular coupling across different vigilance states might be able to enlighten clinicians on how to make earlier diagnosis of certain brain pathologies which have neurovascular origin such as stroke.

In this study, the neurovascular coupling of the brain was investigated in eighteen subjects (mean age =23.5 years, standard deviation = 2.7 years) in three different vigilance states, including eyes-open state (EO), eyes-closed state (EC), and sleep-stage 1 state (SS1). Whole-head resting-state brain activity from all subjects was collected under both eyes-open and eyes-closed conditions using a dual-modality EEG-FNIRS instrumentation setup. Furthermore, sleep scoring [94] of the EEG data during eyes-closed state was performed to define sleep-stage 1 and sleep-stage 2 from eyes closed state and separate/split simultaneous EEG-fNIRS data in eyes-closed state into three different states. Four regions of interest on the head were selected to analyze EEG-fNIRS coupling; the left frontal location (EEG channel ‘Fp1’ and corresponding FNIRS channel ‘5’), the right frontal location (EEG channel ‘Fp2’ and corresponding FNIRS channel ‘7’), the left occipital location (EEG channel ‘O1’ and corresponding FNIRS channel ‘124’), and the right occipital location (EEG channel ‘O2’ and corresponding channel ‘126’). Wavelet coherence analysis was then applied to the simultaneous EEG-fNIRS data in each vigilance state

at each region of interest. Specifically, three separate frequency bands of EEG time series [i.e., theta (4-8 Hz), alpha (8-12 Hz), and beta (12-30 Hz)] were used to analyze coupling with the simultaneous fNIRS time series of oxyhemoglobin; and the neurovascular coupling calculation covered all vigilance states (eyes-open, eyes-closed, sleep-stage 1 & sleep-stage 2). Furthermore, the endogenic (0.01-0.2 Hz), neurogenic (0.02-0.04 Hz), and myogenic (0.04-0.15 Hz) components of EEG-fNIRS coupling were assessed in each vigilance state separately in the three EEG frequency bands. By using wavelet coherence approach, the aim of this study was to make the first step in quantitatively understanding the changes in EEG-fNIRS coupling as the brain transitions from awake to sleep state.

4.2 Methods

4.2.1 Subjects

18 young subjects (15 males and 3 females) with a mean age of 23.5 years (standard deviation = 2.5 years) were recruited for this study. These subjects were chosen from the student population of University of Texas at Arlington. The inclusion criteria were as follows: either sex (male or female), and in an age range of 18 – 29 years old. The exclusion criteria were as follows: (1) diagnosed with a psychiatric or sleeping disorder, (2) history of a neurological condition, or severe brain injury, or violent behavior, (3) have ever been institutionalized/imprisoned, (4) current intake of any medicine or drug, or (5) currently pregnant. In addition, none of the participants were smokers or had diabetes. The study protocol was approved by the institutional review board (IRB) at The University of Texas at Arlington and complied with all applicable federal and NIH guidelines. Informed consent was obtained from each participant prior to the experiments.

4.2.2 EEG-fNIRS Instrumentation

Resting-state brain activity from all subjects was acquired using a dual-modality instrumentation set-up. Specifically, the data were collected using both a 64-channel EEG instrument (Biosemi, Netherlands) and a 133-channel fNIRS instrument (Shimadzu corporation, Japan). Furthermore, a dual-modality cap (Shimadzu corporation, Japan) was used to acquire both EEG and fNIRS measurements from each subject. The dual-modality cap positioned the fNIRS optodes according to a whole-head layout which was already designed in the Shimadzu FNIRS machine. Furthermore, the 64 EEG channels were inserted into the holes of the dual-modality cap to cover specific fNIRS channels. The fNIRS machine uses three wavelengths of 780nm, 805nm, and 830nm to calculate oxy-, deoxy-, and total hemoglobin concentrations at each channel location. Furthermore, the sampling rate for the EEG data acquisition was 1 kHz, while the sampling rate for the fNIRS data acquisition was 8 Hz. In addition, the simultaneous EEG-fNIRS acquisition was controlled by a desktop computer which was connected to both the EEG instrument and fNIRS instrument via a USB port. Figure 4.1 shows the instrumentation setup which was used in this study.

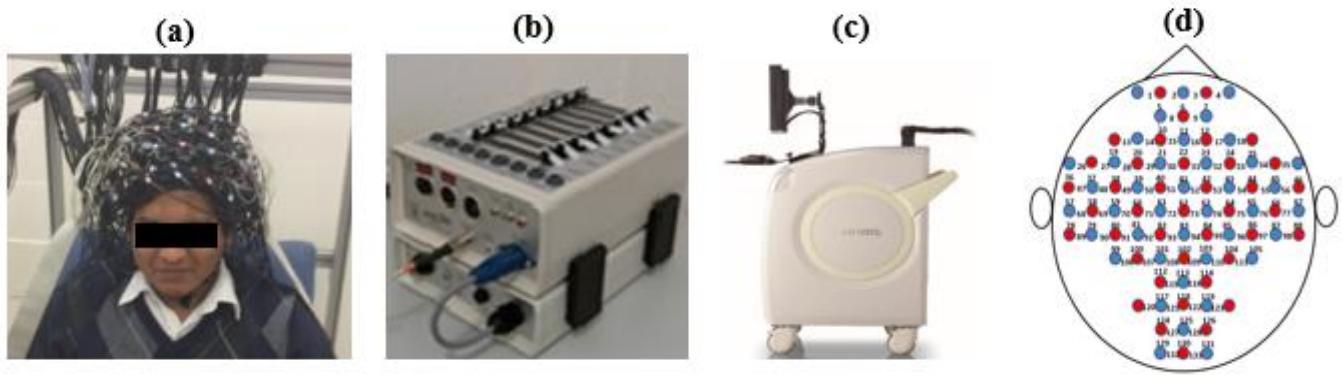

Figure 4.1: Instrumentation setup used for neurovascular coupling study. The simultaneous EEG-FNIRS acquisition was carried out on a subject using a dual-modality head cap which was placed on the subject's head as shown in (a). The simultaneous EEG-FNIRS acquisition was performed using (b) 64-channel EEG instrument and (c) 133-channel FNIRS measurement. The 133 channels of FNIRS were positioned according to the channel layout shown in (d). Red circles in the channel layout correspond to FNIRS sources (40 sources), while blue circles correspond to FNIRS detectors (40 detectors).

4.2.3 Simultaneous EEG-fNIRS Data acquisition

Each subject was seated in a comfortable chair for the whole duration of the experiment. Simultaneous EEG-fNIRS acquisition of resting-state brain activity was acquired in two separate stages. In the first stage of data acquisition, each subject was asked to keep his or her eyes open for five minutes. Then, the resting-state brain activity of each subject under this condition of eyes-open was acquired. In the second stage of data acquisition, each subject was then asked to close his or her eyes and fall asleep for ten minutes. Then, the resting-state brain activity of each subject under this condition of eyes-closed was also acquired. In addition, the measurements were conducted in a well-ventilated room with minimal noise. Also, phones and other electromagnetic devices were not allowed in the lab or on the subject during the whole duration of the experiment. Furthermore, each subject was positioned away from electrical sources to prevent contamination of data by 60 Hz power line noise.

4.2.4 EEG data processing

Data preprocessing of EEG data in both eyes-open and eyes-closed resting states was performed using the EEGLAB toolbox. EEGLAB is a well-known electrophysiological toolbox that has been developed for EEG data analysis [26]. Firstly, all the EEG datasets were exported into the EEGLAB toolbox which was installed in MATLAB 2017 software. Next, the datasets were down-sampled to 256 Hz. Next, a bandpass filter with a frequency range of 1 – 80 Hz was applied to each EEG dataset to remove unwanted signals. Furthermore, each subject's EEG data channel locations were set to match standard MNI coordinates in EEGLAB. Then, the EEG time series signal at each EEG electrode was inspected for extremely large amplitudes and electromyographic artifacts. Such noisy electrodes were corrected using spherical interpolation method in EEGLAB toolbox. After channel interpolation, the EEG data were re-referenced to an average reference for each subject. Furthermore, power line noise in the data was removed using the Clean line algorithm in EEGLAB, with the parameters set to default values. Finally, an Independent Component Analysis (ICA) algorithm was applied to the cleaned EEG data for each subject to remove eye movement artifacts, muscle noise, and eye blink artifacts [20]. This algorithm was also implemented using the EEGLAB toolbox.

4.2.5 Sleep scoring of dual-modality data in eyes-closed vigilance state

For each of the EEG datasets in the eyes-closed state, they were further examined for different sleep stages with the help of a qualified medical doctor. Specifically, the eyes-closed EEG data for each subject was first segmented into separate thirty-second (30 s) epochs. Then, with the help of the doctor, each thirty-second (30 s) epoch was assigned to either stage 0 (eyes-closed and awake, or EC), stage 1 (sleep stage 1 or SS1), or stage 2 (sleep stage 2 or SS2). The sleep scoring was performed in accordance with the American Association of Sleep Medicine (AASM) guidelines[78]. After sleep scoring, each subject's resting-state eyes-closed EEG dataset was

separated into both sleeping-stage 1 EEG dataset and sleeping-stage 2 EEG dataset, in preparation for EEG-fNIRS wavelet coherence analysis. Table 1 shows the total duration (in minutes) of each subject's EEG dataset in the eyes-opened state (EO), eyes-closed state (EC), sleeping-stage 1 (SS1) state, and sleeping-stage 2 (SS2) state.

Table 4.1: The table shows the total duration (in minutes) of eyes-opened (EO), eyes-closed (EC), sleep-stage 1 (SS1), and sleep-stage 2 (SS2) EEG datasets for each of the eighteen subjects that were recruited for neurovascular coupling study. EEG data in EO, EC, and SS1 states were then used for wavelet coherence analysis

Subject	1	2	3	4	5	6	7	8	9	10	11	12	13	14	15	16	17	18
EO	5	5	5	5	5	5	5	5	5	5	5	5	5	5	5	5	5	5
EC	10	9.5	8.5	10	5	10	5.5	1.5	1	9.5	2	5.5	0	3	0.5	10	10	0.5
SS1	0	0.5	1.5	0	5	0	4.5	4.5	4	0.5	3	4.5	3	1.5	2.5	0	0	1.5
SS2	0	0	0	0	0	0	0	4	5	0	5	0	7	5.5	7	0	0	8

4.2.6 Calculation of EEG power from aEEG in all vigilance states

Amplitude-integrated EEG, or aEEG, is a recent method used for analyzing EEG to provide a more precise interpretation of neuronal signals originating from the scalp [28]. From the raw EEG signals, the data are first preprocessed (filtering for noise removal), before calculating the envelope of the signal. The envelope of the signal is referred to as the aEEG signal, which can then be used for other forms of analysis. In this study, aEEG analysis was used to calculate EEG power signal in three different EEG frequency bands (theta, alpha, and beta). After preprocessing of all EEG datasets in EEGLAB, each subject's cleaned EEG data in each vigilance state (eyes-opened or EO; eyes-closed or EC; sleep-stage 1 or SS1; and sleep-stage 2 or SS2) was further separated into three EEG frequency bands which were theta (4-8 Hz), alpha (8-12 Hz), and beta (12-30 Hz). The bandpass filtering was performed using an FIR bandpass filter implemented in

EEGLAB. Then, each subject's 64-channel EEG data in each vigilance state was transformed into 64-channel power data by first calculating the envelope of the signal at each EEG electrode using the Hilbert transform. Then, power in each frequency band was calculated by squaring the complex-magnitude envelope. This step was performed for each frequency band in each vigilance state. The Hilbert transform is a well-known method for calculating power in different frequency bands [58, 59]. Then, the power at each EEG electrode was down-sampled to 8 Hz using a window-averaging process for each frequency band. Specifically, a moving window of length 0.5s with a step size of length 0.125s was used to perform the down-sampling to 8 Hz. The down-sampling was performed to match the sampling rate of EEG data to that of the fNIRS data, in preparation for wavelet coherence analysis. These down-sampled EEG power signals were then used for wavelet coherence analysis. Fig. 4.2 shows a flowchart which outlines the procedure of EEG data processing used in this study. Also, section A2 in the appendix shows the mathematical procedure of the Hilbert transform.

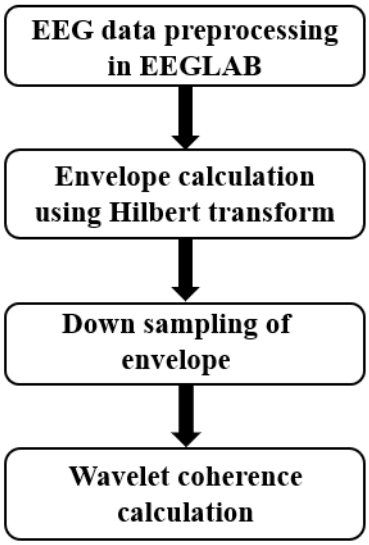

Figure 4.2: Flowchart of EEG data processing for neurovascular coupling study. This procedure was performed for all the EEG datasets shown in Table 4.1

4.2.7 FNIRS data preprocessing

The fNIRS raw files of oxy-, deoxy, and total hemoglobin concentrations for each subject in both eyes-open (EO) and eyes-closed state (EC) were exported to MATLAB 2017 software for further analysis. In MATLAB 2017, an FIR bandpass filter with a frequency range of 0.01-0.2 Hz was applied to the fNIRS oxy-hemoglobin time series data for each subject in both EO and EC state. This filtering operation was implemented to remove unwanted physiological signals such as cardiac signals and respiratory artifacts from the data. Next, the preprocessed fNIRS files in the eyes-closed state were sectioned into both sleep-state 1 (SS1) and sleep-stage 2 (SS2) data, using the information gathered from the sleep scoring of the eyes-closed EEG data for each subject.

4.2.8 Wavelet coherence analysis of simultaneous EEG-FNIRS data

To perform wavelet coherence analysis of simultaneous EEG-FNIRS data, four locations or regions of interest were selected on the head. These four regions of interest were; the left frontal location, which was covered by EEG electrode 'Fp1', and corresponding FNIRS channel '5'; the right frontal location, which was covered by EEG electrode 'Fp2', and corresponding FNIRS channel '7'; the left occipital location, covered by EEG electrode 'O1', and corresponding FNIRS channel '124'; and the right occipital location, covered by EEG electrode 'O2', and corresponding FNIRS channel '126'. Figure 4.3 shows the four regions of interest that were selected for wavelet coherence analysis of simultaneous EEG-FNIRS data.

The wavelet coherence analysis of simultaneous EEG-FNIRS data was performed using the 'wcoherence' function in MATLAB 2017 software. For each region of interest, the wavelet coherence between the window-averaged envelope from the EEG electrode and the oxy-hemoglobin time series signal from the corresponding fNIRS channel was calculated. This procedure was performed in three vigilance states (EO, EC, and SS1) for each frequency band

seperately. This step yielded a wavelet time-frequency coherence map for each subject in each vigilance state and for each frequency band. In addition, the wavelet coherence calculation was performed over a five-minute period. Subsequently, all the time-frequency coherence maps in each vigilance state were averaged across all subjects for each frequency band. This step formed an averaged time-frequency coherence map in each vigilance state for each frequency band across all subjects.

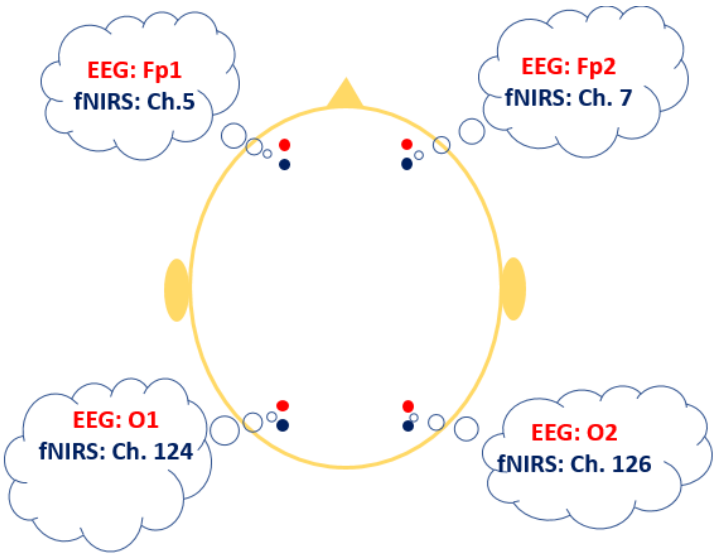

Figure 4.3: The four regions of interest on the head used for wavelet coherence of simultaneous EEG-FNIRS data in neurovascular coupling study. The left frontal location was covered by EEG channel 'Fp1' and corresponding FNIRS channel '5'. The right frontal location was covered by EEG channel 'Fp2' and corresponding FNIRS channel '7'. The left occipital location was covered by EEG channel 'O1' and corresponding FNIRS channel '124'. The right occipital location was covered by EEG channel 'O2' and corresponding FNIRS channel '126'

4.2.9 Analysis of endogenic, neurogenic, and myogenic components of EEG-fNIRS coherence

Each subject's wavelet time-frequency coherence map yielded a set of separate wavelet frequencies from 0.004 Hz up to 3.8 Hz. Then, from each subject's time-frequency map, all

coherence values in the endogenic component band (0.01-0.02 Hz) which were outside the cone of influence (COI) were extracted and averaged. This step was performed in each vigilance state (EO, EC, and SS1) and for each frequency band. The cone of influence is shown as a white dashed line on the coherence maps generated in this study. Coherence values inside the dashed line are free of edge artifacts. All the averaged coherence values of the endogenic component were then grouped together across all subjects to form a bar plot of average coherence in each vigilance state and for each frequency band. Thus, for the endogenic component (0.01-0.02 Hz) of EEG-fNIRS coherence, there were three (3) separate bar plots of averaged coherence values for each of eyes-opened (EO), eyes-closed (EC), and sleep-stage 1 (SS1) respectively in each of theta, alpha, and beta frequency bands. Then, a one-way ANOVA test ($p < 0.05$) was performed on the averaged coherence values of the endogenic component in eyes-open, eyes-closed, and sleep-stage 1 to test for statistical significance. This was performed separately for each frequency band. If the ANOVA test showed significance, a subsequent post-hoc analysis using Tukey-Kramer method was performed to detect the significant differences. Following the procedure just described, the neurogenic (0.02-0.04 Hz) and the myogenic components (0.04-0.15 Hz) of EEG-fNIRS coherence were also analyzed separately for each region of interest shown in Figure 4.3. Figure 4.4 shows a flowchart which outlines the steps of the procedure described here.

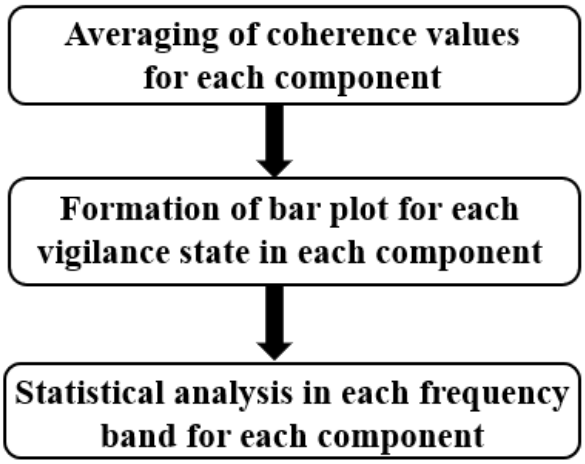

Figure 4 4: Flowchart of steps for analysis of components of EEG-FNIRS coherence

4.3 Results

4.3.1 EEG-fNIRS coherence/coupling in left frontal location for alpha band

For the alpha band, EEG-fNIRS coherence/coupling in the left frontal location occurred in all three vigilance states (Figure 4.5). In the eyes-open state, EEG-fNIRS coherence/coupling occurred predominantly within a frequency range of 0.016-0.25 Hz (Figure 4.5a). In the eyes-closed state, EEG-fNIRS coherence/coupling also occurred at a frequency range of 0.016 – 0.25 Hz (Figure 4.5b), In the sleep state (SS1), the predominant frequency range of EEG-fNIRS coherence/coupling also remained within 0.016-0.25 Hz (Figure 4.5c).

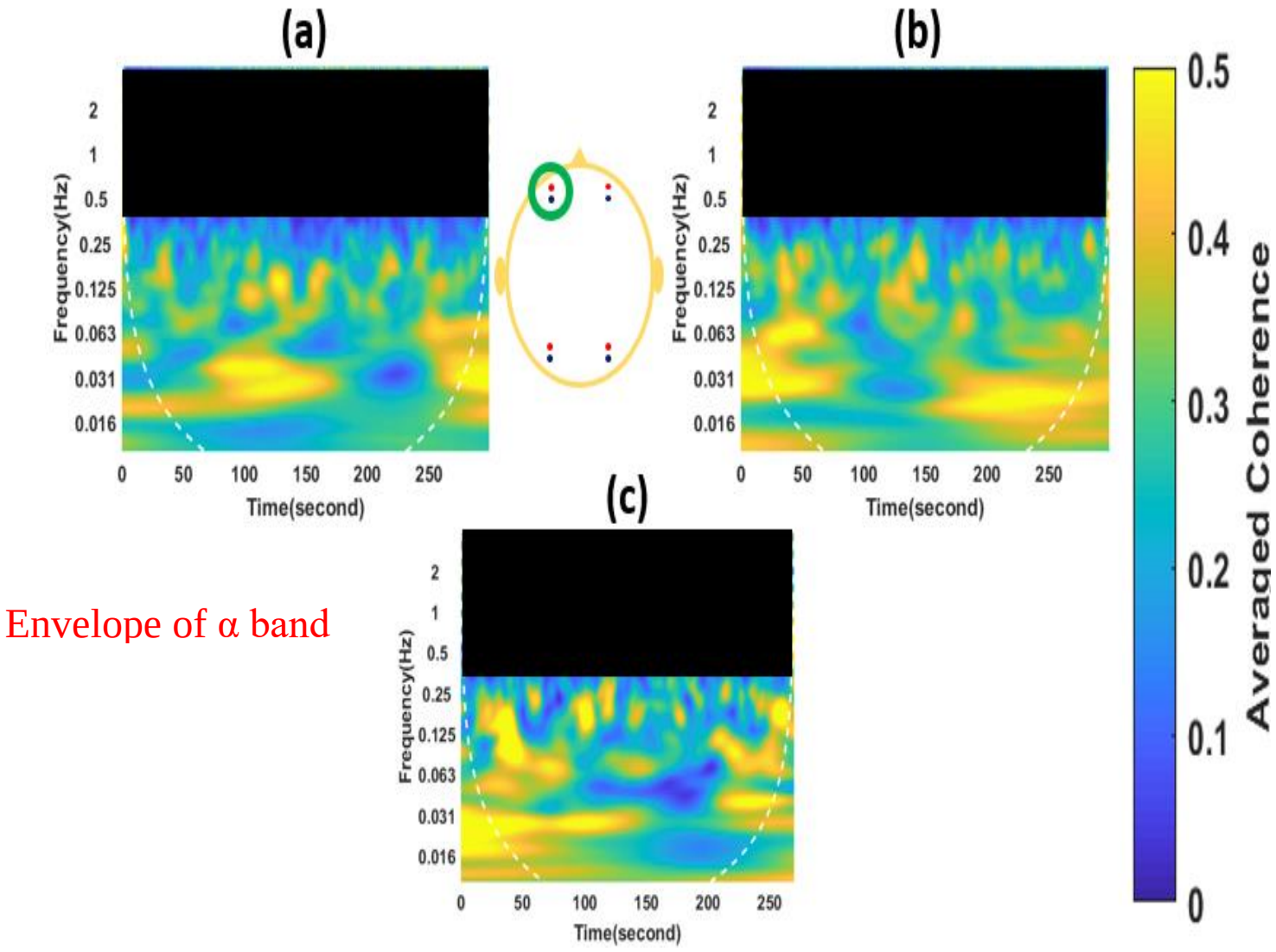

Figure 4.5 Averaged time-frequency coherence maps of EEG-FNIRS coherence in the left frontal location for the alpha-band envelope for (a) eyes-open (EO), (B) eyes-closed (EC); and (c) sleep-stage 1. The cone of influence is shown as areas on the maps that are outside the white-colored dashed line. The blacked-out area covers coherence values of noisy origin. The color bar represents averaged coherence values across all subjects.

4.3.2 EEG-fNIRS coherence/coupling in left frontal location for theta band

For the theta band, EEG-fNIRS coherence/coupling in the left frontal location occurred in all three vigilance states (Figure 4.6). In the eyes-open state, EEG-fNIRS coherence/coupling occurred predominantly within a frequency range of 0.016-0.2 Hz (Figure 4.6a). In the eyes-

closed state, EEG-fNIRS coherence/coupling also occurred at a frequency range of 0.016 – 0.2 Hz (Figure 4.6b). In the sleep state (SS1), the predominant frequency range of EEG-fNIRS coherence/coupling also remained within 0.016-0.2 Hz (Figure 4.6c)

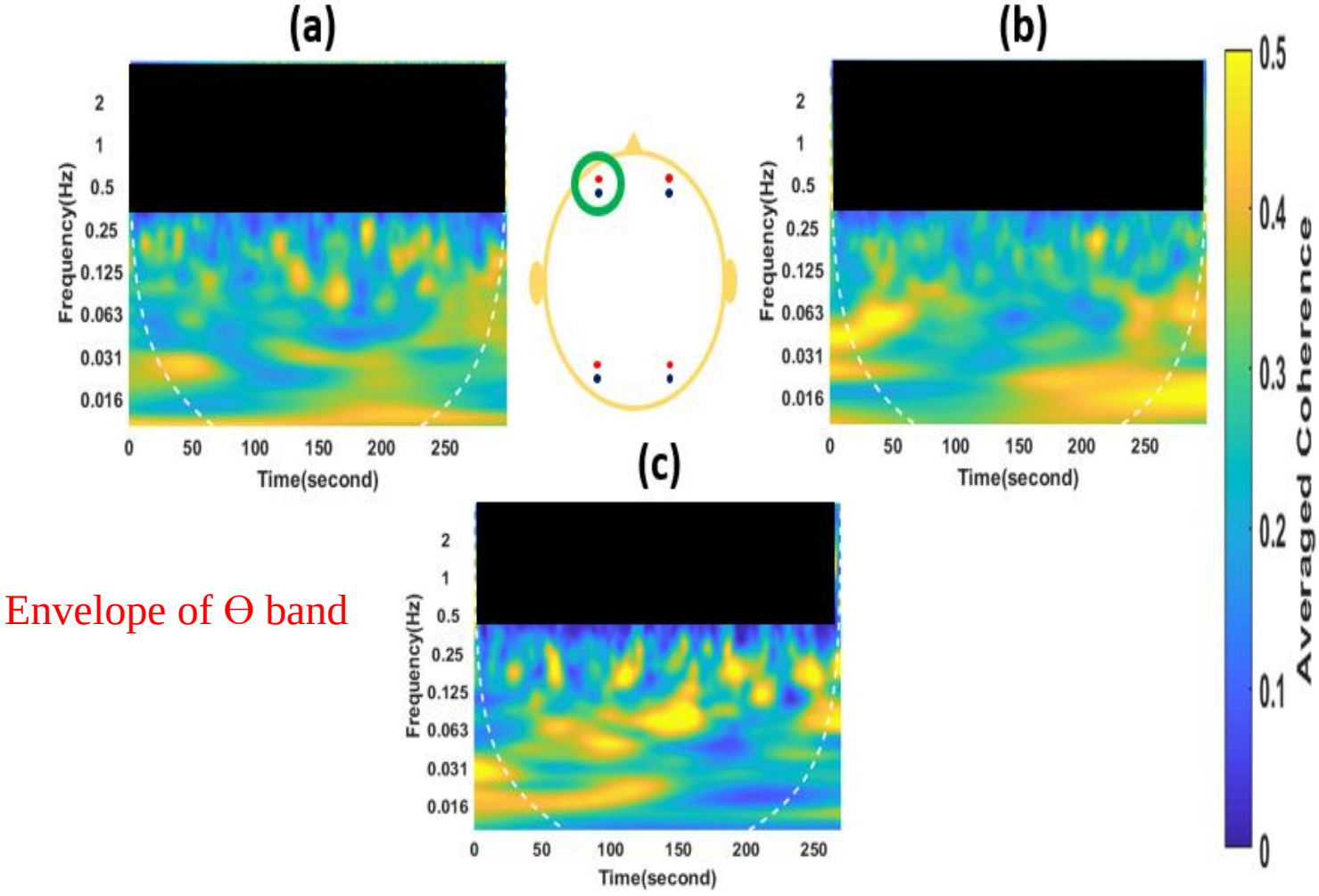

Figure 4.6: Averaged time-frequency coherence maps of EEG-FNIRS coherence in the left frontal location for the theta band envelope in (a) eyes-open (EO); (b) eyes-closed (EC); and (c) sleep-stage 1 (SS1). The cone of influence is shown as areas on the map that are outside the white-colored dashed line. The blacked-out region covers coherence values generated by noise. The color bar represents averaged coherence values across all subjects.

4.3.3 EEG-FNIRS coherence in left occipital location for alpha band

For the alpha band, EEG-fNIRS coherence in the left occipital location occurred in all three vigilance states (Figure 4.7). In the eyes-open state, EEG-fNIRS coherence/coupling occurred predominantly within a frequency range of 0.016-0.2 Hz (Figure 4.7a). In the eyes-closed (EC) state, EEG-fNIRS coherence/coupling also occurred at a frequency range of 0.016 – 0.2 Hz (Figure 4.7b). In addition, the coherence values in the eyes-closed (EC) state were much stronger compared to values in the eyes-open (EO) state. In the sleep state (SS1), the EEG-fNIRS coherence/coupling remained within a frequency range of 0.016-0.2 Hz (Figure 4.7c). In sleep-stage 1, the EEG-fNIRS coherence persisted over the whole-time period, and its coherence values appeared very brightly compared to all other vigilance states (Figure 4.7c).

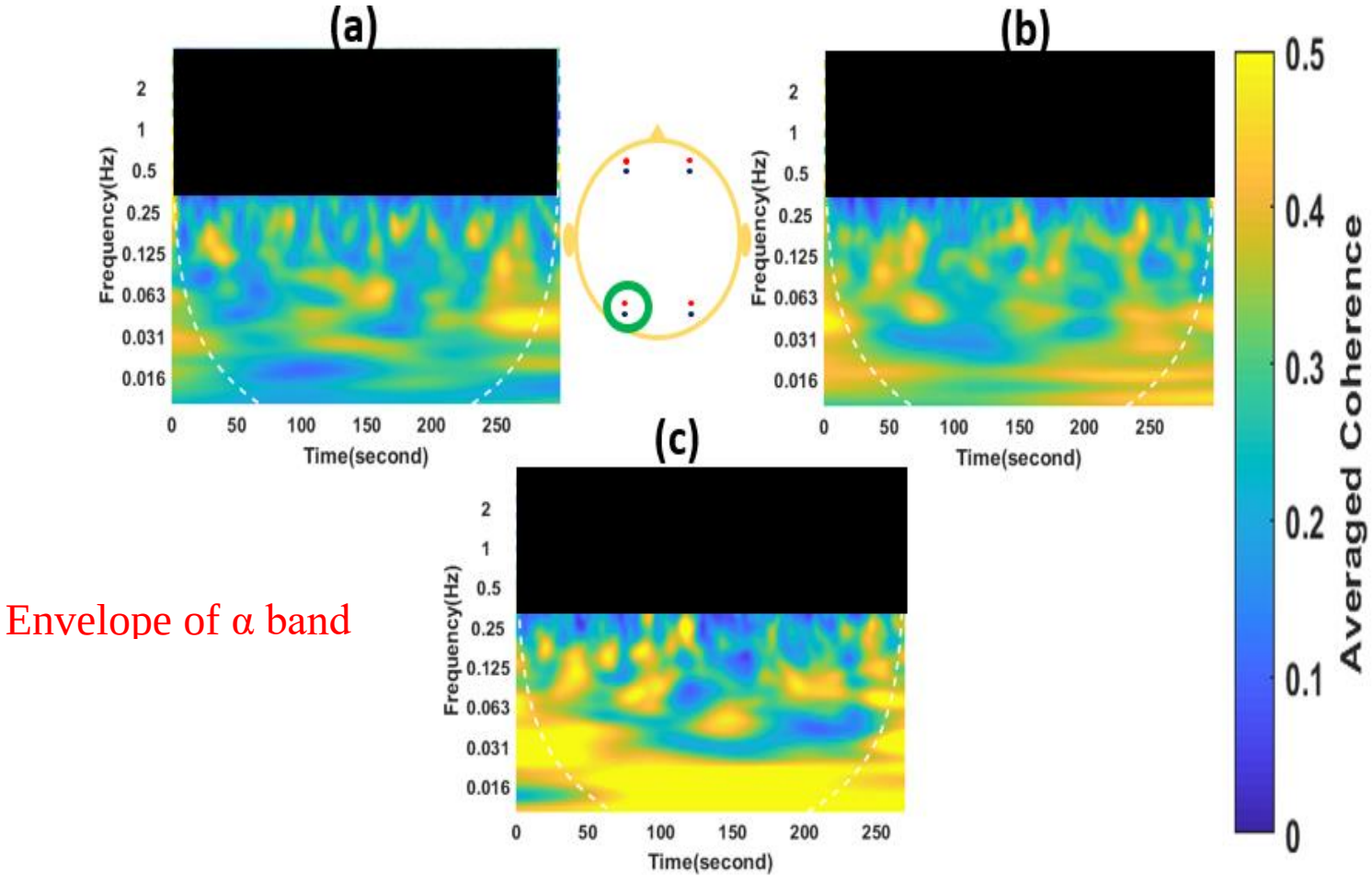

Figure 4.7: Averaged time-frequency coherence maps of EEG=FNIRS coherence in the left occipital location for the alpha band envelope in (a) eyes-open (b)eyes-closed, and (c) sleep-stage 1. The color bar represents averaged coherence values. The cone of influence is shown as areas on the map outside the white-dashed line. The blacked-out region covers coherence values generated by noise

4.3.4 EEG-fNIRS coherence/coupling in right occipital location for alpha band

For the alpha band, the EEG-fNIRS coherence in the right occipital location occurred in each vigilance state (Figure 4.8). In the eyes-open (EO) state, EEG-fNIRS coherence occurred within a frequency range of 0.06-0.2 Hz (Figure 4.8a). In the eyes-closed (EC) state, EEG-fNIRS coherence occurred within a frequency range of 0.016-0.2 Hz (Figure 4.8b). In sleep state (SS1),

EEG-fNIRS coherence occurred within a frequency range of 0.016-0.2 Hz, and the coherence values showed greater intensity than other vigilance state (Figure 4.8c).

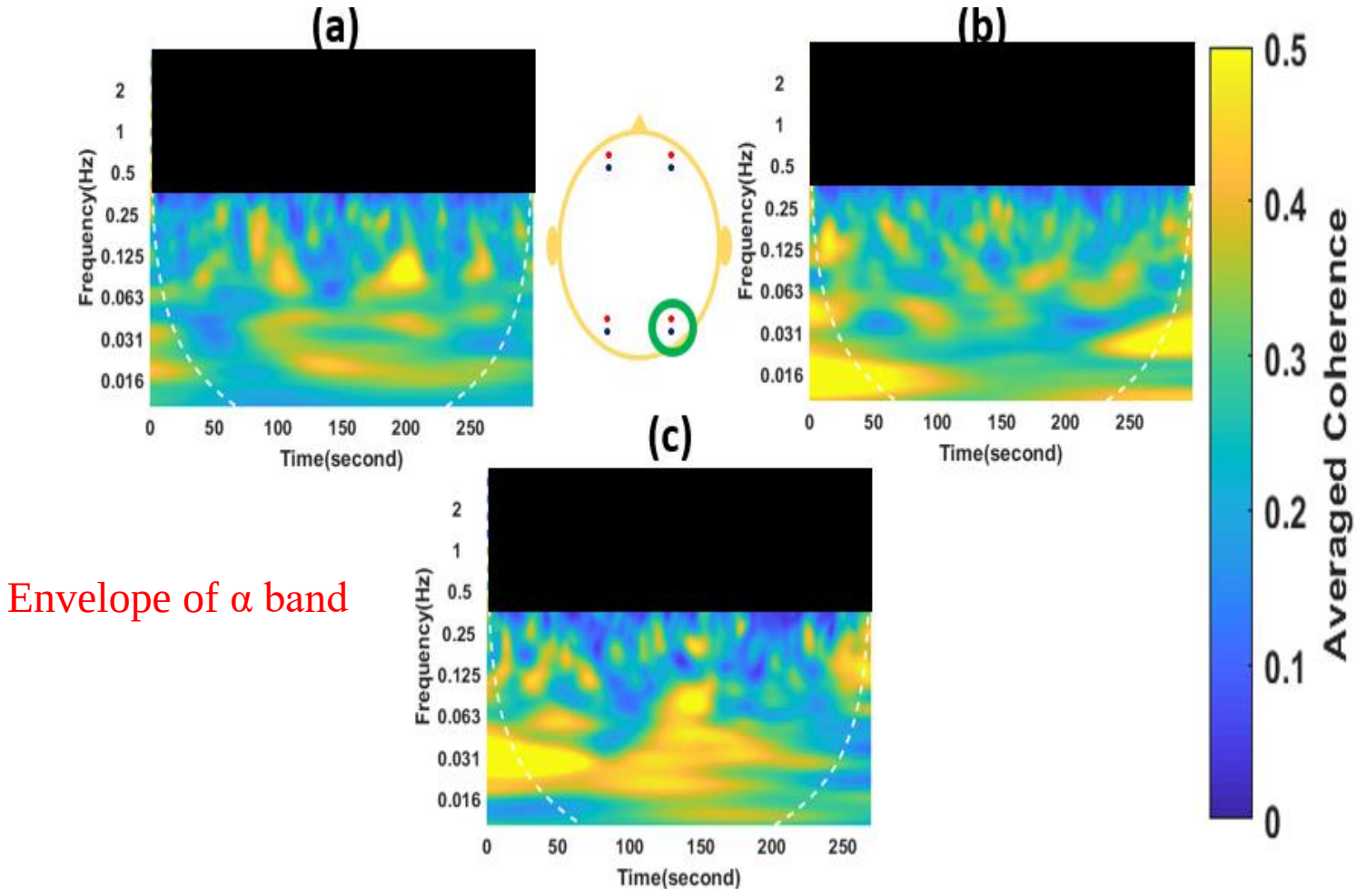

Figure 4.8: Averaged time-frequency coherence maps of EEG=FNIRS coherence in the right occipital location for the theta- band envelope in (a) eyes-open (b)eyes-closed, and (c) sleep-stage 1. The color bar represents averaged coherence values. The cone of influence is shown as areas on the map outside the white-dashed line. The blacked-out region covers coherence values generated by noise

.

4.3.5 Endogenic component of EEG-FNIRS coherence for alpha band in left frontal location.

The maps shown in Figure 4.5 were further analyzed using the method shown in Figure 4.4. The analysis revealed that, in the left frontal location, the endogenic component of EEG-FNIRS coherence for the alpha frequency band was highest in eyes-closed (EC) state and was lowest in eyes-open (EO) state (Figure 4.9). Furthermore, ANOVA test showed a significant difference in average coherence values of the endogenic component across all vigilance states, and post-hoc analysis (Tukey-Kramer method) revealed a significant difference in average coherence of endogenic component between EO and EC states (Figure 4.9).

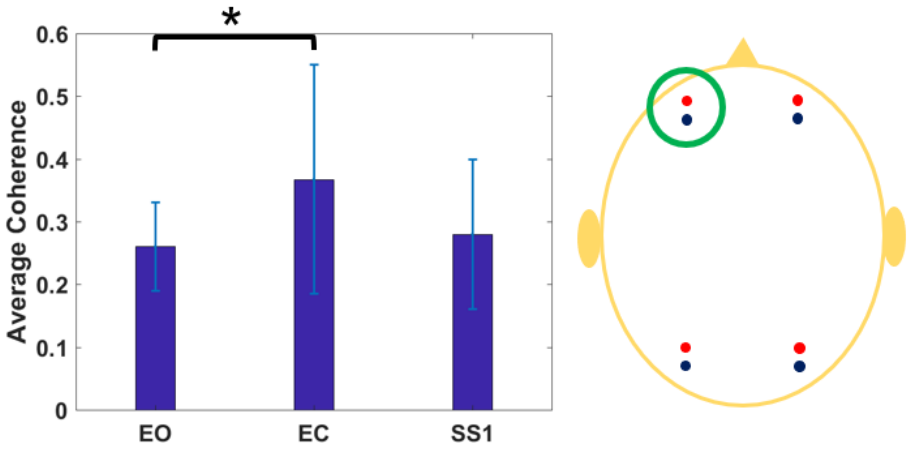

Figure 4.9 : Bar plot showing the average coherence in endogenic component (0.01 – 0.02 Hz) of EEG-FNIRS coherence for alpha band envelope in the left frontal location, in three vigilance states of eyes-open (EO), eyes-closed (EC), and sleep-stage 1 (SS1). The plots marked '*' represent a significant difference ($p < 0.05$, corrected using Tukey-Kramer post-hoc) in endogenic component of coherence between EO and EC states

4.3.6 Myogenic component of EEG-FNIRS coherence for theta band in left frontal location

The maps shown in Figure 4.6 were further analyzed using the method shown in Figure 4.4. The analysis revealed that, in the left frontal location, the myogenic component of EEG-FNIRS coherence/coupling for the theta frequency band was highest in sleep-stage 1 (SS1) state and was

lowest in eyes-open (EO) state (Figure 4.10). Furthermore, ANOVA test showed a significant difference in average coherence values of the myogenic component across all vigilance states, and post-hoc analysis (Tukey-Kramer method) revealed a significant difference in myogenic component between EO and SS1 states (Figure 4.10).

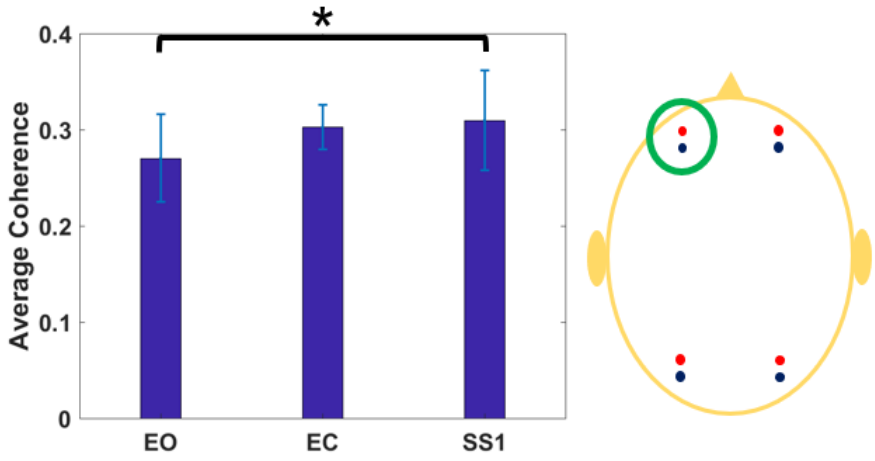

Figure 4.10 : Bar plot showing the average coherence in myogenic component (0.01 – 0.02 Hz) of EEG-FNIRS coherence for theta band envelope in the left frontal location, in three vigilance states of eyes-open (EO), eyes-closed (EC), and sleep-stage 1 (SS1). The plots marked '*' represent a significant difference ($p < 0.05$, corrected using Tukey-Kramer post-hoc) in myogenic component of coherence between EO and SS1 states.

4.3.7 Endogenic component of EEG-FNIRS coherence for alpha band in left occipital location

The maps shown in Figure 4.7 were further analyzed using the method shown in Figure 4.4. The analysis revealed that, in the left occipital location, the endogenic component of EEG-FNIRS coherence/coupling for the alpha frequency band was highest in sleep-stage 1 (SS1) state and was lowest during eyes-open (EO) state (Figure 4.11). Furthermore, ANOVA test showed a significant difference in average coherence values of the endogenic component across all

vigilance states, and post-hoc analysis (using Tukey-Kramer method) revealed a significant difference between EO and SS1 states, and between EC and SS1 states (Figure 4.11).

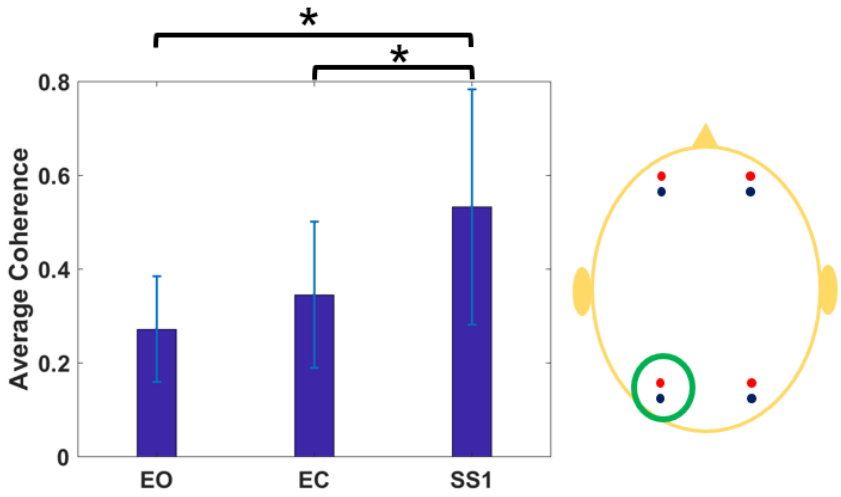

Figure 4.11: Bar plot showing the average coherence in endogenic component (0.01 – 0.02 Hz) of EEG-FNIRS coherence for alpha band envelope in the left occipital location, in three vigilance states of eyes-open (EO), eyes-closed (EC), and sleep-stage 1 (SS1). The plots marked '*' represent a significant difference ($p < 0.05$, corrected using Tukey-Kramer post-hoc) in endogenic component of coherence between EO and SS1 states, and between EC and SS1 states.

4.3.8 Endogenic component of EEG-FNIRS coherence for alpha band in right occipital location

The maps shown in Figure 4.8 were further analyzed using the method shown in Figure 4.4. The analysis revealed that, in the right occipital location, the endogenic component of EEG-FNIRS coherence/coupling in the alpha frequency band was highest in eyes-closed (EC) state and was lowest during eyes-open (EO) state (Figure 4.12). Furthermore, ANOVA test showed a significant difference in average coherence values of the endogenic component across all vigilance states, and post-hoc analysis (Tukey-Kramer method) revealed a significant difference between EO and EC states (Figure 4.12).

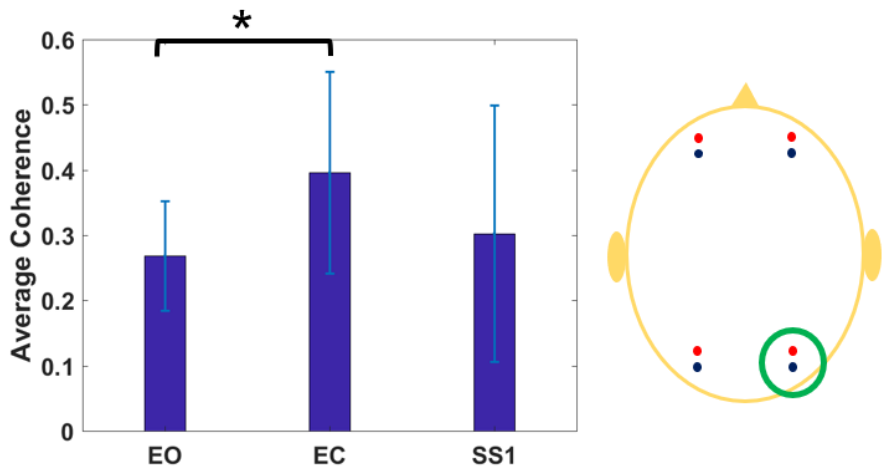

Figure 4.12: Bar plot showing the average coherence in endogenic component (0.01 – 0.02 Hz) of EEG-FNIRS coherence for alpha band envelope in the right occipital location, in three vigilance states of eyes-open (EO), eyes-closed (EC), and sleep-stage 1 (SS1). The plots marked '*' represent a significant difference ($p < 0.05$, corrected using Tukey-Kramer post-hoc) in endogenic component of coherence between EO and EC states.

4.4 Discussion

In this study, analytic envelopes of EEG signals in three different frequency bands (theta, alpha, and beta) were first down sampled to FNIRS sampling rate (8 Hz). Then, wavelet coherence analysis was used to calculate the coherence/coupling in time-frequency between the down sampled EEG signals and FNIRS signals at four different brain locations as shown in Figure 4.3. In addition, statistical analyses were performed to investigate the endogenic, neurogenic, and myogenic components of neurovascular coupling in each of the three separate frequency bands.

4.4.1 Low-frequency oscillations in EEG-FNIRS coherence for three vigilance states

At each of three brain locations (left frontal, left occipital, and right frontal), the EEG-FNIRS coherence occurred in an extremely low frequency range of 0.016 – 0.2 Hz (Figs 4.5-4.8). This finding suggests that EEG-FNIRS coherence/coupling is dominated mainly by low-frequency oscillations. Low-frequency oscillations in brain signals are known as infra-slow oscillations in

the neuroimaging literature. These oscillations have been severally linked with neurovascular coupling processes from previous studies. For example, a study by Nikulin et al detected the occurrence of infra-slow oscillations in EEG signals, with the frequencies in the 0.01 – 0.14 Hz range [79]. In addition, the infra-slow frequencies in EEG showed a strong coherence with NIRS signals in eight subjects [79], which suggests that the infra-slow oscillations in EEG signals have some close relationship with hemodynamic processes. In another study, Roche-Labarbe et al [80] showed that EEG-fNIRS coupling/coherence during quiet sleep in neonates occurred within a frequency range of 0.05-0.1 Hz, which is in the range of infra-slow oscillations. Also, Zanatta et al [71] observed coupling between EEG power and blood flow velocity in the middle cerebral artery (MCA) occurred at a mean frequency of 0.06 Hz in subjects under both moderate and deep anesthesia. The occurrence of infra-slow oscillations during neurovascular coupling in sleep has also been reported in a combined EEG-fMRI study [81]. Infra-slow oscillations in hemodynamic signals are thought to reflect arterial vasomotion, which occurs during neurovascular coupling in the brain [75]. The findings in this study provide strong evidence to support the role of infra-slow oscillations in neurovascular coupling. Furthermore, this finding indicates that the infra-slow frequencies for neuronal signals are found in analytic envelopes of EEG signals in each of the different EEG frequency bands.

Furthermore, the infra-slow oscillations that control EEG-fNIRS coherence/coupling did not occur at just one location; their occurrence was reported at three separate locations on the head (Figures 4.5-4.8). Infra-slow oscillations in EEG signals were also reported at several locations in a previous study, indicating that they are not affected by volume conduction [79]. This finding gives further proof that infra-slow oscillations is tightly linked to neurovascular coupling. Also, wavelet coherence analysis was used to study EEG-fNIRS coupling/coherence during the

transition from wakeful rest to a sleep state in this study. Wavelet coherence analysis has been previously used to show that coupling between amplitude-integrated EEG (aEEG) and NIRS signal occurs within slow frequencies in neonates [76]. Therefore, this study also validates the use of wavelet coherence method as a tool for quantitatively measuring neurovascular coupling in different vigilance states of the brain.

4.4.2 Changes in endogenic component of neurovascular coupling across three vigilance states

The endogenic component of neurovascular coupling changed significantly across vigilance states at three different brain sites (Figs 4.9, 4.11-12). In two locations, there was a significant difference ($p < 0.05$, corrected) between endogenic component in eyes-open state and eyes-closed state only, and both for alpha band (Figs 4.9, 4.12). In another separate brain site, the endogenic component in eyes-open state and in sleep-stage 1 state were significantly different for alpha band, while the endogenic component in eyes-open state and eyes-closed state were significantly different, also for alpha band (Fig. 4.11). A previous fNIRS study has shown predominant endothelial vasomotor activity in the brain during sleep, with higher vasomotor activity during light non-REM sleep compared to deeper non-REM sleep [82]. This finding, coupled with the results from our study, suggests that the transition from an awake to sleep state in the brain may be associated with a gradual increase in endothelial activity of neurovascular activity from eyes-open state to sleep state. In this study, the left occipital location shows a gradual increase in endothelial component activity from eyes-open state to sleep-state 1 (Fig.4.11). This finding points to an important role of endothelial activity within the occipital area during the brain's transition from awake to sleep state. Endothelial activity is causally linked to nitric oxide (NO) release, which is necessary for vasodilation [82]. So, it is possible

that during the brain's transition to sleep state, more NO is released in the occipital area to induce increased blood flow which corresponds to increased neurovascular coupling.

4.4.3 Changes in myogenic component of neurovascular coupling across vigilance states

During the brain's transition from an awake to sleep state, the myogenic component in sleep-state 1 increased significantly compared to that of eyes-open state (Fig.4.10). Myogenic processes refer to activity of smooth muscle cells underlying vessel walls in the brain. The smooth muscle cells undergo contraction and relaxation as blood flow increases or decreases in the brain. Myogenic vasomotor activity in the brain during sleep has also been reported by Zhang et al [25]. In addition, Rosas et al have shown that there is high coherence/coupling between EEG signals in theta band and cerebral blood flow during quiet sleep in neonates [77]. The findings here show that the brain's transition to sleep may also affect myogenic processes of coupling in the brain.

4.4.4 Further work

This study should be considered as a first step in quantitatively measuring neurovascular coupling of the brain in different vigilance states. In further studies, the analysis of EEG-FNIRS coherence in different vigilance states could be extended to more locations or sites on the brain. Furthermore, the coupling between EEG signals in different EEG frequency bands and deoxyhemoglobin or total hemoglobin concentrations could also be examined in each vigilance state using wavelet coherence analysis. Furthermore, the direction of the coupling between EEG signals in different frequency bands and hemodynamic signals from FNIRS could also be investigated using other methods such as Granger causality analysis [83] or phase transfer entropy[84]. Finally, the other components that affect neurovascular coupling could also be studied for a richer understanding of neurovascular coupling in the brain.

4.5 Limitations

A previous study has shown weak correlations between neuronal and hemodynamic signals in resting state of the brain [89]. Therefore, our hypothesis of neurovascular coupling during different vigilance states may be limited by weak interactions between neuronal and hemodynamic signals. Another limitation of this study could be the placement of the EEG electrodes on the scalp; they were not placed according to the standard 10-10 or 10-20 system of EEG electrode placement. In addition, the thirty-second (30 s) sleep data for some subjects may be insufficient for data analysis during sleep. Finally, the maps provide a qualitative result of EEG-FNIRS coherence and may need to be subjected to more rigorous statistical analysis, such as described in ref. 76.

4.6 Conclusion

Overall, this study has demonstrated the use of the simultaneous EEG-FNIRS instrumentation for investigating the coupling between neuronal and hemodynamic signals of the brain during the transition from wakeful resting state to sleep state. In addition, this study shows that the coupling of neuronal and hemodynamic signals occurs within infra-slow oscillations (~0.1 Hz), which corroborates other studies using EEG-FMRI and/or transcranial Doppler flowmetry methods. Also, the brain's transition from an awake state to sleep state was shown to be associated with changes in neurovascular coupling strength. Specifically, the endogenic component of coupling varied significantly across vigilance states from eyes-open to sleep-stage 1, suggesting that the endogenic processes during neurovascular coupling are important signatures of consciousness in the brain.

.

CHAPTER 5

5. Neurovascular coupling in voluntary breath-holding quantified by wavelet coherence analysis

5.1 Background

Neurovascular coupling in the brain refers to the tight coupling between neuronal fluctuations and the corresponding hemodynamic response in the brain [66]. The brain requires a continuous supply of blood to provide energy for its many activities; this continuous supply of blood to the brain is induced by coupling between neuronal activity, cerebral blood flow, and metabolism [67]. According to previous studies, neurovascular coupling is necessary to maintain the cerebral autoregulation in the brain [68]. Also, the impairment of neurovascular coupling in the brain has been linked to some diseases such as ischemic stroke, hypertension, and Alzheimer's disease[11]. In addition, neurovascular coupling may also be impaired in small vessel disease [12].

During apnea, cerebral blood flow to the brain is severely affected due to hypoxia[85]. Hypoxia in turn causes cerebral vasodilation which increases cerebral blood flow to the brain[86]. Hypothetically, the increase in cerebral blood flow should influence neurovascular coupling in the brain. However, the neurovascular coupling in the brain during voluntary apnea has not been previously studied. A core component of neurovascular coupling is the endothelial component or process[75]. The endothelial component of neurovascular coupling occurs within a frequency range of 0.01 – 0.02 Hz.[75]. Endothelial dysfunction has been linked to obstructive sleep apnea disease[85] Thus, knowledge of neurovascular coupling in different conditions of voluntary apnea will provide some insight into how respiratory diseases alter neurovascular coupling in the brain.

The neurovascular coupling in different states of voluntary breath-holding has not been investigated using simultaneous EEG-fNIRS measurement. In this study, a whole-head EEG-FNIRS instrumentation set up was used to collect brain data in three different conditions of voluntary apnea: rest/normal breathing (EO), short breath-hold (BR1), and long breath-hold (BR2). The data were collected from a sample of 8 subjects at the University of Texas at Arlington. Furthermore, envelopes of EEG power in theta, alpha, and beta bands were calculated and then down sampled to match FNIRS sampling frequency (8 Hz). Then, wavelet coherence analysis was used to quantify neurovascular coupling in the brain for each condition of apnea. The analysis was performed at four different locations of the brain: left frontal, left occipital, right frontal, and right occipital locations. The left frontal location was covered by EEG channel 'Fp1' and corresponding channel '5'. The right frontal location was covered by EEG channel 'Fp2' and corresponding channel '7'. Also, the left occipital location was covered by EEG channel 'O1' and corresponding channel '124'. Lastly, the right occipital location was covered by EEG channel 'O2' and corresponding channel '126'.

5.2 Methods

5.2.1 Subjects

8 young subjects (6 males and 2 females) with a mean age of 23.5 years (standard deviation = 2.5 years) were recruited for this study. These subjects were chosen from the student population of University of Texas at Arlington. The inclusion criteria were as follows: either sex (male or female) and in an age range of 18 – 29 years old. The exclusion criteria were as follows: (1) diagnosed with a psychiatric or sleeping disorder, (2) history of a neurological condition, or severe brain injury, or violent behavior, (3) have ever been institutionalized/imprisoned, (4) current intake of any medicine or drug, or (5) currently pregnant. In addition, none of the

participants were smokers or had diabetes. The study protocol was approved by the institutional review board (IRB) at The University of Texas at Arlington and complied with all applicable federal and NIH guidelines. Informed consent was obtained from each participant prior to the experiments.

5.2.2 EEG-FNIRS Instrumentation

Brain activity in all subjects was acquired using a dual-modality instrumentation set-up. Specifically, the data were collected using both a 64-channel EEG instrument (Biosemi, Netherlands) and a 133-channel fNIRS instrument (Shimadzu corporation, Japan). Furthermore, a dual-modality cap (Shimadzu corporation, Japan) was used to acquire both EEG and fNIRS measurements from each subject. The dual-modality cap positioned the fNIRS optodes according to a whole-head layout which was already designed in the Shimadzu fNIRS machine. Furthermore, the 64 EEG channels were inserted into the holes of the dual-modality cap to cover specific fNIRS channels. The fNIRS machine uses three wavelengths of 780nm, 805nm, and 830nm to calculate oxy-, deoxy-, and total hemoglobin concentrations at each channel location. Furthermore, the sampling rate for the EEG data acquisition was 1 kHz, while the sampling rate for the fNIRS data acquisition was 8 Hz. In addition, the simultaneous EEG-fNIRS acquisition was controlled by a desktop computer which was connected to both the EEG instrument and fNIRS instrument via a USB port. Figure 5.1 shows the instrumentation setup which was used in this study.

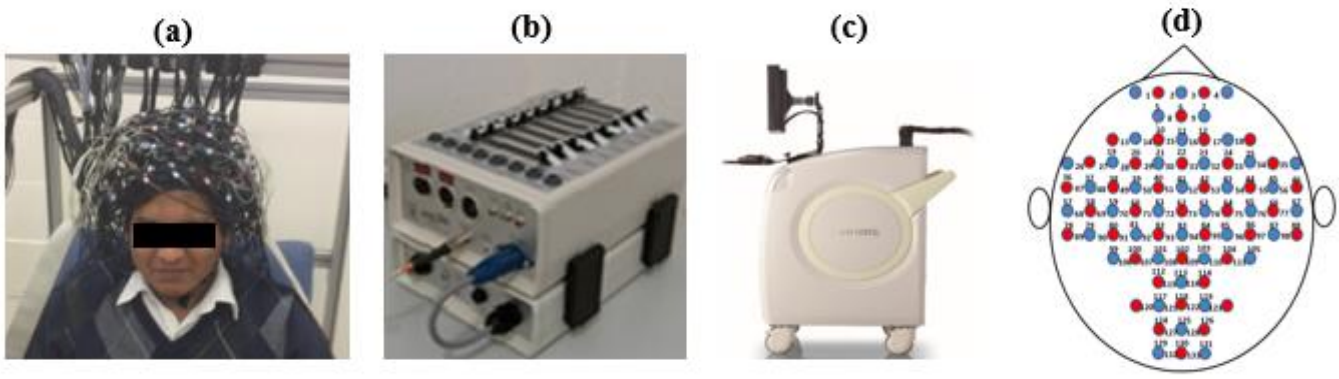

Figure 5.1: Instrumentation setup used for breath hold study. The simultaneous EEG-FNIRS acquisition was carried out on a subject using a dual-modality head cap which was placed on the subject's head as shown in (a). The simultaneous EEG-FNIRS acquisition was performed using (b) 64-channel EEG instrument and (c) 133-channel FNIRS measurement. The 133 channels of FNIRS were positioned according to the whole- head channel layout shown in (d). Red circles correspond to 40 FNIRS sources, while blue circles correspond to 40 FNIRS detectors. The numbers shown in the channel layout represent the FNIRS channels.

5.2.3 Simultaneous EEG-fNIRS Data acquisition

Each subject was seated in a comfortable chair for the whole duration of the experiment. The experimental protocol consisted of, first, a 5-minute period of continuous resting-state data, and then, 10 separate blocks of data acquisition in the breath-hold state. Specifically, in the 5-minute period, simultaneous EEG-fNIRS data was collected in eyes-open (EO) resting state condition. Then, for the first set of 5 blocks, each subject alternated between a 40s period of rest and 10s period of breath-hold in each block (Figure 5.2A). Also, simultaneous EEG-fNIRS data was collected for each block. For the second set of 5 blocks, each subject alternated between a 50s period of rest and 20s period of breath-hold in each block (Figure 5.2B). Simultaneous EEG-fNIRS data was also collected for each block. The total time for the experiment protocol was 900 seconds (15 minutes). The experimental protocol for the study was programmed on a computer screen which the subject viewed and followed the instructions. In addition, the simultaneous

EEG-fNIRS measurements were conducted in a well-ventilated room with minimal noise. Also, phones and other electromagnetic devices were not allowed in the lab or on the subject during the whole duration of the experiment. Furthermore, each subject was positioned away from electrical sources to prevent contamination of data by 60 Hz power line noise.

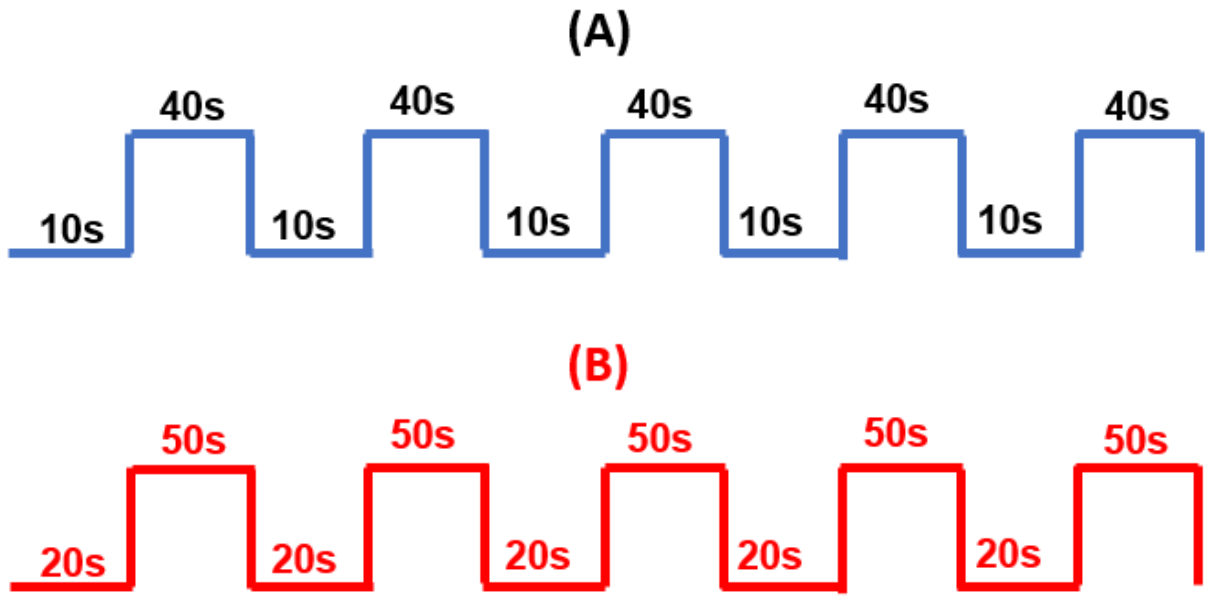

Figure 5.2: Block-type stimulus protocol used for breath-hold study. For the first stage of data acquisition shown in (A), each subject had a 10 second period of rest which was followed by a 40 second period of voluntary breath-holding. This block paradigm was repeated 5 times. For the second stage of data acquisition shown in (B), each subject had a 20 second period of rest which was followed by a 50 second period of voluntary breath-holding. This was also repeated 5 times

5.2.4 EEG data processing

Data preprocessing of EEG data was performed using the EEGLAB toolbox. EEGLAB is a well-known electrophysiological toolbox that has been developed for EEG data analysis [26]. Firstly, all the EEG datasets were exported into the EEGLAB toolbox which was installed in MATLAB 2017 software. Next, the datasets were down-sampled to 256 Hz. Next, a bandpass filter with a frequency range of 1 – 80 Hz was applied to each EEG dataset to remove unwanted signals. Furthermore, each subject's EEG data channel locations were set to match standard MNI

coordinates in EEGLAB. Then, the EEG time series signal at each EEG electrode was inspected for extremely large amplitudes and electromyographic artifacts. Such noisy electrodes were corrected using spherical interpolation method in EEGLAB toolbox. After channel interpolation, the EEG data were re-referenced to an average reference for each subject. Furthermore, power line noise in the data was removed using the Clean line algorithm in EEGLAB, with the parameters set to default values. Finally, an Independent Component Analysis (ICA) algorithm was applied to the cleaned EEG data for each subject to remove eye movement artifacts, muscle noise, and eye blink artifacts [20]. This algorithm was also implemented using the EEGLAB toolbox.

5.2.5 Envelope signal calculation

After preprocessing of all EEG datasets in EEGLAB, each subject's cleaned EEG data for each state (eyes-open or EO, shorter breath-hold or BR1 and longer breath-hold or BR2) was further separated into three EEG frequency bands which were theta (4-8 Hz), alpha (8-12 Hz), and beta (12-30 Hz). The bandpass filtering was performed using an FIR bandpass filter implemented in EEGLAB. Then, each subject's 64-channel EEG data in each breath-hold state was transformed into 64-channel power data by first calculating the envelope of the signal at each EEG electrode using the Hilbert transform, and then squaring the envelope. This step was performed for each frequency band. The Hilbert transform is a well-known method for calculating power in different frequency bands [58, 59]. Then, the power at each EEG electrode was down-sampled to 8 Hz using a window-averaging process for each frequency band. Specifically, a moving window of length 0.5s and a step size of length 0.125s was used to perform the down-sampling. The down-sampling was performed to match the sampling rate of EEG data to that of the fNIRS data, in preparation for wavelet coherence analysis. These down-sampled EEG power signals were then

used for wavelet coherence analysis. Figure 5.3 shows a flowchart which outlines the procedure of EEG data processing used in this study. Also, section A2 in the appendix shows the mathematical explanation of the Hilbert transform.

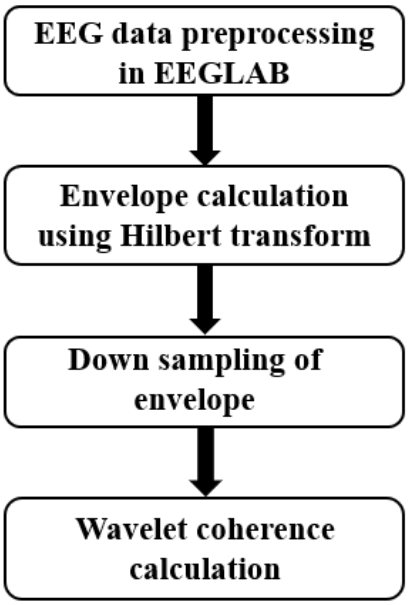

Figure 5.3: Flowchart of EEG data processing pipeline for breath-holding study.

5.2.6 FNIRS data preprocessing

The fNIRS raw files of oxy-, deoxy, and total hemoglobin concentrations for each subject in both eyes-open (EO), shorter breath-hold (BR1), and longer breath-hold (BR2) were exported to MATLAB 2017 software for further analysis. Firstly, the fNIRS oxyhemoglobin data in each condition was detrended to remove trends in the data. Then, an FIR bandpass filter with a frequency range of 0.01-0.2 Hz was applied to the fNIRS oxy-hemoglobin time series data for each subject in the three conditions. This filtering operation was implemented to remove unwanted physiological signals such as cardiac signals and respiratory artifacts from the data.

5.2.7 Wavelet coherence analysis of simultaneous EEG-fNIRS data

To perform wavelet coherence analysis of simultaneous EEG-fNIRS data, four locations or regions of interest were selected on the head. These four regions of interest were; the left frontal location, which was covered by EEG electrode 'Fp1', and corresponding fNIRS channel '5'; the right frontal location, which was covered by EEG electrode 'Fp2', and corresponding fNIRS channel '7'; the left occipital location, covered by EEG electrode 'O1', and corresponding fNIRS channel '124'; and the right occipital location, covered by EEG electrode 'O2', and corresponding fNIRS channel '126'. Figure 5.4 shows the four regions of interest that were selected for wavelet coherence analysis of simultaneous EEG-fNIRS data.

For each region of interest, the wavelet coherence between the window-averaged envelope from the EEG electrode and the oxy-hemoglobin time series signal from the corresponding fNIRS channel was calculated. This procedure was performed under the three different conditions (EO, BR1, and BR2) for each frequency band seperately. This step yielded a wavelet time-frequency coherence map for each subject in each condition and for each frequency band. Subsequently, all the time-frequency coherence maps for each condition were averaged across all subjects for each frequency band to form a single time-frequency coherence map in each condition for each frequency band. The wavelet coherence analysis of simultaneous EEG-fNIRS data was performed using the 'wcoherence' function in MATLAB 2017 software.

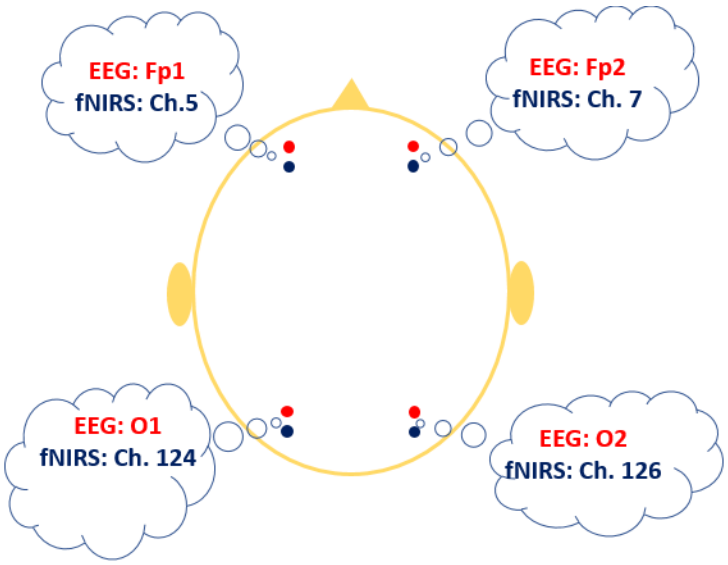

Figure 5.4: The four regions of interest on the human head used for wavelet coherence of simultaneous EEG-FNIRS data in voluntary breath-holding. The left frontal region was covered by EEG channel 'Fp1' and corresponding FNIRS channel '5'. The right frontal region was covered by EEG channel 'Fp2' and corresponding FNIRS channel '7'. The left occipital region was covered by EEG channel 'O1' and corresponding FNIRS channel '124'. The right occipital region was covered by EEG channel 'O2' and corresponding FNIRS channel '126'.

5.2.8 Analysis of endogenic, neurogenic, and myogenic components of EEG-fNIRS coherence

Each subject's wavelet time-frequency coherence map yielded a set of separate wavelet frequencies from 0.004 Hz up to 3.8 Hz. Then, from each subject's time-frequency map, all coherence values for the endogenic component band (0.01-0.02 Hz) which were outside the cone of influence (COI) were extracted and averaged. This step was performed in each condition (EO, BR1, and BR2) and for each frequency band. Then, all the averaged coherence values of the endogenic component for each condition were grouped together across all subjects to form bar plots of average coherence. This was done for each frequency band. Thus, for the endogenic component (0.01-0.02 Hz) of EEG-fNIRS coherence, there were three (3) separate bar plots of averaged coherence values for each of eyes-opened (EO), shorter breath-hold (BR1), and longer breath-hold (BR2) respectively in each of theta, alpha, and beta frequency bands. Then, a one-

way ANOVA test ($p < 0.05$) was performed on the averaged coherence values of the endogenic component in EO, BR1, and BR2 to test for statistical significance. This was performed separately for each frequency band. If the ANOVA test showed significance, a subsequent post-hoc analysis using Tukey-Kramer method was performed to detect the significant differences. Following this procedure just described, the neurogenic (0.02-0.04 Hz) and the myogenic components (0.04-0.15 Hz) of EEG-fNIRS coherence/coupling were also analyzed separately for each region of interest shown in Figure 3. Figure 5.5 shows a flowchart which outlines the steps of the procedure described here.

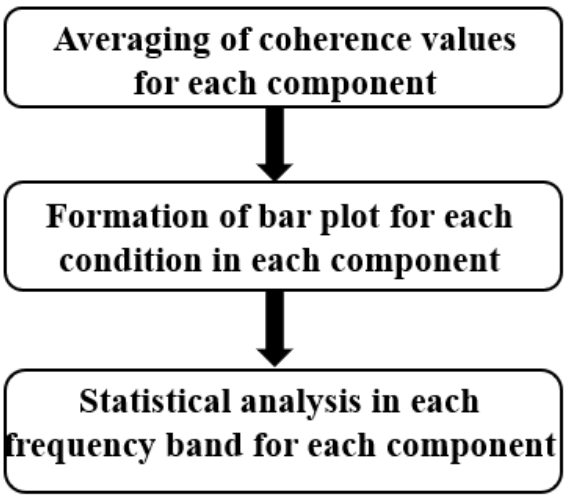

Figure 5.5: Flowchart of the steps in analyzing endogenic, myogenic, and neurogenic components of EEG-FNIRS coherence/coupling.

5.3 Results

5.3.1 EEG-fNIRS coherence in left frontal location for beta band

For beta band, the EEG-FNIRS coherence/coupling in the left frontal location occurred within a frequency range of 0.016 – 0.25 Hz in all three states of voluntary breath-holding (Figure 5.6). For the normal breathing or EO state, the coherence amplitude values showed some intensity

during the time duration (Figure 5.6a). For the short breath-hold or BR1 state, the coherence amplitude values showed less intensity during the time duration (Figure 5.6b). For the longer breath-hold or BR2 state, the coherence amplitude showed greater intensity during the time duration (Figure 5.6c)

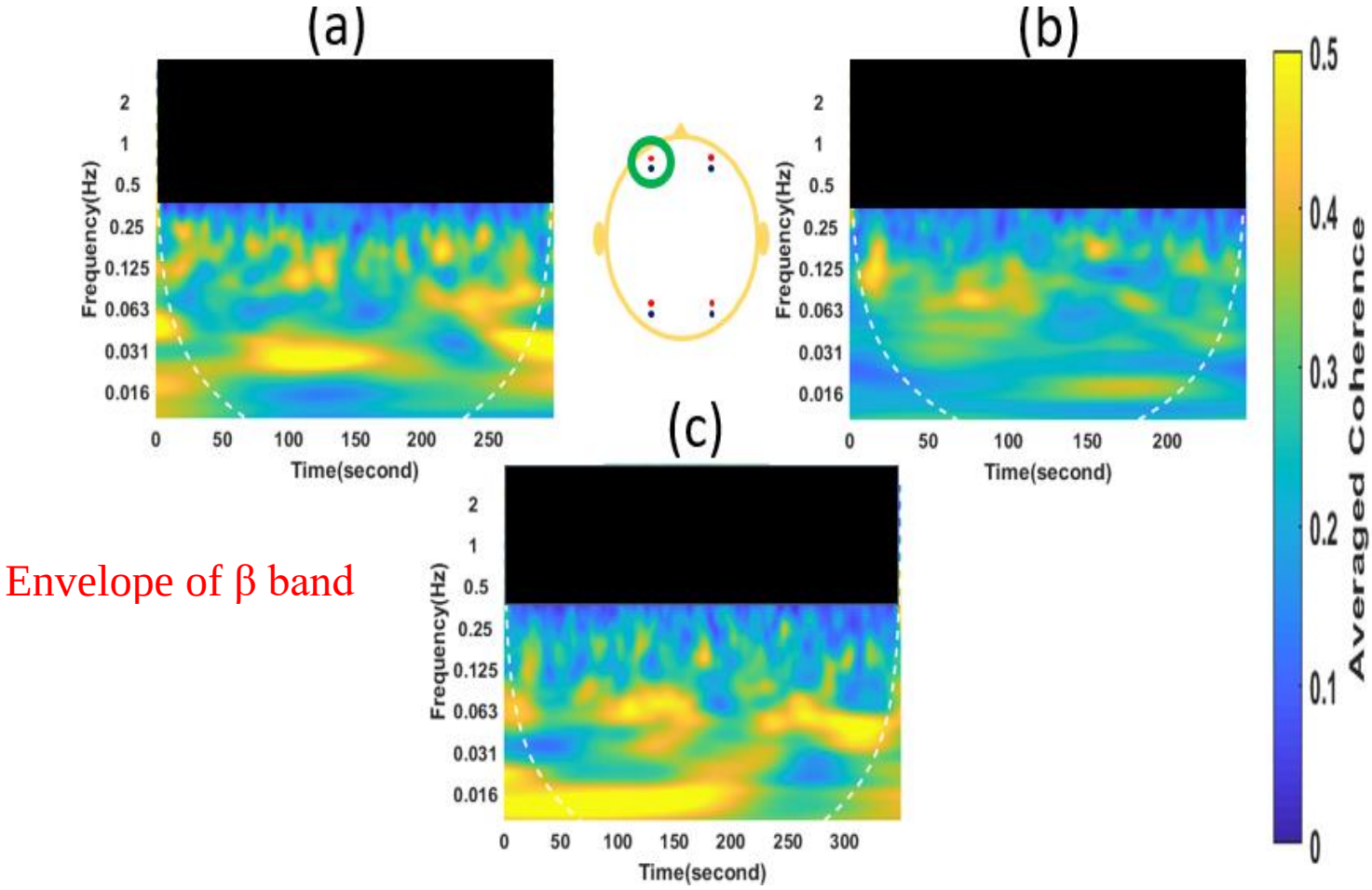

Figure 5.6: Averaged time-frequency coherence maps of beta-band envelope in the left frontal location for (A) normal breathing EO state, (B) short breath-hold or BRI state, and (c) longer breath-hold or BR2 state. The color bar represents the averaged EEG-FNIRS coherence. The cone of influence is shown as areas on the map that are outside the white-colored dashed line. The blacked-out region covers the coherence values generated by noise.

5.3.2 EEG-fNIRS coherence in right occipital location for theta band

For theta band, the EEG-FNIRS coherence in the right occipital location occurred within a frequency range of 0.016 – 0.25 Hz in all three states of voluntary breath-holding (Figure 5.7). For the normal breathing or EO state, the coherence amplitude values showed some bright spots of intensity during the time duration (Figure 5.7a). For the short breath-hold or BR1 state, the coherence amplitude values showed more bright spots of intensity during the time duration (Figure 5.7b). For the longer breath-hold or BR2 state, the coherence amplitude also showed more bright spots of intensity during the time duration (Figure 5.7c)

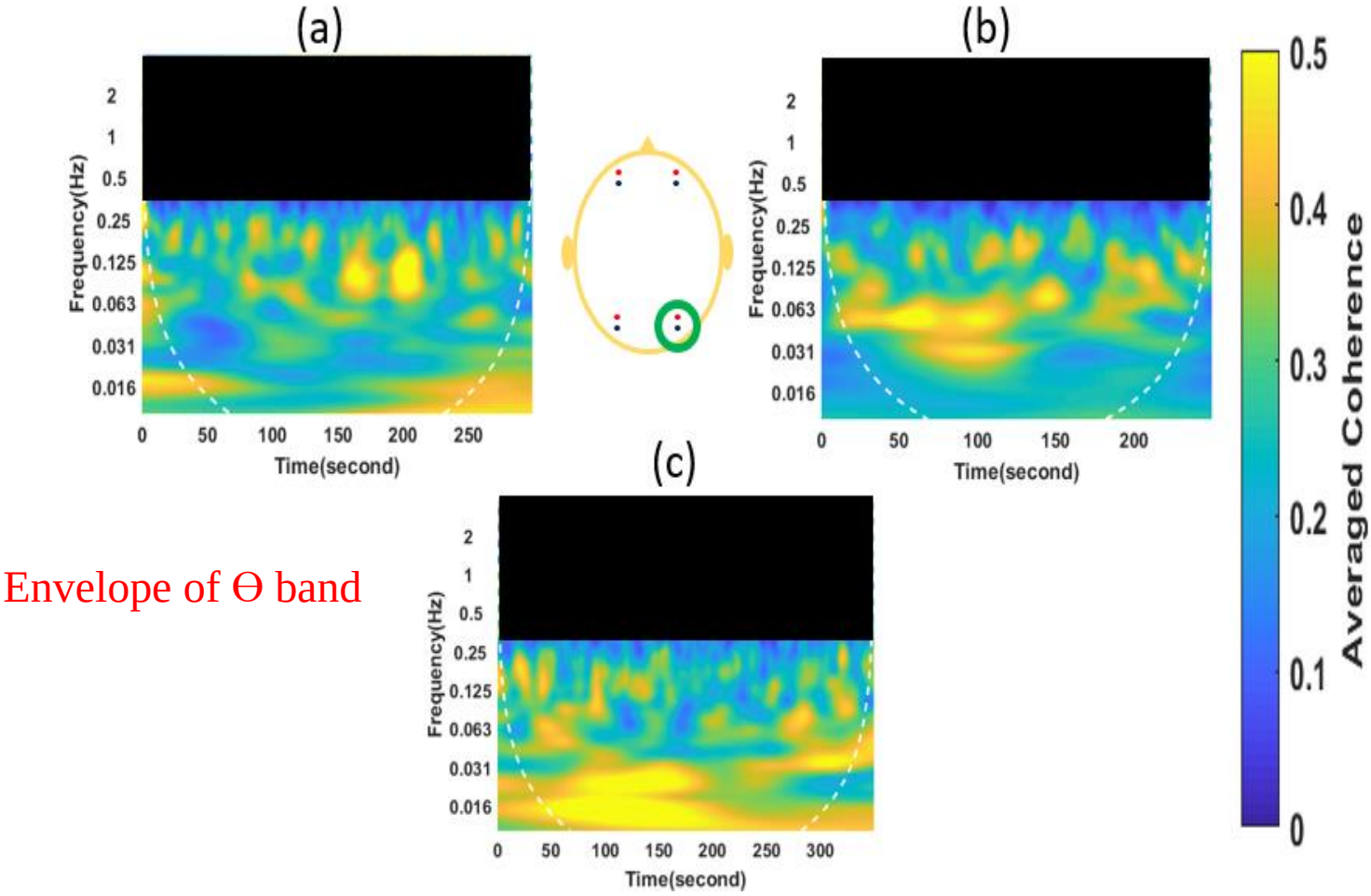

Figure 5.7: Averaged time-frequency coherence maps of theta-band envelope in the right occipital location for (A) normal breathing EO state, (B) short breath-hold or BRI state, and (c) longer breath-hold or BR2 state. The color bar represents the averaged EEG-FNIRS coherence. The cone of influence is shown as areas on the map that are outside the white-colored dashed line. The blacked-out region covers the coherence values generated by noise.

5.3.3 EEG-fNIRS coherence in right occipital location for alpha band

For theta band, the EEG-FNIRS coherence/coupling in the right occipital location occurred within a frequency range of 0.016 – 0.25 Hz in all three states of voluntary breath-holding (Figure 5.8). For normal breathing state, the coherence map showed few bright spots of intensity during the time duration (Figure 5.8a). For the short breath-hold, the coherence map also showed some few bright spots of intensity during the time duration (Figure 5.8b). For the long breath-

hold, the coherence map showed more bright spots of intensity during the time duration (Figure 5.8c).

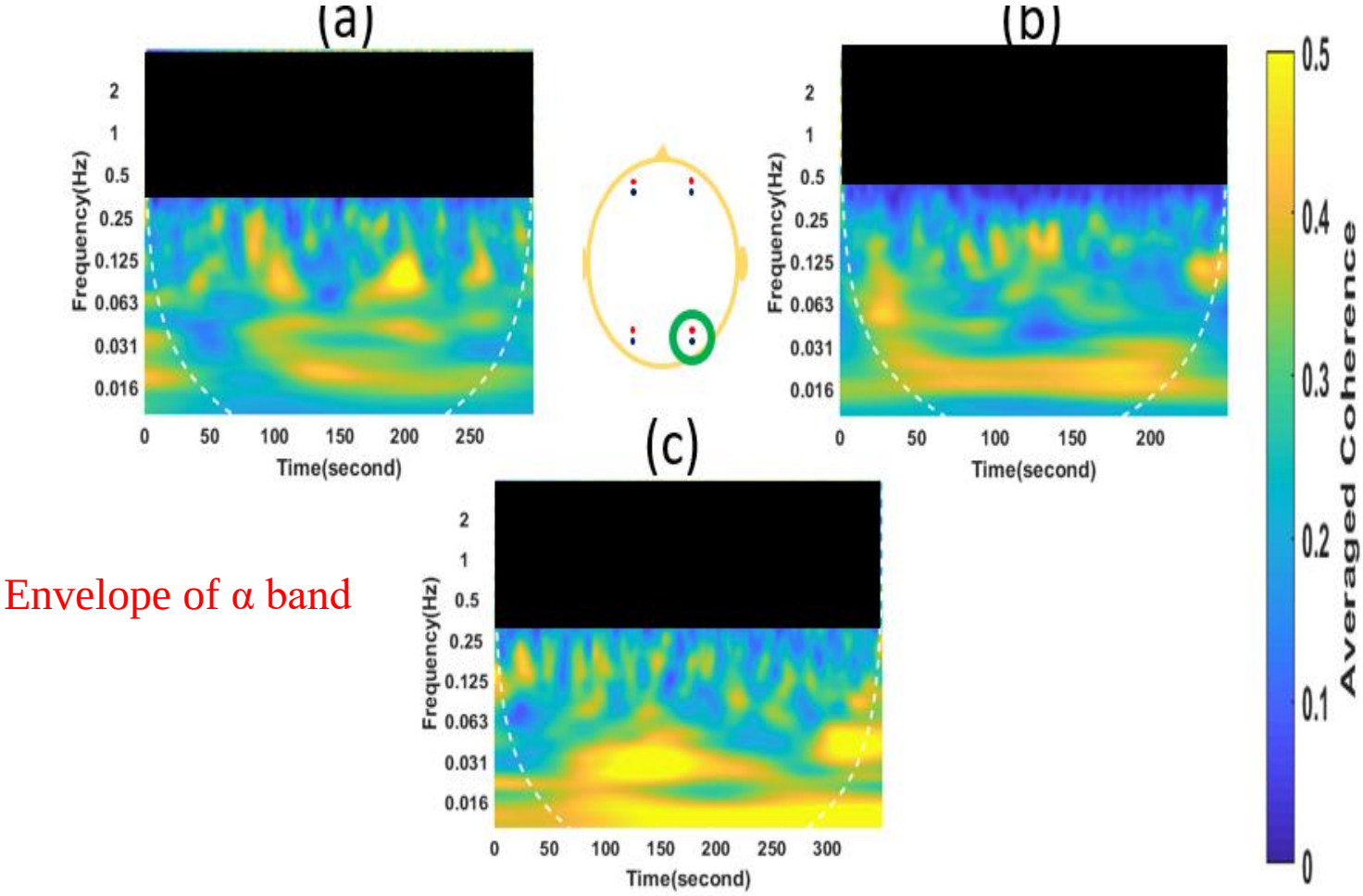

Figure 5.8: Averaged time-frequency coherence maps of alpha-band envelope in the right occipital location for (A) normal breathing EO state, (B) short breath-hold or BRI state, and (c) longer breath-hold or BR2 state. The color bar represents the averaged EEG-FNIRS coherence. The cone of influence is shown as areas on the map that are outside the white-colored dashed line. The blacked-out region covers the coherence values generated by noise.

5.3.4 Endogenic component in left frontal location for beta band

The maps shown in Figure 5.6 were further analyzed using the method shown in Figure 5.5. The analysis revealed that the endogenic component of EEG-fNIRS coherence in the left frontal location for beta band was highest in BR2 state and lowest in EO state (Figure 5.9). Furthermore, ANOVA analysis and subsequent post-hoc test showed that the endogenic component was significantly different between these two states (Figure 5.9)

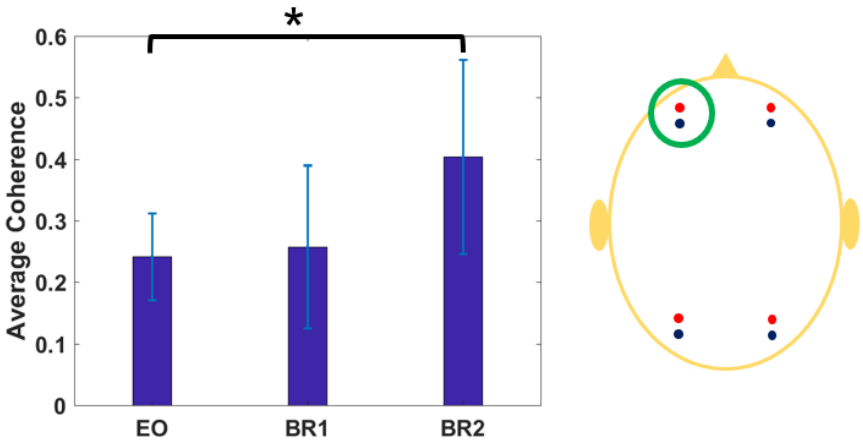

Figure 5.9: Bar plot showing average coherence in endogenic component for beta-band envelope in left frontal location, in three states of eyes-open (EO), short breath-holding (BR1), and longer breath-holding (BR2). The plots marked '*' indicate a significant difference between EO and BR2 states ($p < 0.05$, corrected)

5.3.5 Endogenic component in right occipital location for theta band

The maps shown in Figure 5.7 were further analyzed using the method shown in Figure 5.5. The analysis revealed that the endogenic component of EEG-fNIRS coherence/coupling in the right occipital location for theta band was highest in BR2 state and lowest in BR1 state (Figure 5.10). Furthermore, ANOVA analysis and subsequent post-hoc test showed that the endogenic component was significantly different between the two states (Figure 5.10)

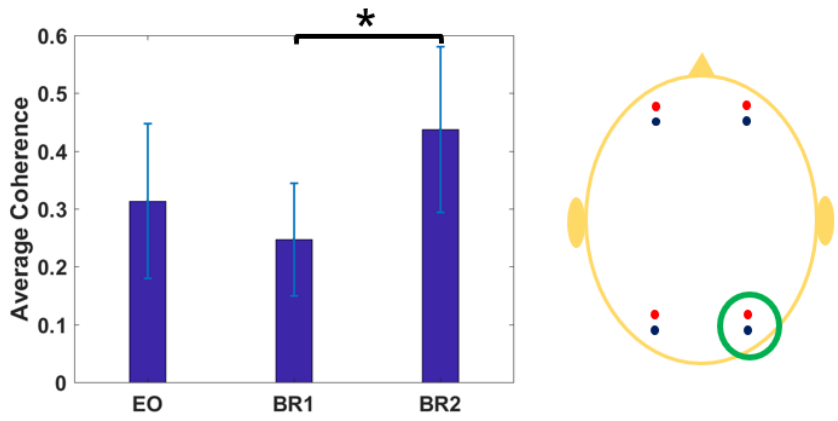

Figure 5.10: Bar plot showing average coherence in endogenic component for theta-band envelope in right occipital location, in three states of eyes-open (EO), short breath-holding (BR1), and longer breath-holding (BR2). The plots marked '*' indicate a significant difference between BR1 and BR2 states ($p < 0.05$, corrected).

5.3.6 Neurogenic component in right occipital location for theta band

The maps shown in Figure 5.7 were further analyzed using the method shown in Figure 5.5. The analysis revealed that the neurogenic component of EEG-fNIRS coherence/coupling in the right occipital location for theta band was highest in BR2 state and lowest in EO state (Figure 5.11). Furthermore, ANOVA analysis and subsequent post-hoc test showed that the neurogenic component was significantly different between these two states (Figure 5.11).

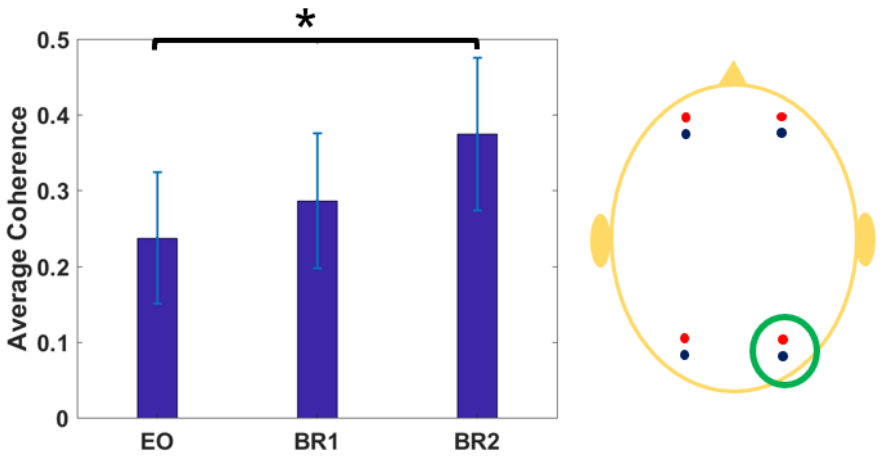

Figure 5.11: Bar plot showing average coherence in neurogenic component for theta-band envelope in right occipital location, in three states of eyes-open (EO), short breath-holding (BR1), and longer breath-holding (BR2). The plots marked '*' indicate a significant difference between EO and BR2 states ($p < 0.05$, corrected)

5.3.7 Endogenic component in right occipital location for alpha band

The maps shown in Figure 5.8 were further analyzed using the method shown in Figure 5.5. The analysis revealed that the endogenic component of EEG-fNIRS coherence in the right occipital location for alpha band was highest in BR2 state and lowest in EO state (Figure 5.12). Furthermore, ANOVA analysis and subsequent post-hoc test showed that the endogenic component was significantly different between these two states (Figure 5.12).

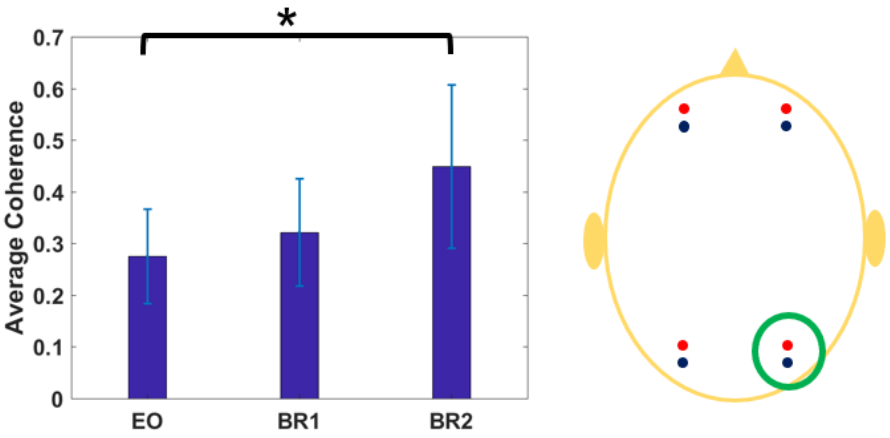

Figure 5.12: Bar plot showing average coherence in endogenic component for alpha-band envelope in right occipital location, in three states of eyes-open (EO), short breath-holding (BR1), and longer breath-holding (BR2). The plots marked '*' indicate a significant difference between EO and BR2 states ($p < 0.05$, corrected).

5.4 Discussion

The aim of this study was to investigate neurovascular coupling in three different states of breath-hold using simultaneous EEG-FNIRS measurements. Data were collected from 8 subjects in three different states of breath-hold namely, normal breathing in eyes-open state (EO), short breath-hold or BR1, and long breath-hold or BR2. Furthermore, the study used wavelet coherence analysis to quantify EEG-FNIRS coupling for each state in four different regions of interest, as shown in Figure 5.4. The study was carried out in compliance with NIH guidelines.

5.4.1 Difference in EEG-fNIRS coupling between EO and BR2 states

A significant difference in EEG-fNIRS coupling between EO and BR2 states was reported in this study. Specifically, the endogenic component of neurovascular coupling was different between these two states in the left frontal location, for beta band (Figure 5.9); and in the right occipital location, for alpha band (Figure 5.12). Also, the neurogenic component of neurovascular coupling was different in these two states at the right occipital location, in theta band (Figure

5.11). These findings of significant difference in EEG-fNIRS coupling between EO and BR2 states indicate that the neurovascular coupling in the brain is significantly altered during longer breath-hold. Specifically, the results show that the neurovascular coupling during the longer breath-hold is increased. A possible explanation for this finding is that during the longer breath-hold, the blood flow to the brain is significantly disrupted, and when normal breathing resumes after the longer breath-hold, the heart supplies a great volume of blood to the brain to compensate for the previous disruption. Because cerebral blood flow is tightly linked to neurovascular coupling, this increased blood flow results in a significant increase in neurovascular coupling. A previous study has shown that there is indeed an increased cerebral blood flow after a period of apnea[86]. Specifically, the study showed that during apnea (long breath-hold), the arterial oxygen content is decreased, hence the need for the body to compensate for this decrement by increasing cerebral blood flow to maintain cerebral delivery of oxygen to the neurons in the brain[86]. Furthermore, from the findings of this study, it is speculated that the endogenic component of neurovascular coupling is significantly altered during voluntary breath-holding. A previous study has shown that there is significant endothelial dysfunction in obstructive sleep apnea disease[85]. The findings here therefore show the significance of endothelial function in neurovascular coupling during breath-holding. The change in neurogenic component should be interpreted with caution, as it was reported in only one site (Figure 5.11). Also, the findings show that the changes in coupling between EO and BR2 are in theta, alpha, and beta frequency bands (Figures 5.9-5.12). A study has reported changes in beta rhythm for sleep apnea patients[87]. Theta and alpha bands are active in wakeful resting-states of the brain, which was the condition of the subjects when the study was conducted. Hence, the theta and alpha bands may indicate that the subjects were in resting-state condition.

5.4.2 Difference in EEG-fNIRS coupling between BR1 and BR2 states

A significant difference of neurovascular coupling strength between BR1 and BR2 state was also reported in this study. This was reported in only one location in theta band (Figure 5.10). This finding could be explained as follows: during short voluntary breath-hold, the amount of compensation needed in the form of increased blood flow is not as much as during longer breath-hold. So, there is more blood flow to the brain after a period of long breath-hold compared to a period of short breath-hold. This results in a higher neurovascular coupling for longer breath-hold than for shorter breath-hold. However, the findings here should also be interpreted with some caution, as this result was not obtained at the other three brain sites.

5.4.3 Limitations

A possible limitation of this study could be the placement of the EEG electrodes on the scalp; they were not placed according to the standard 10-10 or 10-20 system of EEG electrode placement. Also, it is possible that repeated measures ANOVA may provide better statistical results than the one-way ANOVA test that was used in this study.

5.5 Conclusion

Conclusively, this study has reported a significant increase in neurovascular coupling strength in longer periods of voluntary breath-holding compared to periods of normal breathing/rest. This is because, after a longer period of breath-hold, there is a resulting increase in cerebral blood flow to compensate for the decrease in oxygen in the brain, and this result in an increased neurovascular coupling.

CHAPTER 6

6. SUMMARY AND FUTURE WORK

6.1 Summary

My doctoral research work was divided into 3 aims. In Aim 1a, I investigated resting-state EEG functional connectivity at the source level using ELORETA-ICA method. This study was performed to replicate the results of previous work by Aoki et al, and to show the feasibility of ELORETA-ICA method as a tool for EEG functional connectivity analyses. The results of this study were reported in Chapter 2. For Aim 1b, I investigated EEG functional connectivity at the sensor-level in four different vigilance states (eyes-open, eyes-closed, sleep-stage 1, and sleep-stage 2) using graph theory analysis. The results of this study were reported in Chapter 3. In Aim 2, I investigated neurovascular coupling in three different vigilance states (eyes-open, eyes-closed, and sleep-stage 1) using wavelet coherence method. In Aim 3, I investigated neurovascular coupling in three separate periods of voluntary breath-holding (normal breathing, short-period breath-holding, and long-period breath-holding). In addition, 3 frequency components of neurovascular coupling, which were the endogenic (0.01 – 0.02 Hz), neurogenic (0.02 – 0.04 Hz), and myogenic components (0.04 – 0.15 Hz) were quantified for each vigilance state/breath-hold state in each of three EEG frequency bands of theta, alpha, and beta. Furthermore, the neurovascular coupling of the brain for each vigilance state/breath-hold was investigated in four separate brain locations (Figs. 4.3 & 5.4). The study on neurovascular coupling in different vigilance states and in voluntary breath-holding are reported in Chapters 4 & 5 respectively.

In the study of functional connectivity in resting-state, I identified four separate resting state networks and their associated frequency bands from 64-channel EEG data (Figs. 2.4 – 2.7). In

addition, I identified two resting-state networks and their associated frequency bands from 19-channel EEG (Figs. 2,4 – 2.7). The results here indicated that more resting-state networks can be identified from EEG data obtained using many channels (64 channels) compared to EEG data obtained using fewer channels (19 channels). In addition, the results here indicated that EEG modality provides a cheaper and easier alternative of investigating functional connectivity compared to other conventional methods such as FMRI. In the study of functional connectivity in different vigilance states, I reported a decrease in functional segregation (global clustering coefficient) from wakeful states (both eyes-open and eyes-closed state) to sleep states (both sleep-stage 1 and sleep-stage 2) majorly in alpha and beta bands (Fig. 3.4c&d). Also, I reported an increase in functional integration (global efficiency) from wakeful states (both eyes-open and eyes-closed state) to sleep state (both sleep-stage 1 and sleep-stage 2), majorly in alpha and beta bands (Figs 3.5c&d). Also, I reported an increase in nodal clustering coefficient at frontal electrodes from eyes-open to eyes-closed state for alpha and beta bands, with no significant change reported in sleep-stage 1 (Figs 3.6a&b); and a decrease in nodal global efficiency from eyes-open to eyes-closed state for alpha and beta bands, with no significant change reported in sleep-stage 1 (Figs 3.7a&b). Overall, the results here indicated significant alterations in functional connectivity for both the anterior and posterior portions of the default mode network during the transition from awake to sleep states. Thus, this study provides some evidence to support the role of the default-mode brain network in regulating consciousness in the brain.

For neurovascular coupling study in different vigilance states, I reported a significant increase ($p < 0.05$, Tukey-corrected) of endogenic frequency component for alpha band envelope in eyes-closed state compared to eyes-open state at two separate regions of interest (Figs.4.9 & 4.12). Also, I reported a significant increase ($p < 0.05$, Tukey-corrected) of endogenic frequency

component for alpha band envelope in sleep-stage 1 compared to both eyes-open and eyes-closed state at one region of interest (Fig. 4.11). In addition, I reported a significant increase ($p < 0.05$, Tukey-corrected) of myogenic frequency component for theta-band envelope in sleep-stage 1 compared to eyes-open state (Fig. 4.10). These results indicated a significant increase of neurovascular coupling strength during sleep states compared to wakeful/awake state. Also, the results here indicated/suggested that endogenic and myogenic oscillations during neurovascular coupling are significant biomarkers of consciousness in the brain. For neurovascular coupling during voluntary breath-holding, I reported a significant increase ($p < 0.05$, Tukey-corrected) of endogenic component for beta band envelope in long-period breath-hold compared to normal breathing at one region of interest (Fig. 5.9). Also, I reported a significant increase ($p < 0.05$, Tukey-corrected) of neurogenic component for theta-band envelope in long-period breath-hold compared to normal breathing at another location (Fig. 5.11). At this same location, I reported a significant increase ($p < 0.05$, Tukey-corrected) of endogenic component for theta band envelope in long-period breath-hold compared to short-period breath-hold (Fig. 5.10). Finally, I reported a significant increase ($p < 0.05$, Tukey-corrected) of endogenic component for alpha band envelope in long-period breath-hold compared to normal breathing at the same location as the previous two just mentioned (Fig 5.12). These results indicated/suggested a significant increase of neurovascular coupling strength in long periods of breath-holding compared to short breath-holding and normal breathing. This may be indicative of higher metabolic demand during longer breath-hold which causes an increase of blood flow thereby resulting in stronger neurovascular coupling.

6.2 Limitations and Future work

6.2.1 ELORETA-ICA study

For the ELORETA-ICA study, my results did not fully match shown by the previous study of ELORETA-ICA by Aoki et al (see Table 2.1). This could be due to the low sample size; the previous study used 80 subjects. In addition, a lower statistical threshold (z-score of 2) was used in my ELORETA-ICA study, which may have significantly impacted the results. Therefore, future work is suggested to:

(i) collect data from a larger number of subjects to improve the statistical power of the results of ELORETA-ICA analysis. A sample size of 80 is suggested to match the methods of the previous work,

(ii) implement a proper cross validation of the ELORETA regularization parameter to establish an optimal value for meaningful EEG source reconstruction before implementation of ELORETA-ICA method.

6.2.2 Neurovascular coupling study

The study on neurovascular coupling did not yield completely satisfactory results. Specifically, for the study of neurovascular coupling in different vigilance states, I reported only 5 positive results out of a possible 108 cases (Fig A.3). In addition, for the study of neurovascular coupling in breath-holding, I reported only 4 positive results out of a possible 108 cases (Fig A.4). These results could be attributed to the small duration of the data used for the neurovascular coupling study. In previous studies, wavelet coherence method was applied to data with a much longer duration [13]. Hence, in future work,

(i) Simultaneous EEG-FNIRS data should be collected for a much longer duration, especially for sleep study. In sleep studies, a longer duration of data may be required to properly observe brain dynamics during sleep [13].

(ii) a proper statistical model such as a generalized linear model may be more appropriate for the analysis of the time-frequency results of neurovascular coupling.

(iii) the neurovascular coupling analysis could be performed using a source-level analysis to improve the localization accuracy of the simultaneous EEG-fNIRS measurements. For this, an EEG reconstruction algorithm such as ELORETA could be combined with diffuse optical tomography algorithm and digitizer measurements to accurately reconstruct the simultaneous EEG-fNIRS data, before performing neurovascular coupling analysis.

A. Appendix

A1. Graph Theory Analysis: Definition

Graph Theory Analysis is a mathematical method that is used to describe functional connectivity of brain networks. In graph theory analysis, a network is comprised of vertices and edges (Fig. A1). For EEG functional connectivity analyses, nodes represent EEG electrodes and edges represent connectivity strengths between different pairs of EEG electrodes [58]

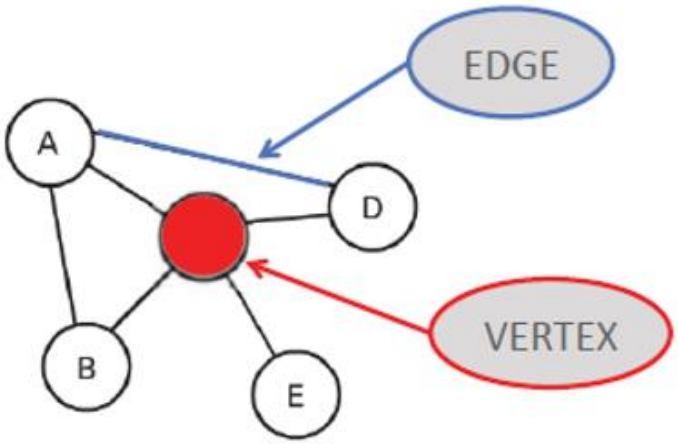

Figure A.1: A diagram of a network represented as a graph containing vertex and edge.

Graph theory analysis uses several metrics to quantify functional connectivity. Four of these metrics were utilized in the analysis of EEG functional connectivity in different vigilance states from wakeful state to sleep state. The subsequent subheadings describe each of these metrics and their mathematical formula.

A1.1 Nodal clustering coefficient

The nodal clustering coefficient of a specific EEG electrode describes how that electrode is connected to its neighbors. For example, an electrode with a high nodal clustering coefficient

indicates that this electrode and its neighbors form a cluster within the whole network. Likewise, an electrode with a low clustering coefficient indicates that this electrode is not well connected with its neighboring electrodes. In addition, a nodal clustering coefficient map shows the clustering coefficient of each node.

For an EEG electrode *i*, the nodal clustering coefficient is the proportion of electrodes that are connected to *i* which are also connected with each other. It is represented as a fraction: the denominator is the number of vertices which have edges to electrode *i*, while the numerator is the number of these vertices that are connected to each other. Mathematically, the nodal clustering coefficient, C_i is given by [62]:

$$\boldsymbol{C_i = \frac{no\ of\ connected\ adjacent\ vertices\ of\ node\ i}{total\ no\ of\ edges\ of\ node\ i}} \qquad \text{(I)}$$

Where *i* refers to each EEG electrode,
C_i is the nodal clustering coefficient for EEG electrode i,

A1.2 Global clustering coefficient

The global clustering coefficient is the average of the nodal clustering coefficients for all vertices of a network. Mathematically, it is given as [62]

$$\mathbf{C} = \frac{\mathbf{1}}{\boldsymbol{N}} \sum_{\boldsymbol{i=1}}^{\boldsymbol{N}} \boldsymbol{C_i} \qquad \text{(II)}$$

Where C_i is the nodal clustering coefficient for each electrode;
N is the number of electrodes

A1.3 Global efficiency

Global efficiency is a measure of the functional integration within a network. An electrode with a high global efficiency indicates that information is readily passed across the network, and vice versa. In addition, a global efficiency map displays hubs of information flow within a network. Global efficiency is calculated from path length. The path length between two vertices is defined as the minimum number of edges that must be passed through from one vertex to another [58]. The global efficiency is the inverse of the minimum path length between each pair of nodes. Mathematically, the global efficiency is calculated as follows [62]:

$$\boldsymbol{E_g = \frac{1}{N(N-1)} \sum_{i,j \in N, i \neq j} \frac{1}{d_{i,j}}} \qquad \text{(III)}$$

Where E_g is the global efficiency,

N is the number of electrodes,

d_{ij} is the path length between electrode pairs i and j

A1.4 Nodal efficiency

The nodal efficiency is the global efficiency at each vertex or electrode i. It is defined as the inverse of the path length between a vertex i and all other vertices in the network. Mathematically, this is given as [62]:

$$\boldsymbol{E_{nodal} = \frac{1}{(N-1)} \sum_{J \in N} \frac{1}{d_{i,j}}} \qquad \text{(IV)}$$

Where N is number of electrodes

d_{ij} is the path length distance between electrode pairs i and j

A1.5 Graph Theory Example

Consider the network shown in Fig.A2. It has 5 nodes or vertices which are labelled A, B, C, D, and E. Also, it has 6 edges or links (number of blue lines)

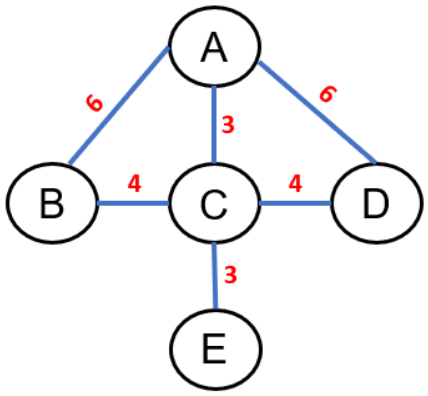

Figure A.2: A network graph consisting of 5 vertices A, B, C, D, and E. The edges of the network are represented as blue lines which connect one vertex to another. Numbers on the edges represent the distance (path length) from one vertex to another.

Graph metrics of the network shown in Fig. A2 are obtained using equations 1 to IV as follows:

Nodal clustering coefficient $C_A = {}^{2}/_{3}$

Nodal clustering coefficient $C_B = {}^{2}/_{2} = 1$

Nodal clustering coefficient $C_C = {}^{2}/_{4}$

Nodal clustering coefficient $C_D = {}^{2}/_{2} = 1$

Nodal clustering coefficient $C_E = 0$

Global clustering coefficient of whole network, $C = \frac{{}^{2}/_{3}+{}^{2}/_{2}+{}^{2}/_{4}+{}^{2}/_{2}+0}{5} = \mathbf{0.63}$

Nodal efficiency for node A = $\left.\frac{1}{6}+\frac{1}{6}+\frac{1}{3}+\frac{1}{6}\right/_{4}$ = 0.69

Nodal efficiency for node B = $\left.\frac{1}{6}+\frac{1}{4}+\frac{1}{7}+\frac{1}{8}\right/_{4}$ = 0.17

Nodal efficiency for node C = $\frac{\frac{1}{3}+\frac{1}{3}+\frac{1}{4}+\frac{1}{4}}{4}$ = 0.29

Nodal efficiency for node D = $\frac{\frac{1}{4}+\frac{1}{6}+\frac{1}{7}+\frac{1}{8}}{4}$ = 0.17

Nodal efficiency for node E = $\frac{\frac{1}{3}+\frac{1}{6}+\frac{1}{7}+\frac{1}{7}}{4}$ = 0.19

Global efficiency of network = $\frac{0.81+0.675+1.16+0.675+0.77}{5(5-1)} = 0.2045$

A1.6 Statistical analysis of binary thresholds

The statistical significance of each of the binary thresholds used in the graph theory analysis study (Chapter 3) was tested for each frequency band that was analyzed. Firstly, the correlation maps in each frequency band were averaged across all subjects. Then, the averaged correlation map in each frequency band was thresholded in a binary form using each of the thresholds from 0.1 to 0.9 in increments of 0.1. At each threshold, the remaining edges were normalized using Fisher transform. Then, the normalized edges were tested for statistical significance using a one-sample t-test ($p < 0.05$). Table A.1 shows the results of the significance testing for each threshold in each of the frequency bands. This analysis was performed for the maps in the eyes-open resting state condition (EO) only.

Table A.1: Significance testing of binary thresholds from 0.1 to 0.9 in graph theory analysis study. Spaces marked '*' indicate retention of significant edges/connections ($p < 0.05$) for the associated frequency band. Spaces marked blank indicate no significant edges were retained at this threshold. Numbers enclosed in brackets indicate the number of surviving edges/connections after binary thresholding. The frequency bands are delta (δ), theta (Θ), alpha (α), and beta (β).

	0.1	0.2	0.3	0.4	0.5	0.6	0.7	0.8	0.9
δ	* (1481)	* (922)	* (552)	* (273)	* (108)	* (46)	* (6)		
Θ	* (1923)	* (1114)	* (722)	* (416)	* (190)	* (91)	*(32)	* (3)	
α	* (2016)	* (1978)	* (1261)	* (787)	* (439)	* (219)	*(94)	* (23)	
β	* (2010)	* (1274)	* (782)	* (428)	* (218)	* (115)	*(34)	* (4)	

A1.7 MATLAB code for repeated measures ANOVA analysis of graph theory metrics

```
%% Global Clustering coefficient: repeated anova model
clear;
clc;
load ('beta_gta.mat','Cp_eo','Cp_ec','Cp_ss1','Cp_ss2');
x = [1,11,21,31,41,51,61,71,81];
for i = 1:length(x)
   group = [Cp_eo(:,x(i)); Cp_ec(:,x(i));Cp_ss1(:,x(i));Cp_ss2(:,x(i))];
   COND =
{'EO';'EO';'EO';'EO';'EO';'EO';'EO';'EO';'EO';'EO';'EO';'EO';'EO';'EO';'EO';'EO';...
   'EC';'EC';'EC';'EC';'EC';'EC';'EC';'EC';'EC';'EC';'EC';'EC';'EC';'EC';'EC';'EC';...

'SS1';'SS1';'SS1';'SS1';'SS1';'SS1';'SS1';'SS1';'SS1';'SS1';'SS1';'SS1';'SS2';'SS2';'SS2';'SS2';'
SS2';'SS2';'SS2'};

t = table(COND, group,group,group,group,'VariableNames',[88'group3','group4']);

Meas = dataset([1 2 3 4]','VarNames',{'Measurements'});

rm = fitrm(t,'group1-group4~condition','WithinDesign',Meas);
ranovatb1 = ranova(rm);

tbl = multcompare(rm,'condition');

save([num2str(x(i)) 'cp'],'ranovatb1','tbl');
end

%% Global efficiency: repeated anova model
clear;
clc;
load ('beta_gta.mat','Eg_eo','Eg_ec','Eg_ss1','Eg_ss2');
x = [1,11,21,31,41,51,61,71,81];
for i = 1:length(x)
group = [Eg_eo(:,x(i)); Eg_ec(:,x(i));Eg_ss1(:,x(i));Eg_ss2(:,x(i))];
%group = group';

COND =
{'EO';'EO';'EO';'EO';'EO';'EO';'EO';'EO';'EO';'EO';'EO';'EO';'EO';'EO';'EO';'EO';'EO';...
   'EC';'EC';'EC';'EC';'EC';'EC';'EC';'EC';'EC';'EC';'EC';'EC';'EC';'EC';'EC';'EC';'EC';...

'SS1';'SS1';'SS1';'SS1';'SS1';'SS1';'SS1';'SS1';'SS1';'SS1';'SS1';'SS1';'SS2';'SS2';'SS2';'SS2';'
SS2';'SS2';'SS2'};
```

```
t =
table(COND,group,group,group,group,'VariableNames',{'condition','group1','group2','group3','
group4'});

Meas = dataset([1 2 3 4]','VarNames',{'Measurements'});

rm = fitrm(t,'group1-group4~condition','WithinDesign',Meas);
ranovatb1 = ranova(rm);

tbl = multcompare(rm,'condition');

save([num2str(x(i)) 'eg'],'ranovatb1','tbl');
end
%% fitting the repeated anova model

for j = 1:64
   group = [EO(j,:), EC(j,:), SS1(j,:), SS2(j,:)];
   group = group';

COND =
{'EO';'EO';'EO';'EO';'EO';'EO';'EO';'EO';'EO';'EO';'EO';'EO';'EO';'EO';'EO';'EO';'EO';...
   'EC';'EC';'EC';'EC';'EC';'EC';'EC';'EC';'EC';'EC';'EC';'EC';'EC';'EC';'EC';'EC';'EC';...

'SS1';'SS1';'SS1';'SS1';'SS1';'SS1';'SS1';'SS1';'SS1';'SS1';'SS1';'SS1';'SS2';'SS2';'SS2';'SS2';'
SS2';'SS2';'SS2'};


t =
table(COND,group,group,group,group,'VariableNames',{'condition','group1','group2','group3','
group4'});

Meas = dataset([1 2 3 4]','VarNames',{'Measurements'});

rm = fitrm(t,'group1-group4~condition','WithinDesign',Meas);
ranovatb1 = ranova(rm);

tbl = multcompare(rm,'condition');

save([num2str(j) 'nodalEg_0.7.mat'],'ranovatb1','tbl');
end
```

A1.8 MATLAB code for detecting statistical significance of graph network thresholds

```
%%
clear;
clc;

rho_delt =zeros(64,64,18);
rho_thet =zeros(64,64,18);
rho_alph =zeros(64,64,18);
rho_beta =zeros(64,64,18);

for j = 1:18
   load (['delta' num2str(j) '_eo']);
   load (['theta' num2str(j) '_eo']);
   load (['alpha' num2str(j) '_eo']);
   load (['beta' num2str(j) '_eo']);

   rho_delt(:,:,j) = rho_d;
   rho_thet(:,:,j) = rho_t;
   rho_alph(:,:,j) = rho_a;
   rho_beta(:,:,j) = rho_b;
end

avg_delt_eo = mean(rho_delt,3);
avg_thet_eo = mean(rho_thet,3);
avg_alph_eo = mean(rho_alph,3);
avg_beta_eo = mean(rho_beta,3);
%%
clear
load avg_eo_corr avg_beta_eo

thr = 0.1:0.1:0.9;

for x = 1:64
   for y = 1:64
      if avg_beta_eo(x,y) < thr(9)
         avg_beta_eo(x,y) = 0;
      end
   end
end

X = triu(avg_beta_eo,1);
X = X(:);
X = nonzeros(X);
X_fz = 0.5 .* log((1+X)./(1-X));
h = ttest(X_fz);
```

A2 Hilbert Transform calculation for envelope

The Hilbert transform can be used to calculate the envelope of a signal. The envelope of a signal contains the slowly varying features of the signal. The Hilbert transform calculates the analytic signal, from which the envelope can be derived.

For EEG data, an EEG signal has the following mathematical representation [58]:

$$\boldsymbol{E = M\cos(2\pi ft)} \quad \text{(V)}$$

Where M is amplitude, f is frequency in Hertz, and t is time in seconds. Equation (V) indicates that EEG signals contain only a cosine component. The cosine component is a real number with no imaginary part. Hilbert transform adds a quarter-cycle component to the cosine component to form a complex signal. Thus, using Hilbert transform, equation (v) becomes [58]:

$$\boldsymbol{E_a = M\cos 2\pi ft + jM\sin 2\pi ft} \quad \text{(VI)}$$

In equation (VI), a complex imaginary component is added to the real signal to form a complex signal. The resulting complex signal is known as the analytic signal. Then, the analytic envelope, E_v, is calculated from the analytic signal as follows [58]:

$$\boldsymbol{E_v = abs(E_a)} \quad \text{(VII)}$$

The function "abs" returns the magnitude of the analytic signal. The Hilbert transform of EEG signals was calculated using the "Hilbert" function in MATLAB software.

A3.1 Results of neurovascular coupling in different vigilance states

(a)

	Endo			Neuro			Myo		
	θ	α	β	θ	α	β	θ	α	β
EO-EC	×	✓	×	×	×	×	×	×	×
EO-SS1	×	×	×	×	×	×	✓	×	×
EC-SS1	×	×	×	×	×	×	×	×	×

(b)

	Endo			Neuro			Myo		
	θ	α	β	θ	α	β	θ	α	β
EO-EC	×	×	×	×	×	×	×	×	×
EO-SS1	×	×	×	×	×	×	×	×	×
EC-SS1	×	×	×	×	×	×	×	×	×

(c)

	Endo			Neuro			Myo		
	θ	α	β	θ	α	β	θ	α	β
EO-EC	×	×	×	×	×	×	×	×	×
EO-SS1	×	✓	×	×	×	×	×	×	×
EC-SS1	×	✓	×	×	×	×	×	×	×

(d)

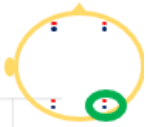

	Endo			Neuro			Myo		
	θ	α	β	θ	α	β	θ	α	β
EO-EC	×	✓	×	×	×	×	×	×	×
EO-SS1	×	×	×	×	×	×	×	×	×
EC-SS1	×	×	×	×	×	×	×	×	×

Figure A.3: Results of neurovascular coupling in vigilance states. Spaces marked 'x' indicate that no change was reported between vigilance states for the specific frequency component. Spaces marked '✓' indicate that a significant difference was reported between vigilance states for the specific frequency component. The frequency components are labelled as 'Endo' for endogenic component; 'Neuro' for neurogenic component; and 'Myo' for myogenic component. The vigilance states are labelled as 'EO-EC' for eyes-open compared with eyes-closed state; 'EO-SS1' for eyes-open compared with sleep-stage 1; and 'EC-SS1' for eyes-closed state compared with sleep-stage 1. The four separate regions of interest are (a) left frontal (b) right frontal; (c) left occipital; and (d) right occipital. Also, EEG frequency bands are represented as 'Θ' for theta band envelope; 'α' for alpha band envelope; and 'β' for beta band envelope.

A3.2 Results of neurovascular coupling in different breath-holding states

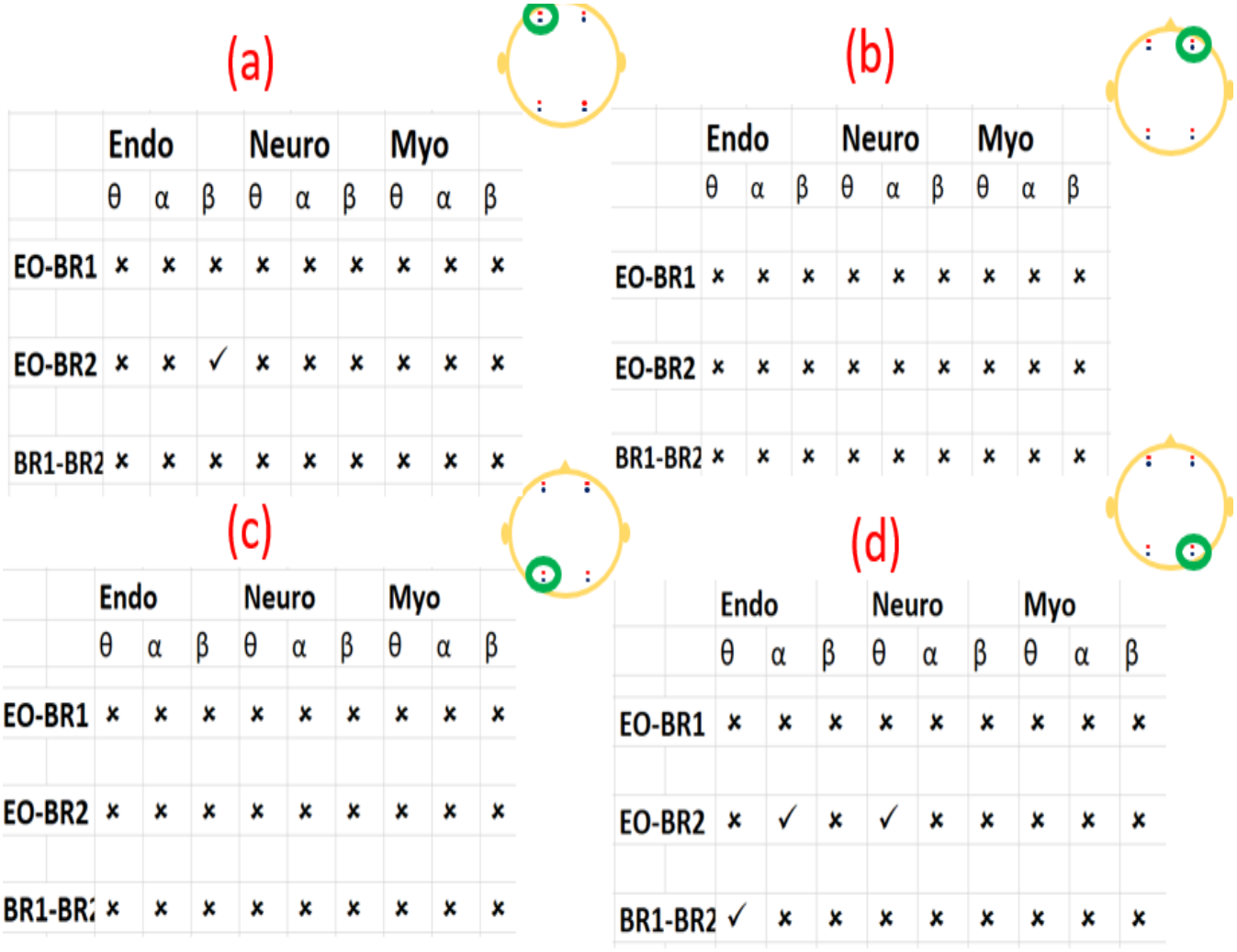

(a)

	Endo			Neuro			Myo		
	θ	α	β	θ	α	β	θ	α	β
EO-BR1	×	×	×	×	×	×	×	×	×
EO-BR2	×	×	✓	×	×	×	×	×	×
BR1-BR2	×	×	×	×	×	×	×	×	×

(b)

	Endo			Neuro			Myo		
	θ	α	β	θ	α	β	θ	α	β
EO-BR1	×	×	×	×	×	×	×	×	×
EO-BR2	×	×	×	×	×	×	×	×	×
BR1-BR2	×	×	×	×	×	×	×	×	×

(c)

	Endo			Neuro			Myo		
	θ	α	β	θ	α	β	θ	α	β
EO-BR1	×	×	×	×	×	×	×	×	×
EO-BR2	×	×	×	×	×	×	×	×	×
BR1-BR2	×	×	×	×	×	×	×	×	×

(d)

	Endo			Neuro			Myo		
	θ	α	β	θ	α	β	θ	α	β
EO-BR1	×	×	×	×	×	×	×	×	×
EO-BR2	×	✓	×	✓	×	×	×	×	×
BR1-BR2	✓	×	×	×	×	×	×	×	×

Figure A.4: Results of neurovascular coupling in breath-hold states. Spaces marked 'x' indicate that no change was reported between breath-holding states for the specific frequency component. Spaces marked '✓' indicate that a significant difference was reported between breath-holding states for the specific frequency component. The frequency components are labelled as 'Endo' for endogenic component; 'Neuro' for neurogenic component; and 'Myo' for myogenic component. The breath-holding states are labelled as 'EO – BR1' for eyes -open compared with short-period breath-hold; 'EO – BR2' for eyes-open compared with long-period breath-hold; and 'BR1 – BR2' for short-period breath-hold compared with long-period breath-hold. The four regions of interest are (a) left frontal (b) right frontal (c) left occipital, and (d) right occipital. Also, EEG frequency bands are represented as 'Θ' for theta-band envelope; 'α' for alpha-band envelope; and 'β' for beta-band envelope.

A3.3 Neurovascular coupling in different vigilance states (more results)

(a)

	Endo			Neuro			Myo		
	θ	α	β	θ	α	β	θ	α	β
EO	0.33	0.28	0.28	0.28	0.32	0.34	0.28	0.3	0.31
EC	0.37	0.39	0.36	0.29	0.28	0.31	0.33	0.3	0.29
SS1	0.48	0.44	0.42	0.35	0.34	0.33	0.34	0.29	0.3

(b)

	Endo			Neuro			Myo		
	θ	α	β	θ	α	β	θ	α	β
EO	0.34	0.3	0.28	0.3	0.31	0.32	0.3	0.3	0.31
EC	0.37	0.36	0.34	0.31	0.33	0.34	0.31	0.31	0.3
SS1	0.44	0.4	0.37	0.27	0.35	0.34	0.34	0.28	0.32

(c)

	Endo			Neuro			Myo		
	θ	α	β	θ	α	β	θ	α	β
EO	0.32	0.28	0.31	0.31	0.32	0.31	0.3	0.32	0.31
EC	0.32	0.37	0.38	0.34	0.3	0.31	0.28	0.33	0.31
SS1	0.35	0.5	0.49	0.34	0.34	0.37	0.32	0.3	0.32

(d)

	Endo			Neuro			Myo		
	θ	α	β	θ	α	β	θ	α	β
EO	0.31	0.29	0.33	0.25	0.3	0.3	0.25	0.3	0.31
EC	0.37	0.41	0.35	0.32	0.33	0.34	0.33	0.28	0.28
SS1	0.32	0.42	0.42	0.3	0.39	0.37	0.35	0.3	0.32

Figure A.5: Values of average coherence amplitude for eyes-open (EO), eyes-closed (EC), and sleep-stage 1 (SS1) vigilance states in endogenic, neurogenic, and myogenic components of neurovascular coupling, for each of theta (δ), alpha (α), and beta (β) bands, at (a) left frontal, (b) right frontal, (c) left occipital, and (d) right occipital locations

A3.4 Neurovascular coupling in breath-holding (more results)

(a)

	Endo			Neuro			Myo		
	θ	α	β	θ	α	β	θ	α	β
EO	0.31	0.27	0.28	0.27	0.31	0.33	0.28	0.31	0.33
BR1	0.34	0.24	0.25	0.3	0.26	0.24	0.29	0.28	0.29
BR2	0.35	0.38	0.41	0.31	0.3	0.31	0.29	0.3	0.32

(b)

	Endo			Neuro			Myo		
	θ	α	β	θ	α	β	θ	α	β
EO	0.34	0.3	0.31	0.28	0.31	0.3	0.31	0.32	0.33
BR1	0.28	0.23	0.29	0.31	0.28	0.3	0.29	0.29	0.29
BR2	0.35	0.37	0.35	0.32	0.27	0.28	0.29	0.29	0.3

(c)

	Endo			Neuro			Myo		
	θ	α	β	θ	α	β	θ	α	β
EO	0.3	0.32	0.31	0.31	0.38	0.34	0.31	0.32	0.31
BR1	0.25	0.26	0.35	0.31	0.27	0.29	0.31	0.27	0.27
BR2	0.42	0.4	0.43	0.33	0.35	0.35	0.29	0.29	0.31

(d)

	Endo			Neuro			Myo		
	θ	α	β	θ	α	β	θ	α	β
EO	0.25	0.28	0.34	0.25	0.28	0.27	0.32	0.3	0.32
BR1	0.24	0.31	0.33	0.27	0.32	0.35	0.32	0.27	0.26
BR2	0.42	0.45	0.39	0.37	0.38	0.36	0.3	0.29	0.3

Figure A.6: Values of average coherence amplitude for eyes-open (EO), short-breathing (BR1), and long breath-hold(BR2) breath-hold states in endogenic, neurogenic, and myogenic components of neurovascular coupling, for each of theta (δ), alpha (α), and beta (β) bands, at (a) left frontal, (b) right frontal, (c) left occipital, and (d) right occipital locations

REFERENCES

[1] E. A. Allen, E. B. Erhardt, E. Damaraju, W. Gruner, J. M. Segall, R. F. Silva, *et al.*, "A baseline for the multivariate comparison of resting-state networks," *Front Syst Neurosci,* vol. 5, p. 2, 2011.

[2] C. M. Anne Hafkemejer, Elise G.P. Dopper, Lize C. Jiskoot, Tijn M.Schouten, "Resting state functional connectivity differences between behavioral variant frontotemporal dementia and Alzheimer's disease," *Frontiers in Human Neuroscience,* vol. 9, 2015.

[3] G. Di Lorenzo, A. Daverio, F. Ferrentino, E. Santarnecchi, F. Ciabattini, L. Monaco, *et al.*, "Altered resting-state EEG source functional connectivity in schizophrenia: the effect of illness duration," *Front Hum Neurosci,* vol. 9, p. 234, 2015.

[4] H. H. Shen, "Core Concept: Resting State Connectivity," *PNAS,* vol. 112, pp. 14115-14116, November 17, 2015 2015.

[5] A. R. B. Silvina G.Horovitz, Walker S. Carr, Dante Picchioni, "Decoupling of the brain's default mode network during deep sleep," *PNAS,* vol. 106, pp. 11376-11381, 2009.

[6] P. M. G. Victor I.Spoormafer, and Michael Czisch, "Frontoparietal connectivity and hierarchial structure of the brain's functional network during sleep," *Frontiers in Neurology,* vol. 3, 2012.

[7] A. P.-L. Arjun Khanna, Christoph Michel, Faranak Fazan, "Microstates in resting-state EEG: Current status and Future Directions," *NeuroScience and Biobehavoral Reviews* vol. 49, pp. 105-113, 2015.

[8] L. Canuet, R. Ishii, R. D. Pascual-Marqui, M. Iwase, R. Kurimoto, Y. Aoki, *et al.*, "Resting-state EEG source localization and functional connectivity in schizophrenia-like psychosis of epilepsy," *PLoS One,* vol. 6, p. e27863, 2011.

[9] F. T. Husain and S. A. Schmidt, "Using resting state functional connectivity to unravel networks of tinnitus," *Hear Res,* vol. 307, pp. 153-62, Jan 2014.

[10] R. D. Pascual-Marqui, D. Lehmann, M. Koukkou, K. Kochi, P. Anderer, B. Saletu, *et al.*, "Assessing interactions in the brain with exact low-resolution electromagnetic tomography," *Philos Trans A Math Phys Eng Sci,* vol. 369, pp. 3768-84, Oct 13 2011.

[11] H. G. a. C. Iadecola, "Neurovascular coupling in the normal brain and in hypertension, stroke, and Alzheimer disease," *J Appl Physiol* vol. 100, pp. 328-335, 2006.

[12] H. B. Clement Huneau, and Hugues Chabriat, "Investigating Human Neurovascular coupling using Functional Neuroimaging: A critical review of dynamic models," *Front Neurosci,* vol. 9, 2015.

[13] T. T. Fenghua Tian, Hanli Liu, Rong Zhang, Lina Chalak, "Wavelet coherence analysis of dynamic cerebral autoregulation in neonatal hypoxic-ischemic encephalopathy," *Neuroimage:Clinical,* vol. 11, pp. 124-132, 2016.

[14] C. Chang, Z. Liu, M. C. Chen, X. Liu, and J. H. Duyn, "EEG correlates of time-varying BOLD functional connectivity," *Neuroimage,* vol. 72, pp. 227-36, May 15 2013.

[15] N. G. P. Ian M. Devonshire, Michael Port, Jason Berwick, Aneurin J. Kennerly, John E.W. Mayhew, Paul G. Overton, "Neurovascular coupling is brain region-dependent," *Neuroimage,* vol. 59, pp. 1997-2006, 2012.

[16] M. T. Talukdar, H. R. Frost, and S. G. Diamond, "Modeling Neurovascular Coupling from Clustered Parameter Sets for Multimodal EEG-NIRS," *Comput Math Methods Med*, vol. 2015, p. 830849, 2015.
[17] D. S. Stephane Sockeel, Melanie Pellegrini-Issac, Habib Benali, "Large-Scale Functional Networks Identified from Resting-State EEG Using Spatial ICA," *PLoS One*, vol. 11, pp. 1-18, 2016.
[18] Y. Liu, M. Liang, Y. Zhou, Y. He, Y. Hao, M. Song, *et al.*, "Disrupted small-world networks in schizophrenia," *Brain*, vol. 131, pp. 945-61, Apr 2008.
[19] M. Pievani, W. de Haan, T. Wu, W. W. Seeley, and G. B. Frisoni, "Functional network disruption in the degenerative dementias," *The Lancet Neurology*, vol. 10, pp. 829-843, 2011.
[20] Tzyy-Ping Jung, Scott Makeig, Colin Humphries, Te-Won Lee, Martin J. Mckeown, Vicente Iragui, *et al.*, "Removing electroencephalographic artifacts by blind source seperation," *Psychophysiology*, vol. 37, pp. 163-178, 2000.
[21] D. K. Pascal-Marqui RD; Kochi K; Lehmann, M; Kinoshita, T, "Functional independent components: revealing cortico-cortical, cross-frequency interactions," *Japanese Journal of Pharmaco-EEG*, pp. 53-58, 2011.
[22] Y. Aoki, R. Ishii, R. D. Pascual-Marqui, L. Canuet, S. Ikeda, M. Hata, *et al.*, "Detection of EEG-resting state independent networks by eLORETA-ICA method," *Front Hum Neurosci*, vol. 9, p. 31, 2015.
[23] C. Open Science, "PSYCHOLOGY. Estimating the reproducibility of psychological science," *Science*, vol. 349, p. aac4716, Aug 28 2015.
[24] C. G. Begley and J. P. Ioannidis, "Reproducibility in science: improving the standard for basic and preclinical research," *Circ Res*, vol. 116, pp. 116-26, Jan 2 2015.
[25] C. G. Begley, A. M. Buchan, and U. Dirnagl, "Robust research: Institutions must do their part for reproducibility," *Nature*, vol. 525, pp. 25-7, Sep 3 2015.
[26] A. Delorme, T. Mullen, C. Kothe, Z. Akalin Acar, N. Bigdely-Shamlo, A. Vankov, *et al.*, "EEGLAB, SIFT, NFT, BCILAB, and ERICA: new tools for advanced EEG processing," *Comput Intell Neurosci*, vol. 2011, p. 130714, 2011.
[27] A. Widmann, E. Schroger, and B. Maess, "Digital filter design for electrophysiological data--a practical approach," *J Neurosci Methods*, vol. 250, pp. 34-46, Jul 30 2015.
[28] T. Mullen, "NITRC: CleanLine: Tool/Resource Info.," 2012.
[29] M. Congedo, "EEG Source Analysis. Neuroscience. Universite de Grenoble," 2013.
[30] D. Mantini, M. G. Perrucci, C. Del Gratta, G. L. Romani, and M. Corbetta, "Electrophysiological signatures of resting state networks in the human brain," *Proc Natl Acad Sci U S A*, vol. 104, pp. 13170-5, Aug 7 2007.
[31] C. T.-B. a. O. Bertrand, "Oscillatory gamma activity in humans and its role in object representation," *Trends Cogn Sci*, vol. 3, pp. 151-162, April 1999 1999.
[32] M. A. G. a. A. D. Milner, "Seperate visual pathways for perception and action," *Trends in NeuroScience*, vol. 15, pp. 20-25, 1992.
[33] P. Ritter, M. Moosmann, and A. Villringer, "Rolandic alpha and beta EEG rhythms' strengths are inversely related to fMRI-BOLD signal in primary somatosensory and motor cortex," *Hum Brain Mapp*, vol. 30, pp. 1168-87, Apr 2009.
[34] A. V. Utevsky, D. V. Smith, and S. A. Huettel, "Precuneus is a functional core of the default-mode network," *J Neurosci*, vol. 34, pp. 932-40, Jan 15 2014.

[35] B. Sajonz, T. Kahnt, D. S. Margulies, S. Q. Park, A. Wittmann, M. Stoy, *et al.*, "Delineating self-referential processing from episodic memory retrieval: common and dissociable networks," *Neuroimage,* vol. 50, pp. 1606-17, May 1 2010.

[36] C. M. Michel and M. M. Murray, "Towards the utilization of EEG as a brain imaging tool," *Neuroimage,* vol. 61, pp. 371-85, Jun 2012.

[37] M. C. Lin Li, Olajide Babawale, and Hanli Liu, "Automated voxel classification used with atlas-guided diffuse optical tomography for assessment of functional brain networks in young and older adults," *Neurophotonics,* 2016.

[38] A. C. B. R. N. K. Luiz Kobuti Ferreira, Maria da Graça Morais Martin, Pedro Paim Santos, Camila de Godoi Carneiro, Daniel Shikanai Kerr, Edson Amaro Jr, Anthony Randal McIntosh and Geraldo F. Busatto, "Aging Effects on Whole-Brain Functional Connectivity in Adults Free of Cognitive and Psychiatric Disorders," *Cerebral Cortex,* 2015.

[39] D. B.-F. Roser Sala-Llonch, Carme Junqué, "Reorganization of brain networks in aging: a review of functional connectivity studies," *Frontiers in Psychology,* vol. 6, 2015.

[40] B. C. Damoiseaux JS, Arigita EJ, Barkhof F, Scheltens P, Stam CJ, Smith SM, Rombouts SA., "Reduced resting-state brain activity in the "default network" in normal aging.," *Cerebral Cortex,* vol. 18, pp. 1856-64, 2008.

[41] K. J. Friston, "Functional and Effective Connectivity: A Review," *Brain Connectivity,* vol. 1, pp. 13-34, 2011.

[42] L. D. Matthew N.DeSalvo, Shigetoshi Takaya, Hesheng Liu, Steven M. Stufflebeam, "Task-dependent reorganisation of functional connectivity networks during visual semantic decision making," *Brain and Behavior,* vol. 4, pp. 877-885, 2014.

[43] a. M. E. R. Yvette I.Sheline, "Resting State Functional Connectivity in Preclinical Alzheimer's Disease: A Review," *Biol Psychiatry,* vol. 74, pp. 340-347, 2013.

[44] D. B. Mary Ellen Lynall, Robert Kerwin, Peter Mckenna, Mnafred Kitzbichler, Ulrich Muller, and Ed Bullmore, "Functional connectivity and brain networks in schizophrenia," *j Neurosci,* vol. 30, pp. 9477-9487, 2010.

[45] V. L. M. Baxter P.Rogers, Allen T. Newton, and John C.Gore, "Assessing Functional Connectivity in the Human Brain by FMRI," *Magn Reson Imaging,* vol. 25, pp. 1347-1357, 2007.

[46] V. P. Paule-Joanne Toussaint, Pierre Bellec, Serge Desarnaud, "Resting-state FDG-PET functional connectivity as an early biomarker of Alzheimer's disease using conjoint univariate and independent component analysis," *Neuroimage,* vol. 61, pp. 936-946, 2012.

[47] C. M. Lu, Y. J. Zhang, B. B. Biswal, Y. F. Zang, D. L. Peng, and C. Z. Zhu, "Use of fNIRS to assess resting state functional connectivity," *J Neurosci Methods,* vol. 186, pp. 242-9, Feb 15 2010.

[48] A. A. Azeez Adebimpe, Emilie Bourel-Ponchei, Mahdi Mahmoudzadeh, and Fabrice Wallois, "EEG Resting state Functional Connectivity Analysis in Children with Benign Epilepsy with Centrotemporal Spikes," *Frontiers in Neuroscience,* vol. 10, 2016.

[49] E. S. L. Martin M. Monti, Mikail Rubinov, Pierre Boveroux, "Dynamic Chnage of Global and Local Information Processing in Propofol-Induced Loss and Recovery of Consciousness," *PLOS Computational Biology,* vol. 9, 2013.

[50] M. S. S. Victor I.Spoormaker, Pablo M.Gleiser, Katia C.Andrade, Martin Dresler, Renate Wehrle, Philipp G.Samann, and Michael Czisch, "Development of a Large-Scale Functional Brain Network during Human Non-Rapid Eye Movement Sleep," *The Journal of Neuroscience,* vol. 30, pp. 11379-11387, 2010.
[51] C. Cao and S. Slobounov, "Alteration of cortical functional connectivity as a result of traumatic brain injury revealed by graph theory, ICA, and sLORETA analyses of EEG signals," *IEEE Trans Neural Syst Rehabil Eng,* vol. 18, pp. 11-9, Feb 2010.
[52] X. Z. a. Y. H. Jinhui Wang, "Graph-based network analysis of resting-state functional MRI," *Frontiers in Systems Neuroscience,* vol. 4, 2010.
[53] H. Niu, Z. Li, X. Liao, J. Wang, T. Zhao, N. Shu, *et al.*, "Test-retest reliability of graph metrics in functional brain networks: a resting-state fNIRS study," *PLoS One,* vol. 8, p. e72425, 2013.
[54] M. J. W. V. d. M. G.Fraga Gonzalez, G.Zaric, M.Bonte, J.Tijms, "Graph analysis of EEG resting functional networks in dyslexic readers," *Clinical Neurophysiology,* vol. 127, pp. 3165-3175, 2016.
[55] O. S. Ed Bullmore, "Complex brain networks: graph theoretical analysis of structural and functional systems.," *Nature,* vol. 10, pp. 186-198, 2009.
[56] X. L. Jiang Zhang, Genyue Fu, Liyang Sai, Huafu Chen, Jianbo Yang, Mingwen Wang, Qi Liu, Gang Yang, Junran Zhang,& Zhen Yuan, "Mapping the small-world properties of brain networks in deception with functional near-infrared spectroscopy," *Sci Rep,* vol. 6, 2016.
[57] O. Sporns, *Networks of the Brain*: MIT Press, 2011.
[58] M. X. Cohen, *Analyzing Neural Time Series Data: Theory and Practice*: MIT Press, 2014.
[59] A. Bruns, "Fourier-, Hilbert, and wavelet-based signal analyses: are they really different approaches?," *Journal of Neuroscience Methods,* vol. 137, pp. 321-332, 2004
[60] X. W. Jinhui Wang, Mingrui Xia, "GRETNA: a graph theoretical network analysis toolbox for imaging connectomics," *Front Hum Neurosci,* 2015.
[61] A. V. P.Guldenmund, M.Boly, "A default mode of brain function in altered states of consciousness," *Archives Italiennes de Biologie,* vol. 150, pp. 107-121, 2012.
[62] H. Y. Xiaoxiao Xu, & Xu Lei, "Activation and Connectivity within the default mode network contribute independently to future-oriented thought," *Scientific Reports,* vol. 6, 2016.
[63] T. Technologies, "Cortical Functions Reference," 2012.
[64] M. M. Boly M., Tononi G, "Theoretical approaches to the diagnosis of altered states of consciousness," *Prog Brain Res,* vol. 177, pp. 383-398, 2009.
[65] X. K. Bo Tan, Ping Yang, "The Difference of Brain Functional Connectivity between Eyes-Open and Eyes Closed Using Graph Theoretical Analysis," *Computational and Mathematical Methods in Medicine,* 2013.
[66] F. H. C. Aaron Philips, Mei Mu Zi Zheng, Andrei Krassioukov, and Philip Ainslie, "Neurovascular coupling in humans: Physiology, methodological advances and clinical implications," *Journal of cerebral blood flow and metabolism,* vol. 36, pp. 647-664, 2016.
[67] M. C. Poornima Venkat, Jieli Chen, "New insights into coupling and uncoupling of cerebral blood flow and metabolism in the brain," *Croat. Med J.,* vol. 57, pp. 223-228, 2016.

[68] J. Z. Rong Zhang, Kenichi Iwasaki, Thad Wilson, Craig G. Crandall, Benjamin Levine, "Autonomic Neural control of dynamic cerebral autoregulation in humans," *Circulation*, vol. 106, pp. 1814-1820, 2002.

[69] Y. M. Yu-Rong Gao, Qingguang Zhang, Aaron T. Winder, Zhifeng Liang, Lilith Antinori, Patrick J.Drew, and Nanyin Zhang, "Time to wake up: Studying neurovascular coupling and brain-wide circuit function in the un-anesthetized animal," *Neuroimage*, vol. 153, pp. 382-398, 2017.

[70] E. C. C. C.K Willie, P.N Ainslie, C.E Taylor, K.J. Smith, P.Y.W. Sin, Y.C. Tzeng, "Neurovascular coupling and distribution of cerebral blood flow during exercise," *Journal of Neuroscience Methods*, vol. 198, pp. 270-273, 2011.

[71] G. M. T. Paolo Zanatta, Elisa Sarton, Anna Bet, Fabrizio Baldanzi, Nivedita Agarwal, Eugene Golanov, "The human brain pacemaker: Synchronised infra-slow neurovascular coupling in patients undergoing non-pulsatile cardiopulmonary bypass," *Neuroimage*, vol. 72, pp. 10-19, 2013.

[72] P. W. Stefan Koch, Jens Steinbrink, Pascal Fries, Hellmuth Obrig, "Stimulus Induced and state dependent sustained gamma activity is tightly coupled to the hemodynamic response in humans," *Journal of Neuroscience* vol. 29, pp. 13962-13970, 2009.

[73] J. Niessing, B. Ebisch, K. E. Schmidt, M. Niessing, W. Singer, and R. A. Galuske, "Hemodynamic signals correlate tightly with synchronized gamma oscillations," *Science*, vol. 309, pp. 948-51, Aug 5 2005.

[74] H. M. Sam Harris, Mingrui Zhao, Luke Boorman, Ying Zheng, Aneurin Kennerley, "Coupling between gamma-band power and cerebral blood volume during recurrent acute neocortical seizures," *Neuroimage*, vol. 97, pp. 62-70, 2014.

[75] A. B. Blanca Martin Bosch, Guido Ferreti, Sophie Schwartz, Kinga Igloi, "Effect of cerebral vasomotion during physical exercise on associative memory: a near-infrared spectroscopy study," *Neurophotonics*, vol. 4, 2017.

[76] F. T. Lina chalak, Beverly Adams-Huet, Diana Vasil, Abbot Laptook, Takashi Turumi, Rong Zhang, "Novel wavelet real time analysis of neurovascular coupling in neonatal encephalopathy," *Sci Rep*, vol. 7, 2017.

[77] D. A. Botero Rosas, Infantosi, A.F.C., Simpson, D.M, Maldonado Arango, M.I, "EEG and cerebral blood flow in newborns during quiet sleep," *International Journal of Bioelectromagnetism*, vol. 10, pp. 261-268, 2008.

[78] M. M.Grigg-Damberger, "The AASM Scoring Manual Four Years Later," *Journal of Clinical Sleep Medicine* vol. 8, 2012.

[79] T. F. Vadim Nikulin, Jan Mehnert, Axel Lipp, Cornelia Noack, Jens teinbrink, Gabriel Curio, "Monochromatic ultra-slow (~0.1Hz) oscillations in the human electroencephalogram and their relation to hemodynamics," *Neuroimage*, vol. 97, pp. 71-80, 2014.

[80] N. Roche-Labarbe, F. Wallois, E. Ponchel, G. Kongolo, and R. Grebe, "Coupled oxygenation oscillation measured by NIRS and intermittent cerebral activation on EEG in premature infants," *Neuroimage*, vol. 36, pp. 718-27, Jul 1 2007.

[81] S. G. H. Dante Picchioni, Maaki Fukunaga, Walter S.Carr, Jed A. Meltzer, Thomas J.Balkin, "Infraslow EEG oscillations organise large-scale cortica-subcortical interactions during sleep: a combined EEG/FMRI study," *Brain Res*, vol. 1374, pp. 63-72, 2011.

[82] Z. Z. a. R. Khalami, "Predominant endothelial vasomotor activity during human sleep: a near-infrared spectroscopy study," *European Journal of Neuroscience,* vol. 40, pp. 3396-3404, 2014.

[83] T. Mullen, C. Kothe, Y. M. Chi, A. Ojeda, T. Kerth, S. Makeig, *et al.*, "Real-time modeling and 3D visualization of source dynamics and connectivity using wearable EEG," *Conf Proc IEEE Eng Med Biol Soc,* vol. 2013, pp. 2184-7, 2013.

[84] P. T. Arjan Hillebrand, Edwin van Dellena, Meichen Yua, Ellen W. S. Carboc, Linda Douwc,Alida A. Gouw, Elisabeth C. W. van Straaten and Cornelis J. Stam, "Direction of information flow in large-scale restingstate networks is frequency-dependent," *PNAS,* vol. 113, pp. 3867-3872, 2016.

[85] D. Z. Jing Feng, Banyaun Chen, "Endothelial mechanisms of endothelial dysfunction in patients with obstructive sleep apnea," *Sleep Breath,* vol. 16, pp. 283-294, 2012.

[86] P. N. A. Chrstopher K.Willie, Ivan Drvis, David MacLeod, Anthony R Bain, "Regulation of brain blood flow and oxygen delivery in elite breath-hold divers," *Journal of cerebral blood flow and metabolism,* vol. 35, pp. 66-73, 2015.

[87] G. H. Haslaile Abdullah, Irena Cosic, Dean Cvetknovic, "Correlation of sleep EEG frequency bands and Heart Rate Variability," *IEEE EMBS,* 2009.

[88] T. Y. Taira Uehara, Tsuyoshi Okamoto, "Efficiency of a "Small World" barin network depends on consciousness level: A resting-state FMRI study," *Cerebral Cortex,* vol. 24, pp. 1529-1539, 2013.

[89] Winder et al, “Weak correlations between hemodynamic signals and ongoing neural activity during the resting state,” *Nature Neuroscience,* vol.20, pp.1761-1769, 2017.

[90] A.W. Ward, D. G McLaren, A.P.Schultz, J.Chhatwal, “Daytime Sleepiness is associated with decreased default mode connectivity in both young and cognitively intact elderly subjects,” *SLEEP.* Vol 36(11), 2013.

[91] J. S Crone, G.Ladurner, Y.Holler, S.Golaszewski, “Deactivation of the default mode network as a marker of impaired consciousness: An FMRI study”, *PLOS ONE,* vol.6(11), 2011.

[92] A.Vanhaudenhuyse, Q. Noirhomme, Luaba J.F .Tshibanda, “Default network connectivity reflects the level of consciousness in non-communicative brain-damaged patients”, *BRAIN,* vol.133, pp 161-171, 2009.

[93] T.Uehara, T.Yamasaki, T.Okamoto, T.Koike, “Efficiency of a small-world brain network depends on consciousness level”, *Cerebral Cortex,* vol.24, pp 1529-1539, 2013.

[94] D.Moser, P.Anderer, G.Gruber, S.Parapatics, “Sleep Classification according to AASM”, *SLEEP.* Vol 32(2), 2008

[95] J. Y. S.-P. Gennady G. Knyazev and L. V. P. Andrey V. Bocharov, "The default mode network and EEG alpha oscillations: An independent component analysis," *Brain Research,* vol. 1402, pp. 67-79, 2011.

Biographical Information

Olajide Babawale M. was born on June 6, 1989, in Ijebu Igbo, Ogun state, Nigeria. He received the Bachelor of Engineering degree in Electrical and Electronics Engineering from Covenant University, Ota, Ogun State, Nigeria, in 2009. In Fall 2012, he began his doctoral study in Bioengineering Department, the University of Texas at Arlington, Arlington, TX, USA. He is in the medical imaging track and under the supervision of Dr. Hanli Liu. His plan is to complete his Doctor of Philosophy in Biomedical Engineering at the joint graduate program of the University of Texas at Arlington and University of Texas Southwestern at Dallas in May 2018. His research interests include functional brain imaging in fMRI, fNIRS and MEG/EEG.